DOTTORATO DI RICERCA IN "RISCHIO E SOSTENIBILITA' NEI SISTEMI DELL'INGEGNERIA CIVILE, EDILE E AMBIENTALE"
XXX Ciclo - Nuova Serie (2014-2017)
DIPARTIMENTO DI INGEGNERIA CIVILE, UNIVERSITÀ DEGLI STUDI DI SALERNO

SUSTAINABLE MANAGEMENT OF STORMWATER IN A CHANGING ENVIRONMENT UNDER MEDITERRANEAN CLIMATE CONDITIONS

ING. (DOTT.) MIRKA MOBILIA

Relatore:
PROF. ING. ANTONIA LONGOBARDI

Coordinatore
PROF. ING.FERNANDO FRATERNALI

SUSTAINABLE MANAGMENT OF STORMWATER IN A CHANGING ENVIRONMENT UNDER MEDITERRANEAN CLIMATE CONDITIONS

TABLE OF CONTENTS

LIST OF FIGURES

LIST OF TABLES

ABSTRACT

The problem of the increase in the magnitude and frequency of flooding events in urban areas can be approached by means of techniques of sustainable urban stormwater management. In this PhD dissertation, the effectiveness of one of these technologies namely the green roof (GR), has been investigated. For this purpose, a daily scale hydrological model for GRs, mainly based on meteorological data and with three levels of complexity has been proposed. Since, the evapotranspiration (ET) fluxes impact the GR retention performances, a study of the dynamics involved in ET process has been carried out. The use of green roofs technology in Mediterranean climate is very limited so two GR experimental benches has been placed in the campus of University of Salerno and preliminary results about the hydrological performances depending on the climate and constructions characteristics have been illustrated. Subsequently, the effectiveness of the proposed technology for the sustainable urban drainage management have been tested at a large scale and Sarno peri-urban basin has been presented as case study since it represents a hydrogeological hazard prone system. The analysis focused on the potential hydrological benefits in terms of peak runoff, peak delay and volume runoff in respect of several hypothetical scenarios of rainfall and GR retrofitting percentage. In high urbanized areas, the implementation of GRs at basin scale, allows a reduction of runoff rainwater from roofs close to 100% for some rainfall and greening scenarios. Where the GR retrofit potential is very low, satisfactory performances in terms of water management can be reached coupling this green technology to other sustainable techniques.

ABOUT THE AUTHOR

Mirka Mobilia Ing. Mirka Mobilia earned a Bachelor's degree in Environmental Engineering at University of Salerno in 2011. In 2014 she earned Master's degree in Environmental Engineering, at University of Salerno. In November 2014,she started a Ph.D. course in "Risk and sustainability in civil, environmental and construction engineering", at the Civil Engineering Department ,University of Salerno. Her research interest is about the sustainable stormwater management for urban drainage systems, with a particular focus on urban greening. During her studies, she spent three research periods abroad at the University of Applied Sciences of Trier, at the Technical University of Darmstadt and at the Institute of Bio- and Geosciences (Forschungszentrum) of Jülich, where she had the opportunity to deepen her knowledge about experimental site monitoring and hydrological modelling.

1 INTRODUCTION

Many cities around the world are increasingly called to deal with the two major challenges of climate change and urbanization. Both of them cause an increase in the magnitude and frequency of flooding in urban areas. In order to face these criticisms, adaptation measures are required for conventional drainage systems with limited capacity and flexibility. They help the urban drainage infrastructures to improve their resilience against the adverse impact of climate change and rapid urbanization in a context where reducing risk of flooding becomes more and more urgent. Among adaptations approaches, techniques of sustainable urban stormwater management like Green infrastructures (GIs) represent a very attractive issue because of the variety of benefits, beyond the hydrological perspective, they can provide for urban environments. They are conceived as a network of greenspaces around urban landscapes providing environmental, social and economic benefits to the community indeed. Among these the green roofs (GRs) technique are an effective tool for pursuing the concept of a sustainable stormwater management. The technology of green roofs induces important hydraulic benefits compared to a traditional roof, such as decrease in runoff volume, peak discharge attenuation and increase in the peak delay. With reference to the hydrological issue related to GIs application within the European geographical context, the sustainable urban drainage management has been widely implemented in the Nordic countries characterized by oceanic climate with warm summers and cool winters and a negligible seasonal pattern. In these regions, the hydrological performances of the green techniques in terms of retention capacity have been investigated in detail and many contributions exist in the specific literature from which it appears that their behavior is not yet fully understood because affected by multiple factors like the types of rainfall event, the climate condition of the study area and the construction type of the roof. In the Mediterranean climate, the uncertainty in GIs hydrological performances is even more evident because of the marked climate stress and differences between the seasons and because of a limited number of test beds providing experimental data. In light of this,

the reported research work has contributed to the understanding of this question with the proposal of a conceptual model strongly grounded on the meteorological conditions for an accurate prediction of green roofs' hydrological behavior at the building scale and with the setup of an experimental site located within the University of Salerno campus. With a particulr focus on a mediterranean catchment characterized by evolving climate and land use conditions, the main aim of the present thesis is the investigation of the sensitivity of the cathment stormwter response to the use of green infrastructures, as a valid tool for the mitigation of hydrogeological risk in urban and peri-urban environments.

In this respect, after a review of the state of the art set out in the chapter 2 of the present work, in the chapter 3, a study of the evapotranspiration dynamics that is a key process affecting the hydrological behavior of green roofs, has been carried out. In the chapter 4, as a result of a modeling with increasing levels of complexity, a daily scale hydrological model for GRs, mainly based on meteorological data, has been proposed. Finally, in the chapter 5, the GR experimental site located in the campus of University of Salerno has been illustrated and preliminary results about the hydrological performances depending on the climate and constructions characteristics have been shown.

In the second part of the thesis, arguing about the limits of a traditional urban drainage system management model where urban flooding prevention is achieved with the use of centralized strategies, generally corresponding to underground concrete tanks connected to the main drainage network, the effectiveness of the proposed technologies for the sustainable urban drainage management have been tested at a large scale. As already said, because of the lack of experimental sites in Italy, especially for what concerns the catchment scale, the research work has been mainly focused on a sensitivity analysis aiming at verify the potential improvement related to the use of GI, from the hydrological point of view. The case study is represented by the Sarno peri-urban basin (Campania region), selected as it represent a hydrogeological hazard prone system and is characterized by an extremely fragile equilibrium at the urban level.

Pursuing this line, in the chapters 6 and 7, the analysis of the hydrological performances of green roof at basin scale in terms of peak runoff, peak delay and volume runoff, has been performed. The susceptibility of the hydrological response to spatial distribution, scale of aggregation and percentage of retrofitted roofs has been tested. A wide

range of situations have been simulated from scenarios related to virtual basin and design storms to scenarios referring to actual catchment and real events occurred in the past. Finally, the analysis investigates the impacts of the sustainable urban stormwater management infrastructures at the basin scale and the potential for such infrastructures to be effectively and diffusely accounted for in planning and managing the urban environment on the way for a sustainable environment.

2 STATE OF ART

Many cities around the world are increasingly called to deal with the two major challenges of climate change and urbanization (Zhou 2014). Both of them cause an increase in the magnitude and frequency of flooding in urban areas (Huong et al. 2013, Leopold 1968, Semadeni-Davies et al. 2008, Zhou et al. 2012). According to several scholars (Willems et al. 2012, Arnbjerg-Nielsen et al. 2012, Ekström et al. 2005), the climate change could address in the coming years more frequent rain of increased peak intensity leading inevitably to more sewer floods because of the overloading of the urban drainage systems, designed with a certain return period. The urbanization has same impacts on sewer infrastructure as climate change. The United Nations (UN, 2014) predict that, the world's population will increase between 1950 and 2100 of about 9 billion people with more than 66% living in urban areas. The increase in urban population involves a sprawl sealing surfaces including industrial commercial and residential settlements. In cities with extensive impermeable areas, the amount of occurring runoff is higher than in case of low urbanization and consequently the risk of flooding increases too (Huong et al. 2013). The dynamic of urbanization can be monitored with SAR images guaranteeing observations and measurements at high spatial and temporal resolution (Taubenböck, et al. 2012, Ban et al. 2012). SAR images acquired over the same area at different times allow to map the process of urbanization in time, and comparing this data with a database of urban flooding events, the identification of a relationship between the occurrences of flooding and the land use changes could be possible. In time many authors have used the SAR images for different research purposes (Di Martire et al. 2016, Weijie et al. 2015, Zhu et al. 2016). Some authors have used this kind of images to investigate the spatial evolution of urbanization (Ban et al. 2012, Zhu et al. 2012, Fu et al. 2014, Ma et al. 2014), few of them have used Synthetic aperture radar images for hydraulic aims (Haas et al. 2014, Dewan et al. 2008). In order to face the criticism of flooding in urban areas, adaptation measures are required for conventional drainage systems with limited capacity and flexibility (Jha et al. 2011). They help the urban sewer infrastructures to improve their resilience against the adverse impact of climate change and

rapid urbanization in a context where reducing risk of flooding becomes even more urgent. The adaptations options include techniques of sustainable management of urban stormwater known around the world with different denominations but with similar principles. In North America and New Zealand, the term LID or low impact development is used to indicated a variety of practices that mimic natural processes in the management of stormwater (Fletcher et al. 2015). In United States and Canada, BMP (Best management practices) refers to practices aiming to prevent pollution (Fletcher et al. 2015). In UK and in general in Europe, sustainable urban drainage systems (SUDS) consist of technologies able to drain rainwater as closely as possible to the natural drainage from a site before development (Woods-Ballard et al. 2007). Green infrastructures (GIs) are an integral part of SUDS (Mguni et al. 2016). They are conceived as a network of greenspaces around urban landscapes providing environmental, social and economic benefits to the community (Benedict et al. 2002, Sartor et al. 2018). GIs exactly fit, in terms of water management and urban flooding prevention, within the philosophy of SUDs, because they aim to provide a hydrological/drainage network being complementary and linking green space with built infrastructure (Ahern 2007). These techniques include green roofs, filter drains and filter strips, permeable surfaces, swales(shallow drainage channels), infiltration trenches, detention basins (Woods-Ballard et al. 2007).

Among these, in a relatively recent past, many scientific studies have demonstrated the potential of green roofs (GRs) (Carter et al. 2006, Shaharuddin et al. 2011, Mobilia et al. 2015a,b) in pursuing the concept of a sustainable stormwater management. These technologies induce important hydraulic benefits compared to the conventional rooftop: decrease in runoff volume (VanWoert et al. 2005, Berndtsson 2010), peak discharge attenuation (Trinh et al. 2013, Fioretti et al. 2010) and increase in the peak delay (Gibler 2015, Stovin et al. 2015). With reference to the green roof retention properties, different authors have reported significantly different hydrological performances with reduction of the total volume of precipitation ranging from 40 to 90% (Mentens et al. 2006, Teemusk et al. 2007, Jarrett et al. 2006). The retention capacity of a GR is obviously a function of the system configuration (Stovin et al. 2012) but especially of the climate conditions of the area where the roof is placed. The hydrological effectiveness of the eco-roofs changes in different weather conditions, even if a complete picture of the situations

can't be presented due to lack of experimental sites in some climatic regimes. For instance, in Europe, green roof infrastructures are mainly implemented in northern regions such as Germany, (Zimmer et al. 1997, Mentens et al. 2006), Sweden and Denmark (Villarreal et al. 2005, Bengtsson 2005, Locatelli et al. 2014), UK (Kasmin et al. 2010, Stovin et al. 201), Stovin et al. 2013) where their hydrological effectiveness is well documented in literature and their performances in term of peak flow and runoff volume reduction and peak time delay have been investigated in detail. The use of green roofs technology in Mediterranean climate is more limited. There are few experimental sites aiming mostly to monitor other aspects of the behavior of green roofs, in particular the thermal one. Consequently, the effects in terms of stormwater mitigation of GRs require additional investigations (Olivieri et al. 2013, Lazzarin et al. 2005, Fioretti et al. 2010).

Together with the system configuration and the climate conditions, the hydrological processes occurring also play an important role in the assessment of stormwater related benefits of green roofs and especially the evapotranspiration loss, as discussed in many recent works, because it directly impacts the green roof retention performances (Poë et al. 2015, Starry et al. 2016, Feitosa et al. 2016, Voyde et al. 2010). Evapotranspiration (ET) continuously restores the retention capacity of a storage system consequently it is the major component in the water balance of hydrological systems (McMahon et al. 2013) and the uncertainty in its assessment would propagate through the hydrological soil water balance (Abbaspour et al., 2015). Long term AET (Actual Evapotranspiration) measurements are complex and costly to be obtained, and even if observational data exists, methods to assess AET fluxes are time-consuming (Burba et al. 2010). For these reasons, many authors have proposed various approaches for indirect AET modeling (Mobilia et al 2016a). Under the Budyko framework AET is dominated either by precipitation P or by potential evapotranspiration PET (Budyko 1974). AET rates approach precipitation values in case of dry climates (water availability limited conditions) and potential evapotranspiration values in case of wet climates (energy limited conditions). Introducing the aridity index P/PET, water availability limited systems and energy limited systems are characterized respectively by $P/PET < 1$ and $P/PET > 1$. Beyond a long term characterization, water availability an energy limited conditions can alternate in time for a given system, as the results of the intra-annual variability of

climatological variables and thus in evapotranspiration rates, that switch from actual to potential rates (Ryu et al. 2008, Zhang et al. 2016). Opposed to more physically based methods, requiring soil physical properties and soil moisture and vegetation monitored data, actual evapotranspiration modeling can be performed through the use of a class of methods, simply based on routinely measured meteorological variables. Among these methods the Antecedent Precipitation Index (API) model, the Advection-Aridity (AA) model (Brutsaert et al. 1979), the Granger and Gray (GG) model (Granger et al. 1989), the CRAE model (Morton 1978), the modified advection aridity (MAA) model proposed by Otsuki et al. 1984 can be listed. Despite the large number of scientific contributions existing in the specific literature, there is still no a method for the assessment of actual evapotranspiration losses, starting from simple meteorological data and able to: i) identify the temporal switching between water availability and energy limited conditions, in order to recognize time period where the evapotranspiration losses are dominated by PET; ii) model the evapotranspiration losses seasonal pattern moving from potential to actual rates, respectively during energy limited and water availability limited conditions.

The GR hydrological behavior is modeled by soil water balance approaches and evapotranspiration loss plays an important role into retention modeling frameworks. In time, a broad range of models, conceptual or more physically based, oriented to the event or to the continuous time scale, suitable for single building or catchment scale, have been proposed by numerous authors (Berthier et al. 2010, Sherrard et al 2011, Stovin et al. 2013, Jim et al. 2012, Poë et al 2015, Hardin et al. 2012). Their implementation generally requires a high number of input parameters related to the soil hydraulic properties including textural class of the soil, residual soil water content, saturated soil water content, saturated hydraulic conductivity, or related to the water flow boundary condition, and the initial condition in terms of the pressure head or the water content (Hilten et al. 2008, Hakimdavara et al. 2014). Model implementation to predict the effectiveness of a planned green-roof installation in a particular area is mostly complex, due to the above-mentioned required data and parameters of the hydraulic system to be simulated, which are usually not readily available without laboratory or field experiments. It is well known indeed how model complexity affects model performances. Relatively simpler approach are frequently

preferred to over complex one as low calibration requirements are associated to a more robust parameters estimation (Burstza-Adamiak et al. 2013, Carson et al., 2015, Starry et al. 2016). In view of this, a conceptual model approach essentially using only few basic input parameters and weather data recorded by inexpensive monitoring installations in the area of interest is required as an answer to mentioned limitations. It should be taken into account that if the green infrastructures want to be used for the mitigation of urban flooding events, in addition to the complexity related to the understanding of their behavior at single building scale, efforts should be made to figure out how they perform at a larger scale. In the latter case, the corresponding experimental sites do not exist and the relative contributions refer to sensitivity analysis aiming at verifying the potential hydrological impacts (Masseroni et al. 2016, Versini et al. 2016, Zimmerman et al. 2016, Mobilia et al. 2018a). In this kind of study, a key role has been played by the analysis of the dynamics occurring in different climate conditions but also of the extent of implementation of this technology according to the characteristics of the existing urban built heritage.

3 EVALUATION OF METEOROLOGICAL DATA BASED EVAPOTRANSPIRATION MODELS

In a water balance, evapotranspiration represents the largest component and therefore, errors in estimating ET loss, assume great significance. The assessment of hydrological performances of green roof requires the quantification of evapotranspiration loss that plays a key role in reducing stormwater input because it directly acts on its moisture content, and thus on its ability to retain water after rainfall events. In order to measure evaporation fluxes, very sophisticated techniques can be used but they require more experimental data and instrumentation than are normally available. Given this premise, a methodology for actual evapotranspiration losses only based on meteorological data has been proposed. The approach is very simple to implement because the data required as input are commonly and directly measured in weather stations or can be derived with the help of direct or empirical relationships. To this aim micro-meteorological data at the Rollesbroich experimental site have been analyzed for a period of two years from July 2013 to June 2015. The analysis highlights a seasonal pattern in Budyko index so based on the observed seasonal switch between water-limited and energy-limited conditions, a threshold approach, combining potential evapotranspiration formulation and empirical actual evapotranspiration relationships, has been proposed and validated against eddy covariance assessment. Using several goodness of fit indices (RMSE, RE, MAE, NSE, d and r) the deviation between modeled and measured ET fluxes have been investigated. Penman-Montheith formulation has been considered for the potential evapotranspiration assessment and two different empirical relationships have been applied, namely the advection-aridity "AA" and the "API" non-potential Priestly-Taylor models, as empirical actual losses relationships. At the monthly scale, the lowest error occurs when the API method is used to mimic the water availability limited conditions but further significant improvements in the model can be achieved through the calibration of the Priestly-

Taylor advection coefficient. Because the model prediction of ET agreed well with the estimates obtained with the EC measurements, the approach can be considered well performing in the assessment of the actual evapotranspiration loss to be used in retention models of green roofs (Mobilia et al. 2018b).

3.1 A REVIEW OF EVAPOTRANSPIRATION MODELS

3.1.1 Study area and data collection

The grassland study site of Rollesbroich (50°37'19"N, 6°18'15"E) is located in western Germany close to the Belgian border (Figure 3.1). The catchment has an area of 31 ha and its elevation increases from 474 to 518 m.a.s.l.. The annual mean precipitation and air temperature are respectively about 1033 mm and 7.7 °C (Qu et al. 2016). While the air temperature has a clearly visible seasonal pattern, with minimum and maximum values occurring respectively during the winter and summer seasons, the precipitation amount is substantially and uniformly distributed during the year (Figure 3.1).
The composition of the higher plant species at the site is typical for traditionally managed grassland of the Ranunculus repens–Alopecurus pratensis plant community with the major species of meadow foxtail (Alopecurus pratensis), perennial rye grass (Lolium perenne), rough meadow grass (Poa trivialis) and common sorrel (Rumex acetosa) (Borchard et al. 2015). All components of the water balance (e.g. precipitation, evapotranspiration, runoff, soil water content) are continuously monitored using state-of-the-art instrumentation installed in the center of the field, including weather stations, a micrometeorological station, weighable lysimeters, runoff gauges, cosmic-ray soil moisture sensors, a wireless sensor network that monitors soil temperature, and soil moisture and a 4-component net radiometer. For a detailed description of the site and measurement facilities please see Gebler et al. 2015 and Post et al. 2015. Latent heat flux was obtained by the eddy covariance (EC) technique for time intervals of 30 minutes. The EC post-processing software TK3.1 (Mauder et al. 2011) was used to calculate latent heat flux from the vertical wind velocity obtained by the sonic anemometer (CSAT3,

Campbell Scientific, Inc., Logan, USA) and water vapor density obtained by an infrared gas analyzer (LI7500, LI-COR Inc., Lincoln, NE, USA).

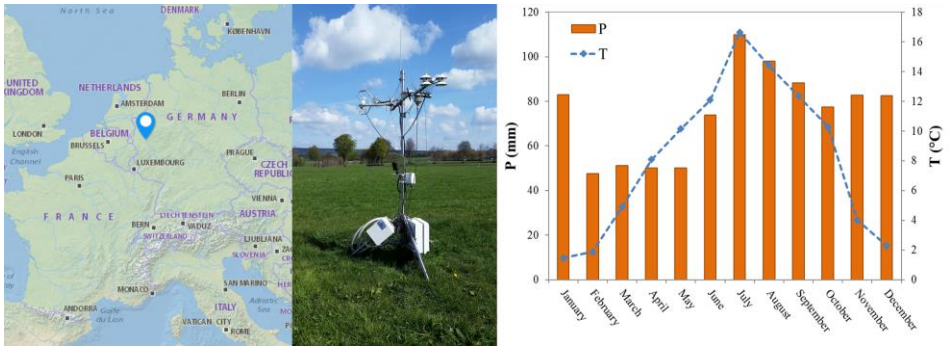

Figure 3.1 Location of the Rollesbroich grassland site in Germany (left) and the Eddy covariance station (right) at the site.

The processing and quality assurance of the EC data followed the corresponding TERENO strategy presented in Mauder et al. 2013. Actual evapotranspiration was calculated from the latent heat flux using:

$$AET = \frac{LH}{\rho_W \cdot L_{water}} \tag{3-1}$$

$$L_{water} = 10^{-3} \cdot (2500.8 - 2.36 \cdot T + 0.0016 \cdot T^2 - 0.000006 \cdot T^3) \tag{3-2}$$

where AET is actual evapotranspiration (mm^{-1}), LH is latent heat flux (Wm^{-2}), ϱ_w is water density ($kg\ m^{-3}$), L_{water} is latent heat of condensation of water in the temperature range from −25 to 40 ◦C ($J\ kg^{-1}$), and T is air temperature (◦C).
Since eddy covariance measurements are inevitably including gaps a standard gap-filling procedure was applied after Reichstein et al. 2005 to calculate the daily, monthly and annual sums actual evapotranspiration.

3.1.2 Complementary relationships for actual evapotranspiration modeling

Complementary relationship (CR) models were introduced by Bouchet 1963, and allow to directly model actual evapotranspiration using conventional meteorological data. These models argue about a mechanism of feedback between actual evapotranspiration (AET) and potential (PET) evapotranspiration rates under condition of minimum advection in a homogeneous area. In other words, in a condition of wet surface, actual evapotranspiration equals the potential one, according to:

$$AET = PET = WET \tag{3-3}$$

also expressed as:

$$AET + PET = 2 \cdot WET \tag{3-4}$$

and finally:

$$AET = 2 \cdot WET - PET \tag{3-5}$$

Where WET is the wet environment evapotranspiration. WET environment or equilibrium evaporation is the evaporation rate occurring when the surface is saturated and energy supply is constant. Equ. 3-3 states that an increase in AET corresponds to an equivalent decrease of PET because when the surface gets dry, a reduction of actual evapotranspiration occurs, it leads to a decrease in humidity and an increase in air temperature, as consequence, the PET increases too by equal amount.
Among well-known complementary relationships, one of the most broadly used approaches, the Advection Aridity model (Brutsaert et al. 1979), has been here selected to quantify actual evapotranspiration losses based on meteorological variables measurements. It considered that AET models require previous calculation of Priestley and Taylor (P-T) 1972 (eq. 3-6) and Penman (eq. 3-7) potential evapotranspiration fluxes PET

$$PET_{P,T} = \frac{1}{\lambda} \cdot \alpha \left[\frac{\Delta}{\Delta + \gamma} \left(R_n - G_{soil} \right) \right] \tag{3-6}$$

$$PET_{P,M} = \frac{1}{\lambda}\left[\frac{\Delta}{\Delta+\gamma}\left(R_n - G_{soil}\right)\right] + \left[\frac{\gamma}{\gamma+\Delta}E_A\right] \tag{3-7}$$

where Δ is the slope of the saturation vapor pressure–temperature curve (kPa °C^{-1}) , given by the formula:

$$\Delta = \frac{4098 e_s}{\left(T+237.3\right)^2} \tag{3-8}$$

e_s is the saturation vapor pressure:

$$e_s = 0.611\exp\left(\frac{17.27 \cdot T}{T+237.3}\right) \tag{3-9}$$

T is the air temperature (°C), γ is the psychrometric constant (kPa °C^{-1}), λ is latent heat of vaporization (MJ kg^{-1}):

$$\lambda = 2.501 - (2.361 \cdot 10^{-3})T \tag{3-10}$$

and E_A is the drying power of the the air expressed as:

$$E_A = 2.6(1+0.54u_2)(e_s - e_a) \tag{3-11}$$

u_2 is the wind speed (ms^{-1}), e_s is the saturation vapor pressure (kPa), e_a is the vapor pressure (kPa), and α the is the advection correction coefficient from the Priestley–Taylor model equation with value 1.26, R_n is the net radiation (MJ m^{-2} d^{-1}), G_{soil} is the soil heat-flux density at the soil surface (MJ m^{-2} d^{-1}), considered to be negligible on a daily time scale (Allen et al., 1998). Actual evapotranspiration derived by the AA Method results from eq. 3-1 where potential evapotranspiration is given by Penman equation for potential evapotranspiration and its subsequent amendments suggested by different authors (e.g., Penman et al. 1951, Tanner et al. 1960, Slatyer et al. 1961, Kohler et al. 1967) while the wet environment evapotranspiration is provided by the Priestley and Taylor equation for PET in which condition of minimal advection is considered and the value of 1.26 is assumed for the advection correction coefficient.

Finally, the AA model calculates AET from PET predicted by coupled P-T and Penman equations, according to the formula (Marasco et al. 2015):

$$AET_{AA} = (2\alpha - 1)0.408\left[\frac{\Delta}{\Delta+\gamma}\left(R_n - G_{soil}\right)\right] - \left[\frac{\gamma}{\gamma+\Delta}E_A\right] \quad (3\text{-}12)$$

3.1.3 API Corrected potential evapotranspiration for actual evapotranspiration modeling

The equilibrium evaporation or wet environment evaporation equation, originally proposed by Slatyet et al. 1961, was subsequently modified by Priestley and Taylor (1972) for estimating potential evapotranspiration (eq. 3-6). From the results of several experiments, they found that the coefficient α was constant and equals to 1.26. Mawdsley et al. 1985 modified the Priestley-Taylor model assuming a variability for α, which is assessed in relation to the Antecedent Precipitation Index (Linsley et al. 1951) as in the following:

$$AET_{API} = 0.408 \cdot \alpha_{API}\left[\frac{\Delta}{\Delta+\gamma}\left(R_n - G_{soil}\right)\right] \quad (3\text{-}13)$$

where the dimensionless coefficient, α_{API}, is expressed as a function of the wetness index API:

$$if \quad API \le 20mm \rightarrow\rightarrow \alpha_{API} = 0.123(API) - 0.0029(API)^2 - 0.0000056(API)^3 \quad (3\text{-}14)$$

Where:

$$API_t = (C \cdot API_{t-1}) + P_t \quad (3\text{-}15)$$

With API_t the antecedent precipitation index computed on day t, C the storm hydrograph recession coefficient and P_t the precipitation of day t. While for values of API lower than the fixed threshold, the non-dimensional coefficient corresponds to the Priestley-Taylor coefficient:

$$if \quad API > 20mm \rightarrow\rightarrow \alpha_{API} = 1.26 \tag{3-16}$$

assuming that for over saturated system (API > 20 mm) AET rates are no longer dependent on soil water content but they are a constant percentage of PET.

3.2 SWITCHING BETWEEN WATER AND ENERGY LIMITED CONDITIONS

Computed on an annual time scale, for the period under evaluation, mean annual precipitation and potential evapotranspiration are respectively about 895 mm and 795 mm, which return an annual scale Budyko index of about 1.2. The energy limited scheme is thus applicable to the investigated system.
If computed at the monthly scale, the Budyko index I appears to be characterized by a seasonal pattern (Figure 3.2). From March to September I = P/PET is overall smaller than the threshold limit P/PET = 1, thus the system can be defined water-limited in this period of the year. Extra-ordinary rainfall events (not consistent with the average behaviour) occurred in July and August 2014 are the reason for I larger than 1. According to Budyko 1974 framework, actual evapotranspiration rates are controlled by precipitation amounts which are visibly significant also during this time window. From October to February I is instead larger than 1. The system switches from a water limited to an energy limited condition in this period of the year. An effective switch occurs in the period from November to February, when I values are significantly larger than 1. A comparison between actual evapotranspiration, derived by eddy covariance observations, and potential evapotranspiration, computed by the Penman Montheith formulation (Figure 3.3), illustrates how during this period (I >> 1) actual rates approach potential one and are instead lower during the remaining periods, especially during the summer season. When compared to meteorological variables available for the study site, it has been found a significant correlation between the net radiation value and the temporal switching between the water limited and energy limited conditions. At the monthly scale, in fact, actual evapotranspiration rates approach potential ones when the net radiation

assumes negative values or when net radiation is below a threshold of about 1.5 MJ/m^{2}d^{-1}.

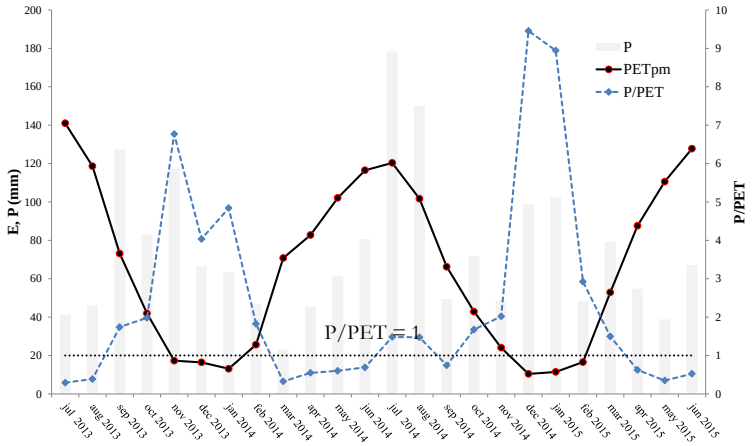

Figure 3.2 Monthly patterns for precipitation (P), eddy covariance actual evapotranspiration (AETec), Penman-Montheith potential evapotranspiration (PETpm) and Budyko aridity index (P/PET). The dotted line P/PET = 1 represents the threshold limit between energy limited and water limited systems.

This finding, assumed valid for the particular climate environment and vegetation type considered, represent an operational result useful for further modelling the actual evapotranspiration losses, which will be constrained by potential values on the base of a threshold model that, as later detailed, can be set on widely available meteorological variables, such as the monitored net radiation.

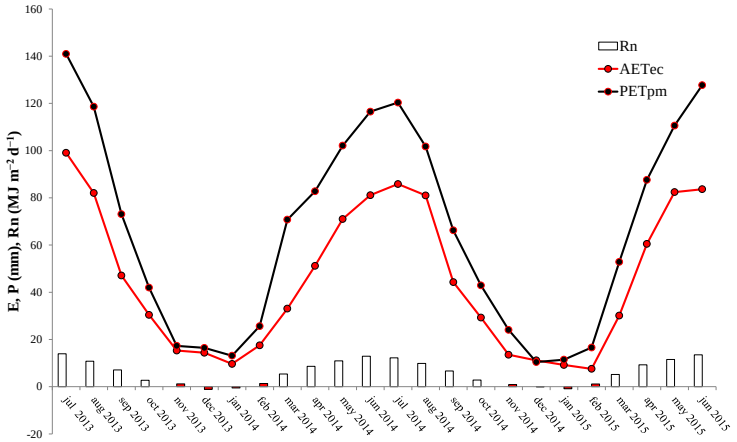

Figure 3.3 Monthly patterns for eddy covariance actual evapotranspiration (AETec), Penman-Montheith potential evapotranspiration (PETpm) and net radiation (Rn).

3.3 MONTHLY AET PREDICTION MODELS

In order to effectively model actual evapotranspiration at monthly scale, four methods have been proposed:
1) The API Antecedent precipitation index method, as described by eq. 3-13
2) The AA Advection Aridity method, as described by eq. 3-12
3) In addition to the above mentioned methods reported by the scientific literature, two threshold combined approaches have been proposed, provided the illustrated findings related to the temporal switching from the water limited to energy limited conditions. The proposed approaches are PM/API and PM/AA models, described by eq. 3-17,3-18, combining the Penman Montheith formulation for PET assessment and the API or AA formulations for AET assessment, where the Priestley-Taylor coefficient has been set to 1.26, as suggested by Mawdsley et al. 1985. The combination between the PET and the AET formulation is proposed according to the observed temporal switch. When energy limited conditions occur, actual evapotranspiration is well described by the potential one computed by PM according to Figure 3.3 while when the system is governed by water limited conditions, actual ET rates can be accurately predicted using API and AA methods. The switch from PM to API or/and AA is detected when net radiation (NR) is below an observed threshold (NR_T) as in the following:

$$if \quad NR < NR_T \rightarrow\rightarrow PET_{P,M} = \frac{1}{\lambda}\left[\frac{\Delta}{\Delta+\gamma}\left(R_n - G_{soil}\right)\right] + \left[\frac{\gamma}{\gamma+\Delta}E_A\right] \tag{3-17}$$

$$if \quad NR > NR_T \rightarrow\rightarrow \begin{cases} AET_{API} = 0.408\left[\frac{\Delta}{\Delta+\gamma}\left(R_n - G_{soil}\right)\right] \\ or \\ AET_{AA} = (2\alpha - 1)0.408\left[\frac{\Delta}{\Delta+\gamma}(R_n - G_{soil})\right] - \left[\frac{\gamma}{\gamma+\Delta}E_A\right] \end{cases} \tag{3-18}$$

4) The last proposed model is the threshold approach PM/API_{CAL}, which combines PM and API, according to the previous considerations, but where a calibration of Pristley-Taylor coefficient is further suggested in order to achieve a better fitting between observed and modelled ET values.

The relationships between AET fluxes modelled using the above described approaches and observed EC measurements have been evaluated by a quantitative fitting analysis. The comparisons help testing the ability of the models in predicting actual evapotranspiration but, what is more important, help detecting the limitations of each approach. The fitting analysis have been performed at monthly and global scales using several goodness-of-fit (GOF) indices: the root-mean-square error (RMSE), the relative error (RE), the mean absolute error (MAE), Nash-Sutcliffe Efficiency coefficient (NSE), Index od agreement (d), the correlation coefficient (r) estimated as follows:

$$RMSE_j = \left[\frac{\sum_{i=1}^{n} (ET_{\mathrm{mod},i} - ET_{obs,i})^2}{n_j} \right]^{\frac{1}{2}} \tag{3-19}$$

$$RMSE_j(\%) = \frac{RMSE_j}{\overline{ET_{obs}}} \cdot 100 \tag{3-20}$$

$$RE_j = \frac{1}{n_j} \sum_{i=1}^{n} \left| \frac{ET_{\mathrm{mod},i} - ET_{obs,i}}{ET_{obs,i}} \right| \tag{3-21}$$

$$MAE_j = \frac{1}{n_j} \sum_{i=1}^{n} \left| ET_{\mathrm{mod},i} - ET_{obs,i} \right| \tag{3-22}$$

$$NSE_j = 1 - \frac{\sum_{i=1}^{n} \left(ET_{obs,i} - ET_{\mathrm{mod},i} \right)^2}{\sum_{i=1}^{n} \left(ET_{obs,i} - \overline{ET_{obs,i}} \right)^2} \tag{3-23}$$

$$d_j = 1 - \frac{\sum_{i=1}^{n} \left| ET_{\mathrm{mod},i} - ET_{obs,i} \right|^2}{\sum_{i=1}^{n} \left(\left| ET_{\mathrm{mod},i} - \overline{ET_{obs,i}} \right| + \left| ET_{obs,i} - \overline{ET_{obs,i}} \right| \right)^2} \quad (3\text{-}24)$$

$$r = \frac{Co\,\mathrm{var}iance(ET_{\mathrm{mod}}, ET_{obs})}{S.D.(ET_{\mathrm{mod}})S.D.(ET_{obs})} \quad (3\text{-}25)$$

Where "j" is the index of the month, "n_j" is the length of the monthly sample, "$ET_{mod,i}$" and "$ET_{obs,i}$" are respectively the monthly values of modeled and observed evapotranspiration, S.D. stands for standard deviation. The monthly and global errors have been further normalized respectively by the mean monthly value and the annual cumulative value of observed AET from EC.

The results reported in Table 3.1 highlights that all of the applied models allow for a good prediction of ET and that the threshold models compared to their corresponding single models perform however better, how confirmed by the low values of RE, RMSE and MAE.

Table 3.1 Global values of the goodness-of-fit indices for the proposed models.

Method	MAE (%)	RMSE (%)	RE (%)	NSE (-)	d (-)	r (-)
API (1.26)	0,878	0,463	27,769	0,842	0,848	0,989
AA	0,973	0,670	36,426	0,836	0,819	0,964
PM/AA	0,869	0,279	29,707	0,855	0,826	0,935
PM/API(1.26)	0,841	0,770	25,793	0,845	0,846	0,985
PM/API(1)	0,466	0,140	20,865	0,953	0,902	0,979

At monthly scale, the results illustrated in Figure 3.4 confirm that the threshold models (eq.3-17, 3-18) have lower errors than the basic empirical models (eq. 3-12) and (eq. 3-13), with an average value of the monthly RE and RMSE respectively of 25% and 20% for PM/API(1.26) and 29% and 20% for PM/AA against 28% and 21% for API(1.26) and 36% and 23% for AA. Differences in terms of performances are evident at the seasonal scale however, with the threshold method PM/API that appear to be the best performing especially during the winter periods. In the meantime, several authors, have proposed a re-examination of the value of Priestley-Taylor coefficient in order to improve the ET prediction. Although the value proposed by Mawdsley et al. 1985 set α

on 1.26, a moderate range of variability has been reported for such coefficient. McNaughton et al. 1973 suggested to use α=1.05, Davies et al. 1973 proposed a coefficient of 1.27 while Morton 1983 of 1.32 similar to 1.3177 proposed by Hobbins et al. 2001. De Bruin et al. 1979 further argued about a variation of α between 1.15 and 1.42. Given the uncertainty in the value to be assigned to the Priestly Taylor coefficient and in order to improve the simulation approach, a calibration of the value of the Priestley Taylor coefficient is also here proposed.

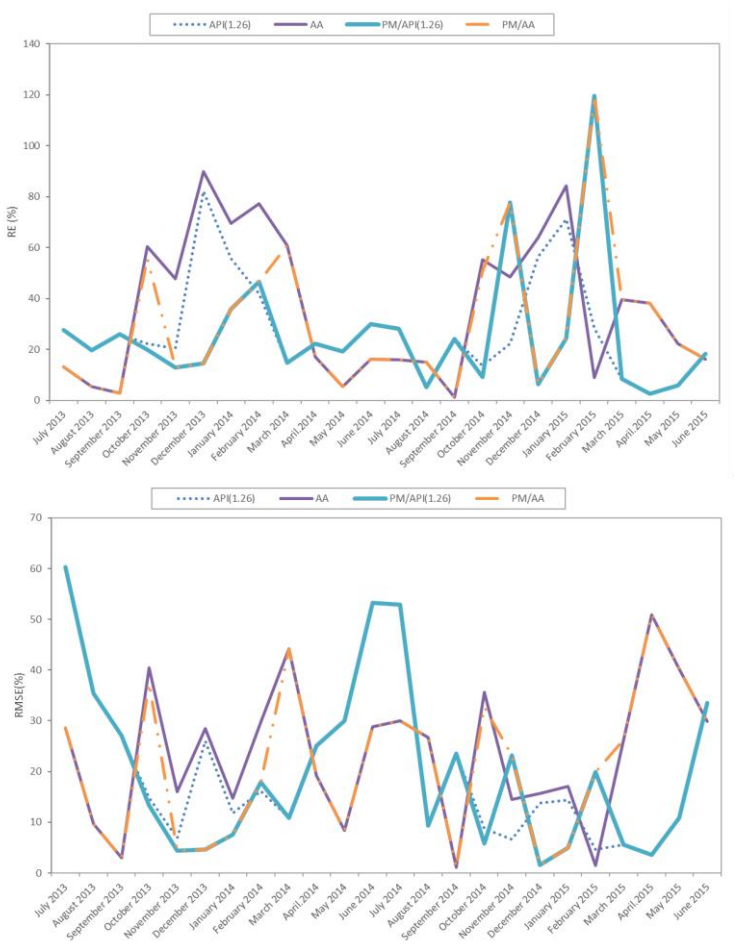

Figure 3.4 Monthly values of RE and RMSE for the proposed models.

The calibration is performed, at the monthly scale, with reference to the API method formulation eq. 3-13 from which the α coefficient is computed according to:

$$\alpha_{j,CAL} = \lambda \cdot AET_{obs,j} \cdot \frac{\Delta + \gamma}{\Delta} \cdot \frac{1}{R_n - G_{soil}} \tag{3-26}$$

where the AET losses is assumed to correspond to the observed eddy correlation values, where "j" is the index of the month.
The calibration particularly concerns only the periods when the system can be defined water-limited excluding those ones where energy limited conditions prevail, as during these periods the evapotranspiration is well described by the potential PET. The monthly calibration (Figure 3.5) show a value of α approximately equal to 1 for all the periods when water limited conditions occur.

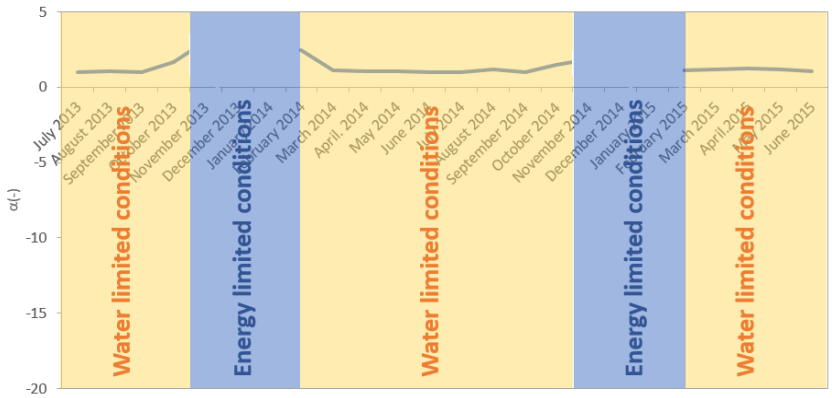

Figure 3.5 Calibrated monthly values of the Priestly Taylor coefficient α.

The accuracy of the ET values provided by the calibrated API models with a_{CAL}=1 has been verified and compared to those ones resulting from the non-calibrated approach using the above said goodness of fit indices (Figure 3.6). The monthly indices computed for the PM/API_{CAL} confirm that the process of calibration involving the adjusted coefficient α allows to a further improvement of the PM/API model with an average monthly RMSE of 11% compared to 20% of the threshold

model PM/API and a minimum value of 0.06 % against 1.53%. At the global scale (Table 3.1), the indices for PM/API$_{CAL}$ model appear overall the best performing in the end, the calibration of the Priestly-Taylor coefficient appears to be a critical issue in the improvement of model performances.

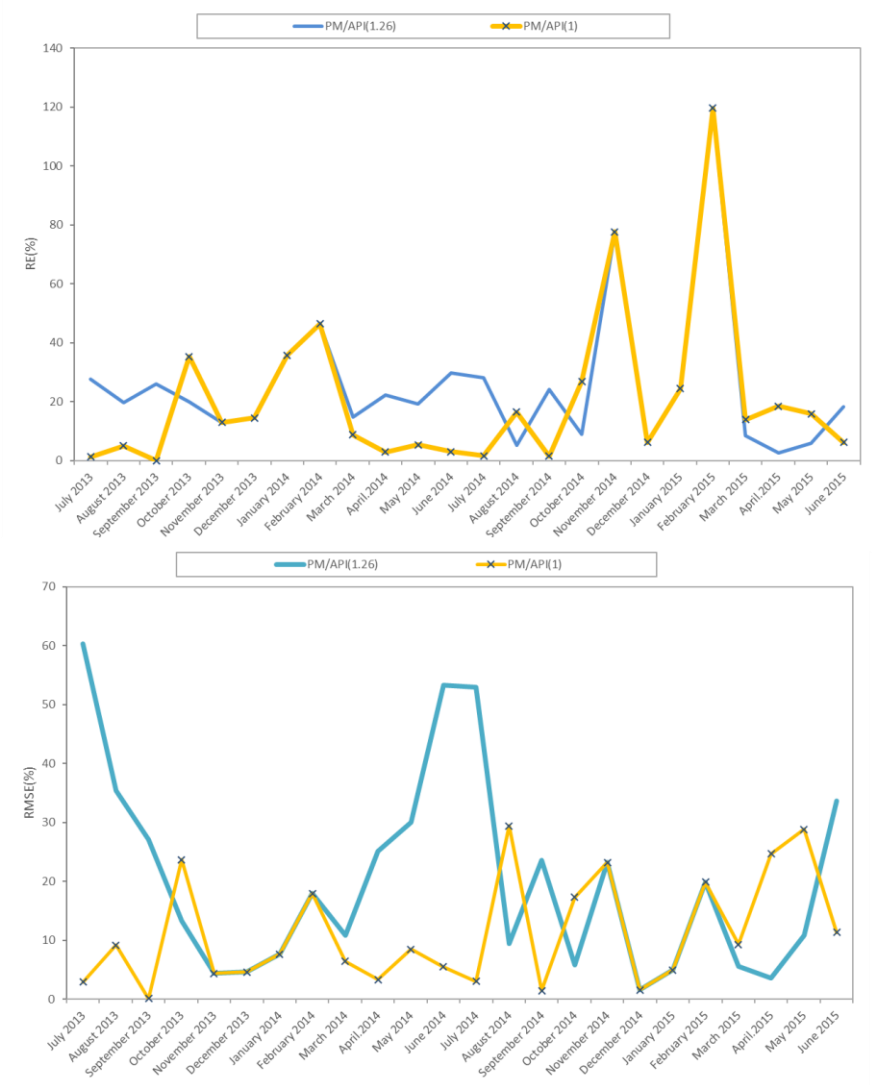

Figure 3.6 Monthly values of RE and RMSE for PM/API(1.26) and PM/API(1).

4 DAILY SCALE WATER BALANCE MODEL

The proposed threshold methodology for an accurate simulation of the actual evapotranspiration loss simply based on meteorological data can be used in retention models for the prediction of green roof retention performances. Until now, questions remain to be answered regarding the relationship between the complexity level of a GR retention model and its performances. Three conceptual models, of increasing complexity in descriptive details, are calibrated and compared to experimental data of runoff recorded over three years from an experimental site located at Bernkastel-Kues, Germany. The case study has enable to determine if higher complexity level leads to better model performance, and therefore to a better prediction of observed hydrological processes. The proposed approaches consist of daily scale hydrological models, based on water balance equations, where the main processes and variables accounted for are the precipitation input, the evapotranspiration losses and the maximum water storage capacity. Model detail increase is achieved moving from a basic approach using potential evapotranspiration and constant storage threshold to an intermediate complexity approach using actual evapotranspiration and a constant storage threshold to an advanced approach using actual evapotranspiration and a variable storage threshold. Potential evapotranspiration has been estimated with the use of the Penman–Monteith equation while actual evapotranspiration with the proposed threshold combined approach. The maximum water holding in the basic and intermediate approach is the only model parameter to be calibrated for hydrological simulation, it depends on substrate layer material properties and represents a constant physical property. In the advanced approach the storage threshold represents a process and it is a variable evolving over time. The model estimates of runoff have been compared with observed runoff data for the entire duration of the study period using two fit indices namely the average of absolute percentage errors (AAPE) and root-mean-square errors (RMSE). The main findings confirm on one side the role played by evapotranspiration modeling and, on the other side, the good accuracy

achieved, in a minimal calibration requirement approach, through the modeling of basic and elemental processes.

4.1 THE STUDY SITE AND DATA

The green roof in analysis is an extensive green roof with an area of 22 m^2 and a slope of about 5°, it is located in Bernkastel-Kues (49° 55' 11" N, 7° 4' 33" E, 145 m above sea level), Rhineland-Palatinate, western part of Germany (Figure 4.1).

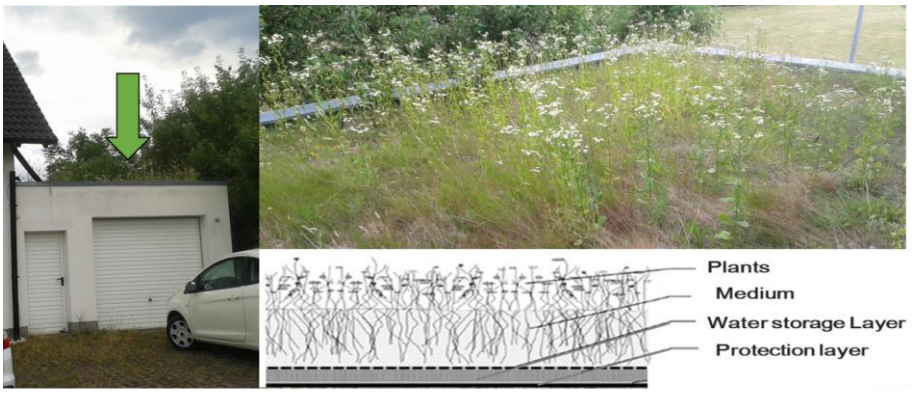

Figure 4.1 Green roof location and composition.

It is made up of three layers: the vegetation layer (spontaneous vegetation), the growing medium (mineral substrate) consisting of a mixture of lava, pumice and humus and a water storage/protective layer (retention Hydrotex membrane). The climate regime is typically oceanic. Average precipitation is about 700–800 mm/year and it is approximately uniformly distributed during the year. Temperature exhibits instead a typical seasonal pattern, with highest monthly mean values during the summer season of about 18 °C and annual average temperature of 9,4° (Figure 4.2).

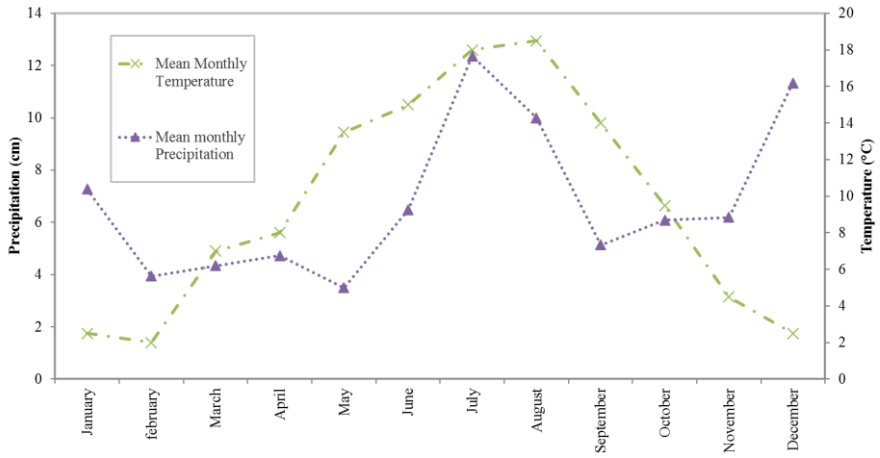

Figure 4.2 Patterns of mean monthly rain and temperature for the study site.

Meteorological data are precipitation recorded at the experimental site and wind speed, air temperature, relative humidity, global radiation collected at the nearest available meteorological station, Bernkastel (AgrarMeteorologie, Rheinland-Pfalz, 2017). Runoff measurements have been recorded, with a daily time step, from March 2004 to May 2007, but some missing data appear during the monitoring period, preventing the total period of observation to be used for modeling purposes. Generally, no significant runoff has occurred, due to freezing of the water, between late December and late March. For this reason, the winter period has not been considered in the simulation approach.

4.2 THE CONCEPTUAL MODELS

The aim of the reported research is an analysis of the impact of the complexity in the description of variables and processes of a green roof hydrological model on the relative parameterization and accuracy, with a focus on the retention capacity of the green infrastructure. To this purpose a daily scale conceptual hydrological model is applied, based on water balance equations whose main input variables are the precipitation, the evapotranspiration loss and the maximum water storage capacity, here called storage threshold (Mobilia et al. 2017). The model is used

with three different settings (mod A, mod B and mod C), characterized by an increasing complexity in the description of the involved variables and processes (Table 4.1).

Table 4.1 Models settings for different model complexity level. Mod A represents the basic approach. Mod B represents the intermediate approach. Mod C represents the advanced approach.

Model	ET	W_{max}
Mod A	PET	Constant
Mod B	AET	Constant
Mod C	AET	Variable

The three settings correspond to: a basic approach based on the use of potential evapotranspiration and a constant storage threshold (mod A); an intermediate approach where actual evapotranspiration and a constant storage threshold are accounted (mod B); an advanced approach where actual evapotranspiration and a variable maximum water holding depth are used (mod C). The three conceptual retention models, of different complexity, are calibrated using the values of runoff measured from the studied infrastructure.

4.2.1 The governing equations

The water balance equations used to simulate the runoff production "R", common to all of the three model settings, are:

$$\begin{cases} V_t = V_{t-1} + P_t - ET_t \le W_{\max} \rightarrow\rightarrow R_t = 0 \\ V_t = V_{t-1} + P_t - ET_t > W_{\max} \rightarrow\rightarrow R_t = V_t - W_{\max} = V_{t-1} + P_t - ET_t - W_{\max} \end{cases} \quad (4\text{-}1)$$

where "t" is the daily time index, "V" the green roof water depth, "P" the observed precipitation, "ET" the modelled evapotranspiration loss, "W_{max}" the maximum water holding depth or storage threshold.
In the basic approach, ET loss is assumed to be set on the potential evapotranspiration (PET) and a constant storage threshold is also considered. The governing equations become:

$$\begin{cases} V_t = V_{t-1} + P_t - PET_t \le W_{\max} \rightarrow\rightarrow R_t = 0 \\ V_t = V_{t-1} + P_t - PET_t > W_{\max} \rightarrow\rightarrow R_t = V_t - W_{\max} = V_{t-1} + P_t - PET_t - W_{\max} \end{cases} \quad (4\text{-}2)$$

where the term "ET_t" is replaced by "PET_t". As PET is rapidly computed from meteorological observation, W_{max} represents the only model parameter to be calibrated.
Potential evapotranspiration represents obviously an ideal process, but for a better model performance, the actual evapotranspiration process should be modeled (Mobilia et al. 2016b). Actual evapotranspiration AET modeling generally requires soil moisture, soil and vegetation properties data, but in order to keep to a minimum the number of needed information, an approach simply based on meteorological variables and on the concept of non-potential Priestley-Taylor model (Mawdsley et al. 1985), is in the following used. In the intermediate complexity approach, ET loss is then assumed to be set on the non-potential Priestley-Taylor evapotranspiration (AET) and a constant storage threshold is accounted for. The governing equations are represented by eq. 4-3 where the term "ET_t" is replaced by "AET_t":

$$\begin{cases} V_t = V_{t-1} + P_t - AET_t \le W_{\max} \rightarrow\rightarrow R_t = 0 \\ V_t = V_{t-1} + P_t - AET_t > W_{\max} \rightarrow\rightarrow R_t = V_t - W_{\max} = V_{t-1} + P_t - AET_t - W_{\max} \end{cases} \quad (4\text{-}3)$$

As in the case of the basic model, also in this case W_{max} represents the only parameter to be calibrated for hydrological simulation. Considered as the amount of water stored between the permanent wilting point and the field capacity, the maximum water holding capacity W_{max} depends on substrate layer material properties and represents a constant physical threshold. The constant physical limit could be however called into discussion, if it is considered that due soil heterogeneity runoff can occur even before the actual capacity is reached and that vegetation provides some additional moisture storage capacity to be accounted for (Poë et al. 2015). W_{max} is more likely to represents a process rather than a physical property and, as exhaustively discussed in Mobilia et al. (2017), a strong correlation is found between the maximum water holding depth on day "t" and the water depth on day "t − 1" as follows:

$$W_{\max,t} \approx V_{t-1} \quad (4\text{-}4)$$

The correlation results from the eq. 4-3, where the GR runoff production is computed at the daily scale as:

$$R_{t,\mathrm{mod}} = V_t - W_{\max} = V_{t-1} + P_t - AET_t - W_{\max} \quad (4\text{-}5)$$

If Eq. 4-5 is reversed, a calculation for W_{max} could be obtained:

$$W_{\max,t} = V_t - R_{t,\mathrm{mod}} = V_{t-1} + P_t - AET_t - R_{t.\mathrm{mod}} \quad (4\text{-}6)$$

Assuming further that for each day t, the modeled runoff (R_{mod}) is equal to the observed one (R_{obs}), a calibrated daily time series for $W_{max,t}$ can be obtained:

$$W_{\max,t} = V_{t-1} + P_t - AET_t - R_{t.obs} \quad (4\text{-}7)$$

Plots for V_{t-1} and $W_{max,t}$ are provided in Figure 4.3, as a ratio of the green roof depth.

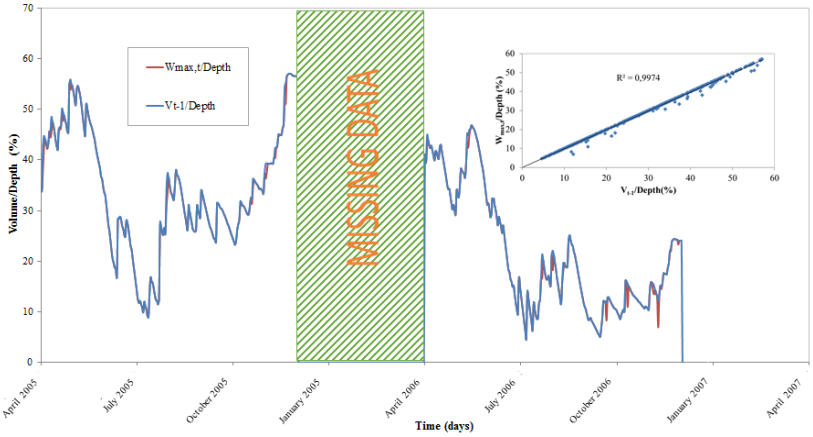

Figure 4.3 Water depth (V) and water holding capacity (W) daily scale patterns as a ratio to soil depth. Actual evapotranspiration losses are computed by the API Method. Overlapped, in the upper right corner, the scatter plot for the two considered variables and the relevant Person correlation coefficient.

Illustration refers to AET computed by the threshold method PM/API(1.26). Considering the above discussed soil physical properties and also probably to balance the a-priori calculation for AET losses, W_{max} becomes a variable for the GR hydrological model itself. Its temporal pattern is nearly coincidental with the water depth pattern. Retention

capacities approach a maximum value of about 55% during the rainy and cold seasons. They decline to about 10% during a short summer period, where the typical large amount of rainfall (high API values in Figure 4.4) is contrasted by high evapotranspiration losses. In 2006, the retention capacity appears moderate also for the autumn season because of enhanced evapotranspiration losses compared to the same period of the previous year (Figure 4.5). Beyond the visual patterns coincidence, the coefficient of correlation between $W_{max,t}$ and V_{t-1} is extremely high (r^2 = 0.99). This result confirms the strong correlation the water holding capacity W_{max} and the stored depth V (eq. 4-4). Thus eq. 4-5 becomes:

$$R_{t,\mathrm{mod}} = V_{t-1} + P_t - AET_t - W_{\max,t} \approx V_{t-1} + P_t - AET_t - V_{t-1} = P_t - AET_t \quad (4\text{-}8)$$

According to such discussion, in the advanced approach, ET loss is assumed to be set on the actual evapotranspiration (AET) and a variable storage threshold is accounted for. "$W_{max,t}$" and "AET_t" respectively replace "W_{max}" and "ET_t" in eq. 4-1 and the water balance equations are:

$$\begin{cases} V_t = V_{t-1} + P_t - AET_t \le W_{\max,t} \rightarrow\rightarrow R_t = 0 \\ V_t = V_{t-1} + P_t - AET_t > W_{\max,t} \rightarrow\rightarrow R_t = V_t - W_{\max,t} = V_{t-1} + P_t - AET_t - W_{\max,t} \end{cases} \quad (4\text{-}9)$$

where the second equation, according to eq. 4-4, can be rewritten as:

$$R_t = P_t - AET_t \quad (4\text{-}10)$$

The runoff production can then be modeled at daily time steps as the result of a surface water balance between input and output fluxes. AET is simulated with the use of indirect methods (empirical relationships) and thus the choice of the particular AET approach would be crucial for model uncertainty. To further consider the ability of the evapotranspiration process to restore the green roof water retention capacity during prolonged dry periods (Stovin et al. 2015), a cumulative soil water balance index (I_{SWB}) over the previous four days is considered in the mod C:

$$I_{SWB} = \sum_{i=1}^{4} P_{t-1} - AET_{t-1} \quad (4\text{-}11)$$

If the index produces a negative value on the day "*i*", the GR retention capacity is assumed to be completely restored. No runoff will be produced on that day, if its actual rainfall does not exceed the GR retention capacity. The four-day interval in Eq. 4-11 has been calibrated on the basis of available monitoring data about dry periods, which represent a negligible set of occurrences (about 3% of total cases), perhaps due to the particular uniform precipitation regime of the studied area. Eq. 4-11 has been applied regardless of the relationship used for actual evapotranspiration modeling. Model details are actually more complex, as more processes are schematized, but contrarily to what expected, model parameterization is lessened, as no parameter has to be calibrated for simulation purposes because GR response to rainfall is simply computed as the difference between observed precipitation and modeled actual evapotranspiration. The three models (mod A,B, C) require an initial value for the depth of water V, which is assumed to correspond to the Antecedent Precipitation Index value, considered as a proxy of soil moisture conditions (Ali et al. 1987). The same index would be used, as illustrated in the previous chapter, to compute AET losses.

4.2.2 PET and AET assessment

In contrast to most common frameworks, in the proposed approach evapotranspiration losses are modeled a-priori, as a function of meteorological parameters, independently of explicit moisture content. Potential evapotranspiration has been assessed with the use of the Penman–Monteith (1948) (eq. 3-7):

$$PET_{P,M} = \frac{1}{\lambda}\left[\frac{\Delta}{\Delta+\gamma}\left(R_n - G_{soil}\right)\right] + \left[\frac{\gamma}{\gamma+\Delta}E_A\right] \qquad (3\text{-}7)$$

For actual evapotranspiration, the threshold combined approach, proposed in the eq. 3-17, 3-18, has been used. The method combines the Potential evapotranspiration suggested by Penman-Montheith and the Antecedent Precipitation Index formulation for AET assessment with P-T coefficient equal to 1.26:

$$if \quad NR < NR_T \rightarrow\rightarrow PET_{P,M} = \frac{1}{\lambda}\left[\frac{\Delta}{\Delta+\gamma}\left(R_n - G_{soil}\right)\right] + \left[\frac{\gamma}{\gamma+\Delta}E_A\right] \qquad (3\text{-}17)$$

$$if \quad NR > NR_T \rightarrow\rightarrow AET_{API} = 0.408\alpha\left[\frac{\Delta}{\Delta+\gamma}\left(R_n - G_{soil}\right)\right] \qquad (3\text{-}18)$$

The threshold method PM/$API_{1.26}$ has been has been preferred over the PM/AA method because it appears to be the best performing. According to eq.3-17,3-18, the temporal switch between the two models occurs for a detected value of net radiation marking the transition from energy limited conditions to water limited conditions (NR_T). The investigation of NR_T has been possible for the study site of Rollesbroich because eddy covariance measurements of evapotranspiration are available. These values of ET fluxes have been compared to the modelled ones in order to identify the threshold. For the study case of Bernkastel-Kues, no data from EC towers were available so there was no possibility to calibrate the NR_T threshold. However, the period when one or the other condition occurs, has been unequivocally characterized by Budiko aridity index. In fact, from March to September when I<1, the system can be defined water-limited and in the other months of the year, the system is energy limited. This finding, assumed valid for Rollesbroich can be extended to Bernkastel-Kues because both of them are located in an oceanic climate region with similar wheatear conditions. Similar considerations can't be applied to the calibrated Priestly-Taylor advection coefficient used in the threshold approach PM/API_{CAL}, combining PM and API with $\alpha_{,CAL}$. The reason is that the two case studies have different vegetation covers which are species of meadow foxtail, perennial rye grass, rough meadow grass and common sorrel for the site of Rollesbroich and sedum with spontaneous vegetation for the site of Bernkastel-Kues as well as the grassland area of Rollesbroich is a natural site while the green roof is made up of synthetic substrates with a thin natural layer on the top. Finally actual evapotranspiration for this site has been described by a PM/$API_{(1.26)}$ approach using $AET_{API,1.26}$ from April to October and $PET_{P,M}$ in November and December. Provided data continuity and reliability, the period chosen for the simulations ranges from April 2005 to December 2006. Main meteorological variables used for AET assessment are illustrated in Figure 4.4. AET and PET monthly

patterns have been reported in Figure 4.5 for the full period of observation (from April 2005 to December 2006).

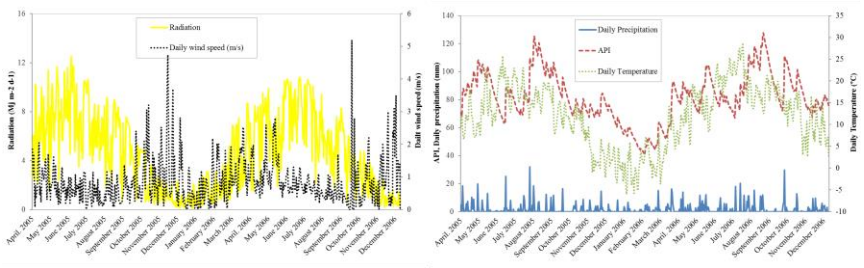

Figure 4.4 Precipitation, antecedent precipitation index (API), air temperature, wind speed, radiation daily pattern for the experimental site.

They are featured by a sinusoidal pattern, with the maximum and minimum values occurring during the summer and autumn period, respectively.

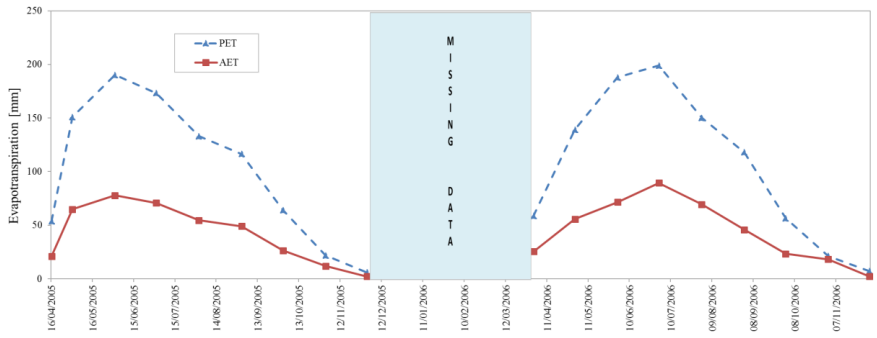

Figure 4.5 Monthly patterns of PET and AET during the period of observation.

4.2.3 Models evaluation

To quantitatively judge the ability of the approaches to reproduce the observed runoff, two fit indices, average of absolute percentage errors (AAPE), root-mean-square errors (RMSE) and the percentage RMSE have been calculated:

$$RMSE_j = \left[\frac{\sum_{i=1}^{n} (R_{\mathrm{mod},i} - R_{obs,i})^2}{n_j} \right]^{\frac{1}{2}} \tag{3-19}$$

$$RMSE_j(\%) = \frac{RMSE_j}{\overline{R_{obs}}} \cdot 100 \tag{3-20}$$

$$AAPE_j = \frac{1}{n_j} \sum_{i=1}^{n} \left| \frac{R_{\mathrm{mod},i} - R_{obs,i}}{R_{obs,i}} \right| \tag{4-12}$$

with "n" the number of points of discontinuity of the cumulated runoff distribution (runoff events occurrences) where the fit is evaluated, R_{mod} is the modeled runoff, R_{obs} the observed runoff and $\overline{R_{obs}}$ the total average observed runoff.

4.3 RESULTS

In the case of mod A and mod B settings, evapotranspiration losses, respectively potential and actual fluxes, represent functions of meteorological variables and can be assesses a-priori and used as a climate forcing for the GR model, not dependent on the stored water depth V. Mod A and mod B hydrological simulation relies thus only on W_{max} calibration. In the case of mod C, as previously discussed W_{max} is assumed to varies during the simulation. This circumstance, as discussed, causes a simplification of the water balance equation, and the hydrological simulation does not require a calibration phase, with runoff production modeled as by eq. 4-10. In the case of mod A and mod B, W_{max} calibration is achieved assuming that total modelled runoff equals total observed runoff, for each period of simulation. Results are illustrated in Figure 4.6 and Figure 4.7. At a first visual inspection, in the case of mod A and mod B a number of runoff events are not modeled and in most cases an overestimation occurs. Mod C appears the best performing among the three different considered model settings.

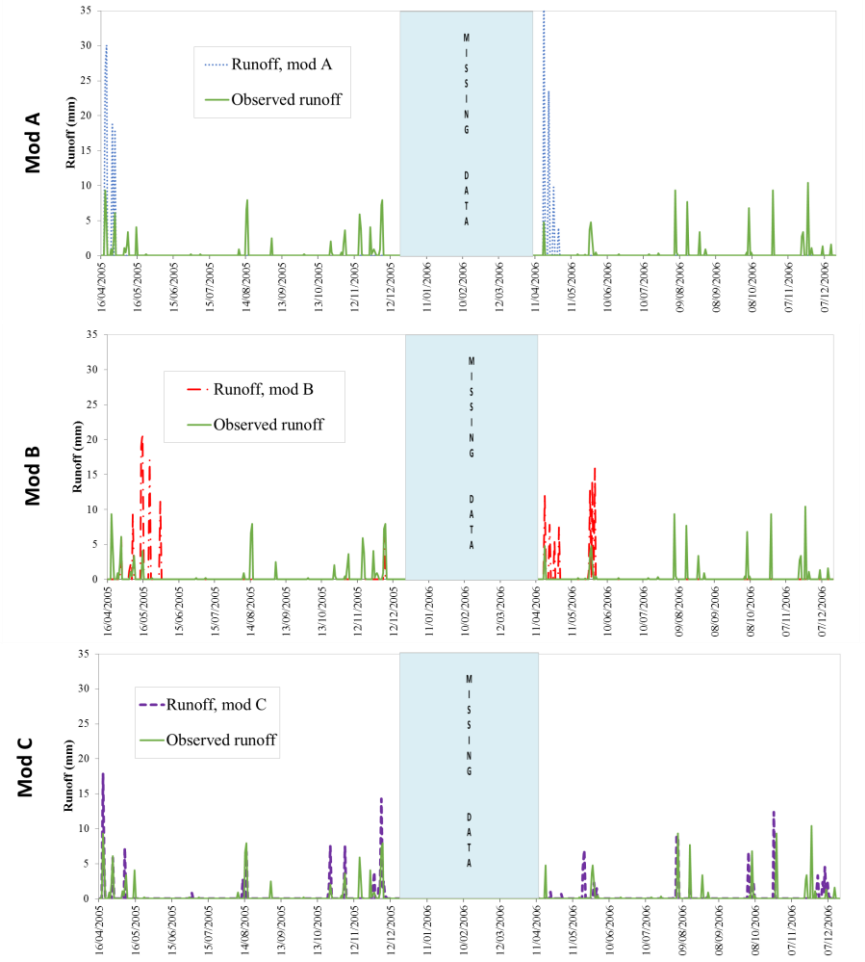

Figure 4.6 Comparison between modelled and observed runoff time series for the different approaches.

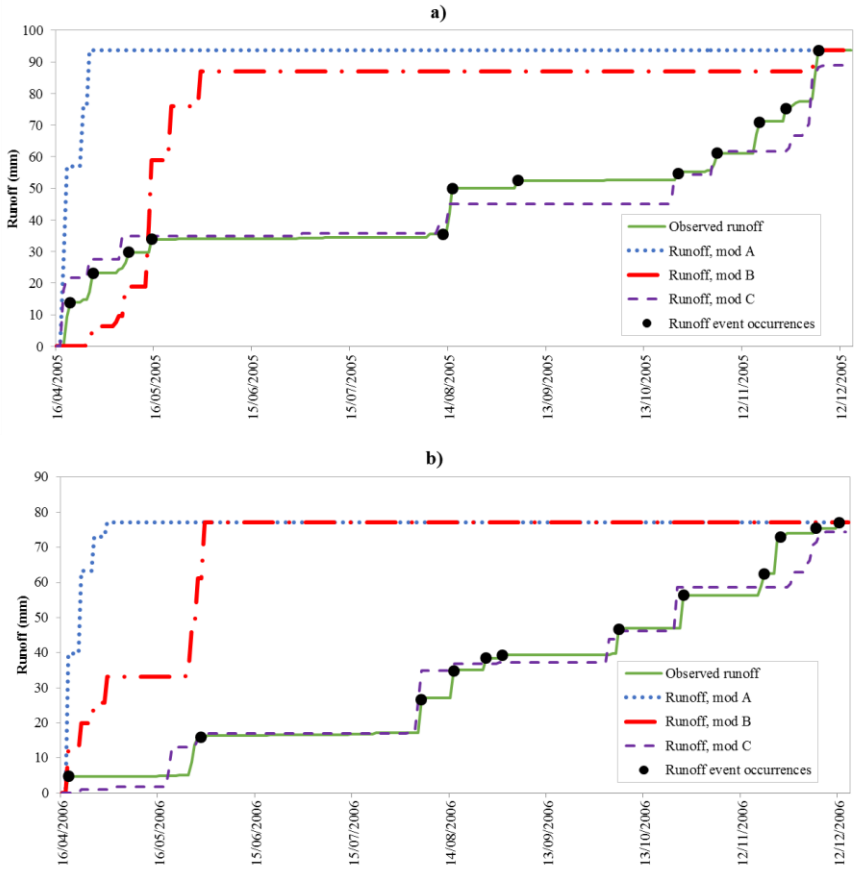

Figure 4.7 Comparison between cumulated observed runoff from the studied green roof and cumulated runoff modelled using the three approaches with increasing level of complexity. a) simulated period: 2005. b) simulated period: 2006.

The results of the analysis of fitting carried out using the indices of model performances (eq. 3-19, 3-20, 4-12) are illustrated in Table 4.2. Although a calibration process has been performed and cumulative simulated runoff equals the observed one, mod A, regardless for the modeled period, is characterized by the largest errors, with RMSE (%) above 14% (in 2005), of average observed runoff, and AAPE approaching 126% (in 2005). Cumulative modeled runoff pattern significantly differs from the observed one and it is practically not at all affected from rainfall occurrences, as the cumulative runoff, for the total

period of observation, is approached in the earlier period of the simulation (Figure 4.7).

Table 4.2 Values of the RMSE and AAPE for the different approaches.

Year	Method	R_{mod} (mm)	RMSE (mm)	RMSE (%)	AAPE (%)
2005	mod A	93.6	13.1	14	126.3
Robs (mm)=	mod B	93.6	2.67	2.85	58.96
93.6	mod C	89.0	0.66	0.7	14.09
2006	mod A	77.0	9.8	12.7	146.5
Robs (mm)=	mod B	77.0	3.02	3.92	89.87
77.0	mod C	74.4	0.55	0.71	16.14

Moving from potential to actual evapotranspiration losses increases model accuracy. RMSE (%) and AAPE values for mod B are indeed lower than in the case of mod A, respectively equal to about 4% and 89% (in 2006), but cumulative simulated runoff pattern is still significantly different from the observed one. A larger sensitivity to rainfall occurrences is detected however compared to mod A (Figure 4.7). Nevertheless the lack of a calibration process, mod C appears to be the best performing method also on a quantitative point of view. RMSE (%) and AAPE indices approach the lowest values of about 0.7% (for both years) and 14% for 2005 and 16% for 2006 respectively. Furthermore, cumulated modeled pattern is very close to the observed one and total cumulated runoff only differs of about 5% from observed one (Figure 4.7).
Calibrated values for the maximum water holding capacities for mod A and mod B are illustrated in Table 4.3 as percentage of total soil depth.

Table 4.3 Calibrated (mod A and mod B) and average (mod C) maximum water holding capacities as percentage of total soil depth.

Year	Mod A (%)	Mod B (%)
2005	26.6	45.4
2006	24.3	38.9

For each method, the maximum water holding capacity in 2006 is lower than in 2005. This is likely due to the reduced value of total annual precipitation occurred in 2006, 367 mm, compared to the total annual precipitation of about 424 occurred in 2005, for a percentage reduction

of about 15%. Differences in total precipitation also causes differences in cumulated runoff, about 77 mm, occurred during 2006 compared to the 93 mm observed during the year 2005, for a percentage reduction of about 20%. Evapotranspiration total amount, for both potential and actual rate, are indeed similar for the two monitored periods. A moderate difference is detected in particular for the actual evapotranspiration larger (of about 6%) in 2005.

4.3.1 Impact of maximum water holding capacity threshold

In the case of mod A and mod B the hydrological simulations require a calibration for the water holding capacity threshold W_{max}. For such approaches it would be important, especially in context where experimental data are not available for calibration, to study the impact of the choice for a particular value of W_{max} on model accuracy.
To this purpose, a sensitivity analysis has been performed, in the case of mod A and mod B, to measure model performances through RMSE and AAPE statistical indices. Results are illustrated in Figure 4.8. For both cases, RMSE and AAPE illustrate how, as a results of the calibration, errors monotonically increase for W_{max} values lower than the calibrated threshold. In the case of mod A, for a given W_{max} value, errors occurring in 2005 and 2006 are different probably because the different cumulated runoff rates (Table 4.2) for the two periods are not balanced by instead very similar potential evapotranspiration cumulate loss for the same time intervals. The largest errors are indeed predicted for the 2005 period, characterized by the largest potential evapotranspiration loss. On the contrary, in the case of mod B, errors occurring in 2005 and 2006 are almost similar, probably because the different cumulated runoff rates (Table 4.2) for the two periods are balanced by a different actual evapotranspiration cumulate loss for the same time intervals. Model errors associated to mod B are, compared to mod A, larger, for W_{max} different from the calibrated threshold. Such circumstance indicates a larger sensitivity of mod B to uncalibrated W_{max} compared to what occur for mod A. Lower evapotranspiration losses (by actual process as formulated in mod B) correspond to lower rainwater storage availability and thus, for a given W_{max}, to larger runoff rates and larger overestimation (Figure 4.6).

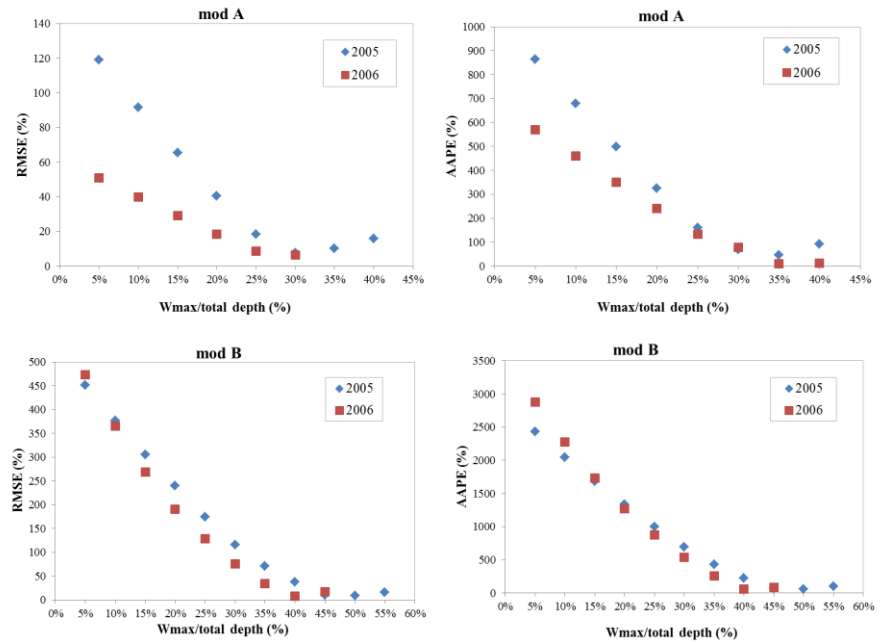

Figure 4.8 Impact of water holding capacity (as a percentage of soil total depth) for mod A (upper panel) and mod B (lower panel).

5 EXPERIMENTAL GREEN ROOFS AT UNISA CAMPUS

Once the models for predicting the hydrological green roof performances have been proposed, it should be taken into account that the stormwater response of a green roof is indeed highly impacted by the climate conditions. The green roof infrastructures are mainly implemented in cold region where their effectiveness is well documented in literature (Zimmer et al. 1997, Mentens et al. 2006, Villarreal et al. 2005). The use of green roofs technology in Mediterranean areas is more limited. The specific climate probably represents a challenge for GRs implementation because it is characterized by long dry periods without rain, that occur mainly during summer periods and that could affect the plants growth of the vegetation layer and consequently the performances of the eco-roof. Even the experimental sites in Mediterranean climate are scarce (Olivieri et al. 2013, Lazzarin et al. 2005, Fioretti et al. 2010) and only a few of them analyze the hydrological behavior of the green roof (Palla et al. 2011, Bonoli et al. 2013, Carbone et al. 2014, Mobilia et al. 2014), consequently few studies about their performances in terms of stormwater management exist. For a better understanding of the behavior of GRs with regard to the climate condition, in particular the Mediterranean one, and the construction type of the roof, two green roof test beds (GR1, GR2) have been located in the campus of University of Salerno and their hydrological performances have been monitored.

5.1 SITE DESCRIPTION

In January 2017 two green roof test beds (Figure 5.1) were installed at the Laboratory of Environmental and Maritime Hydraulic, Department of Civil Engineering of the University of Salerno UNISA (40.770425, 14.789427 altitude of 282 meter) (Mobilia et al. 2017a). UNISA is located in Fisciano, (Southern Italy) and it is featured by a Mediterranean

climate. The two experimental roofs are of extensive type with short-stemmed plants. They differ for the drainage layer setting. They are placed on bench of stainless steel with a surface of 2.5 m^2 (1 x 2.5 m) and a double pitch slope of 1%. All over the walls of the bed, three lines of holes at the height of 0, 2.5 and 5 cm from the bottom of the table, have been planned to drain rainwater to the outlet. The holes have a diameter of 1 cm and they are 8 cm away from each other.

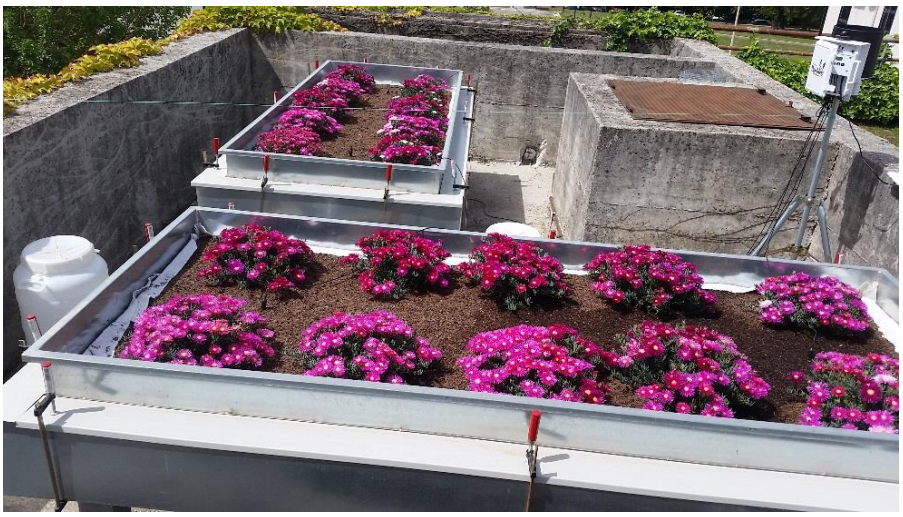

Figure 5.1 Green roofs Experimental site in Salerno.

From the holes, runoff flows in underlying 8 cm wide open channels set up all around the perimeter of the bench. The open channels are equipped with L-section top lids fixed by metallic clamps and removable for periodic inspection. From the channel the flow is collected into a circular outlet section with a diameter of 10 cm. From this section, a pipe channels runoff into a tank. The tank is manually emptied through a water tap every time the maximum capacity of 50 liters is reached. In the Figure 5.2 some details about plans and sections of the benches are provided. The tank weight is continuously monitored to measure the stored water and quantify the amount of runoff during storm events. The two green roofs include three layers: the vegetation layer made up of succulent plants typical of Mediterranean climate (Mesembryanthemum) planted at medium density (4 plants per square meter) in order to provide adequate coverage of the growing substrate, 10 cm deep support

substrate with peat and zeolite and total porosity of 94%, finally the water storage layer with a depth of 5 cm. A non-woven filter mat is interposed between the substrate and the storage layer. For one of the test bed (GR1), the drainage layer is made up of expanded clay with diameters from 8 to 20 mm and it ensures a reserve of 32 liter/m2.

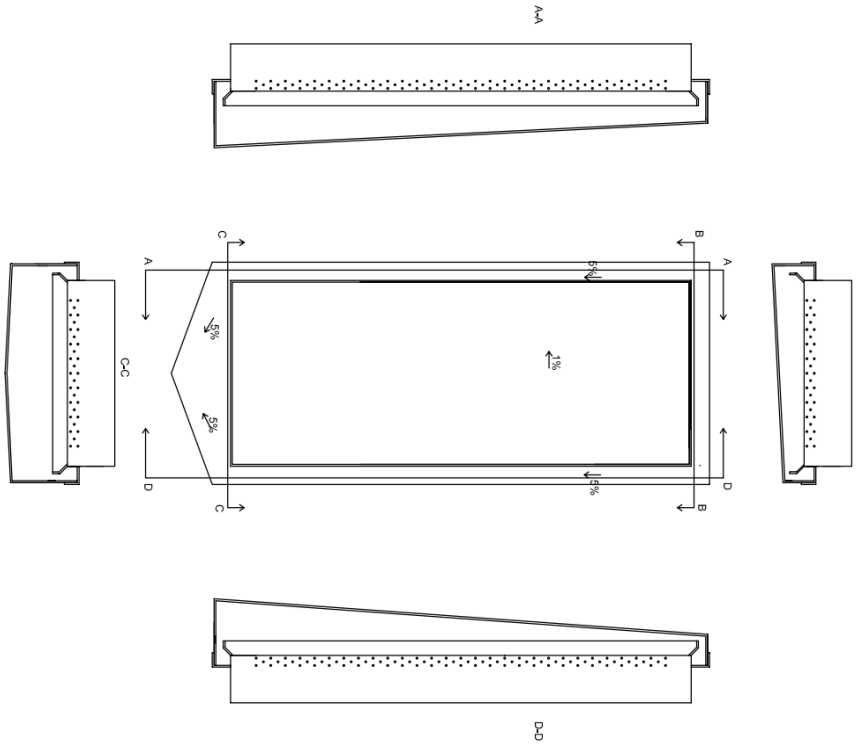

Figure 5.2 Plans and sections of the benches.

For the second installation (GR2), the drainage layer is made up of a commercial drainage panel MODì filled with expanded clay (Figure 5.3). Each panel of 58x58 cm is supplied in 13 trays filled with clay acting as water reservoirs and providing, empty, according to the manufacturer's specification, a reserve of 14 liters/m^2.

Figure 5.3 Drainage layer with clay and commercial panel filled with clay.

The site is fully and continuously (5 minutes resolution) monitored with a meteorological station including a tipping bucket type raingauge for rain with the minimum recordable depth of 0.25 mm rainfall, a thermohygrometer for air humidity and temperature, a pyranometer for solar radiation, 4 soil moisture sensors, 2 for each test bed located upstream and downstream at a distance of 10 cm from the shorted sides (Figure 5.4).

Figure 5.4 Weather monitoring systems.

5.2 IRRIGATION SYSTEM

Green roofs have become a widely used tool for stormwater retention mainly in cold and wet regions where the knowledge about their function and performances is in an advanced state while in Mediterranean climate, the lack of experimental sites concerning the hydrological behavior of GR infrastructures makes the investigation of these aspects difficult.
The reason can be searched in site conditions because for successful establishment and long-lasting vegetation, climate and weather factor like the occurrence of periods of drought and the pattern of annual precipitation are crucial (FLL 2002). The oceanic climate generally is characterized by warm (but not hot) summers and cool (but not cold) winters with evenly distributed rain throughout the year and no significant precipitation difference between seasons. Mediterranean climate is characterized by warm or hot, dry summers and mild or cool, wet winters and at least three times as much rain falls in the wettest month of winter as in the driest month of summer (Koeppen 1931, FAO/SDRN 2017). As an example, these statements are supported by the seasonal pattern of rain for Salerno (located in Southern Italy with a typical Mediterranean climate) and Trier (Western Germany with a typical oceanic Climate) shown in the following figure. (Figure 5.5)

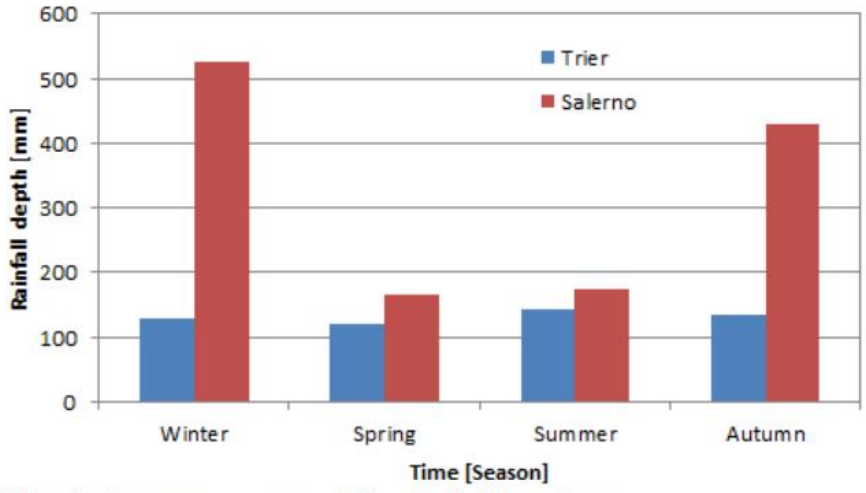

Figure 5.5 Seasonal patterns of rain for Salerno and Trier.

In light of this, the oceanic climate appears to be the perfect place for the placement of green roofs but with some precautions, the technique can be exported also in Mediterranean climate. The precautions in case of experimental test-beds located in the campus of UNISA, have been the use of succulent plants with great drought tolerance and of an irrigation system to be turned on during drier months of the year in order to provide a minimal irrigation to the vegetation.
Given such consideration, the experimental site has also been equipped with an irrigation system (Figure 5.6). The irrigation system has been powered by 9V battery. Is includes 10 drip nozzles for watering individually each plant and directly to its base. The nozzles are connected with a 5-cm-diameter trickle hose forming a closed network. The nozzles are anchored to the vegetation support layer of the roof through ground spikes. A water timer controls the distribution and regulation of the volume of water required for the simulation and it starts and stops watering automatically. The irrigation system borrows water from the distribution network of the campus.

Figure 5.6 Irrigation system for GR1 and GR2.

The system allows to satisfy the irrigation water need (IN) of the plants during the driest months of the year. If the water need is provided entirely by rainfall (P_e), IN is zero, if no precipitation falls during the considered moth, IN equals crop evapotranspiration (ET_{crop}). In other case, the water need is supplied partly by irrigation and partly by rainfall, in such cases IN is the difference between ET_{crop} and P_e. To sum up:

$$\begin{cases} if \quad P_e > ET_{crop} : IN = 0 \\ if \quad P_e = 0 : IN = ET_{crop} \\ if \quad P_e < ET_{crop} : IN = ET_{crop} - P_e \end{cases} \tag{5-1}$$

P_e is the effective rainfall and it represents the amount of total precipitation (P) actually stored in the soil and available for consumptive use of the plants. According to Brouwer et al. 1986, P_e (mm/month) can be described by the following formula:

$$P_e = 0.8P - 25 \quad if \quad P > 75 \frac{mm}{month} \tag{5-2}$$

$$P_e = 0.6P - 10 \quad if \quad P < 75 \frac{mm}{month}$$

P_e depends on the monthly value of precipitation which, for the study site, can be derived by the Figure 5.7 Average monthly precipitation is about 821 mm/year (Climate-data 2017), the drier month is July with 25 mm and the wetter is November with 120 mm.

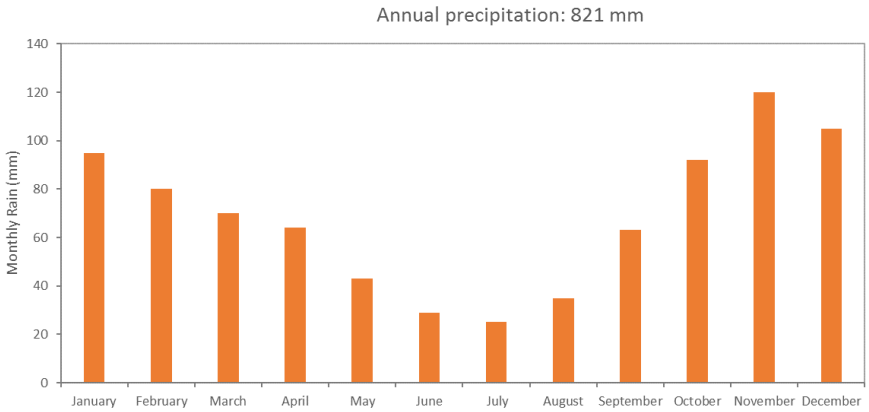

Figure 5.7 Monthly values of rain for the experimental site.

Crop evapotranspiration is given by:

$$ET_{crop} = K_L \cdot ET_0 \tag{5-3}$$

Where ET_0 (mm/day) is the reference crop evapotranspiration estimated using the Blaney-Criddle formula (FAO/SDRN 2017) suggested because it is simple and it uses only measured data on temperature:

$$ET_0 = p(0.46 \cdot T_{mean} + 8) \quad (5\text{-}4)$$

With "p" mean daily percentage of annual daytime hours provided in literature for different latitudes (Table 5.1.a) and T_{mean} (°C) mean daily temperature (Table 5.1.b). K_L is the adjustment factor for landscape plants: (Salinity Management Guide 2007)

$$K_L = K_S \cdot K_D \cdot K_{MC} \quad (5\text{-}5)$$

K_S is the species factor, in the case of equals to 0.25 for the Mesembryanthemum belonging to the Cotyledon species (cotyledon), K_D is the vegetative-density factor equaling 1 for an average density halfway between sparsely and densely planted area, K_{MC} is the microclimat factor depending on the landscapes's temperature, humidity, exposure to wind/sunlight which assumes the low value of 0.7 because the benches are under a building's overhang. A summary of the irrigation water needs has been provided in Table 5.1.b. The results show that the irrigation system, in order to ensure the survival of the plants in Mediterranean climate, should work from May to August. In case of the presented test benches, irrigation has been provided only during August according to the minimum quantities suggested in Table 5.1.b. Despite the small amount of water supplied, at the end of the dry period, the vegetation layer of the experimental green roofs was in good health and fully functional. Finally, the quantity of water required for the wellness of the plants is negligible just like the resulting energy and water consumptions. From this point of view, green roofs can be installed in Mediterranean without any major difficulties as long as they have significant performances.

Table 5.1 Parameters used for the calculation of irrigation water need.

a

Northern hemisphere												
Latitude	**January**	**February**	**March**	**April**	**May**	**June**	**July**	**August**	**September**	**October**	**November**	**December**
60	0,15	0,20	0,26	0,32	0,4	0,41	0,4	0,34	0,28	0,22	0,17	0,13
55	0,17	0,21	0,26	0,32	0,4	0,39	0,38	0,33	0,28	0,23	0,18	0,16
50	0,19	0,23	0,27	0,31	0,3	0,36	0,35	0,32	0,28	0,24	0,2	0,18
45	0,2	0,23	0,27	0,3	0,3	0,35	0,34	0,32	0,28	0,24	0,21	0,2
40	0,22	0,24	0,27	0,3	0,3	0,34	0,33	0,31	0,28	0,25	0,22	0,21
35	0,23	0,25	0,27	0,29	0,3	0,32	0,32	0,3	0,28	0,25	0,23	0,22
30	0,24	0,25	0,27	0,29	0,3	0,32	0,31	0,3	0,28	0,26	0,24	0,23
25	0,24	0,26	0,27	0,29	0,3	0,31	0,31	0,29	0,28	0,26	0,25	0,24
20	0,25	0,26	0,27	0,28	0,3	0,3	0,3	0,29	0,28	0,26	0,25	0,25
15	0,26	0,26	0,27	0,28	0,3	0,29	0,29	0,28	0,28	0,27	0,26	0,25
10	0,26	0,27	0,27	0,28	0,3	0,29	0,29	0,28	0,28	0,27	0,26	0,26
5	0,27	0,27	0,27	0,28	0,3	0,28	0,28	0,28	0,28	0,27	0,27	0,27
0	0,27	0,27	0,27	0,27	0,3	0,27	0,27	0,27	0,27	0,27	0,27	0,27

b

Component	**January**	**February**	**March**	**April**	**May**	**June**	**July**	**August**	**September**	**October**	**November**	**December**
Tmean (°C)	7,6	7,9	9,7	12,4	16	20,3	22,9	23	20,4	16	11,9	8,8
P (mm/month)	95	80	70	64	43	29	25	35	63	92	120	105
P_e (mm/month)	51	39	32	28,4	16	7,4	5	11	27,8	48,6	71	59
P_e (mm/DAY)	1,65	1,39	1,03	0,95	0,51	0,25	0,16	0,35	0,93	1,57	2,29	1,90
p (-)	0,22	0,24	0,27	0,30	0,32	0,34	0,33	0,31	0,28	0,25	0,22	0,21
ET0(mm/day)	2,53	2,79	3,36	4,11	4,97	5,89	6,12	5,76	4,87	3,84	2,96	2,53
K_L (-)	0,18			K_S=		0,25	K_D=		1,00	K_{MC}=		0,70
ET_{corp} (mm/day)	0,44	0,49	0,59	0,72	0,87	1,03	1,07	1,01	0,85	0,67	0,52	0,44
IN (mm/day)	0	0	0	0	0,36	0,78	0,91	0,65	0	0	0	0

5.3 DATA COLLECTION

The monitoring campaign has started on 16th February 2017. It includes real (10 events) and simulated (9 events) rainfall/runoff events. The measures collected during February and March have been discarded

because during that period the system was at an early stage. The root system was not fully developed so the roof was unable to operate according to the requirements. The real events have been monitored during February (2 events), March (3 events), July (1 event), September (2 events), October (1 event) and November (1 event). For some of these events, it has been possible to recorder the temporal evolution while for other ones some inconvenience occurred related to the overflow of the system or to the shutdown of the scale due to blackout .

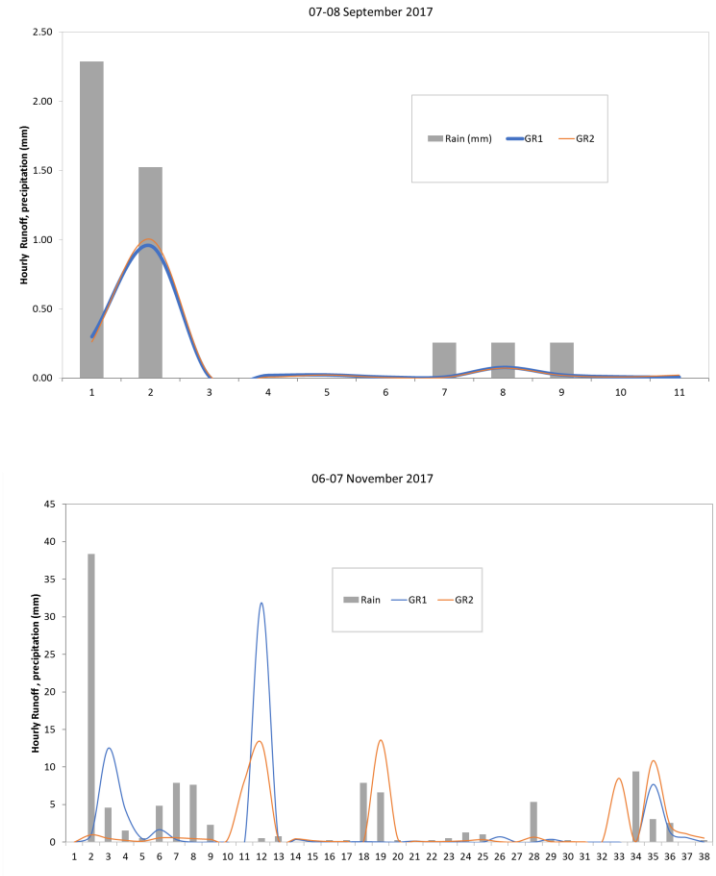

Figure 5.8 Temporal evolution of two rainfall events.

The simulation of the rain has been performed during the spring/summer period (from May to June) when no real events occurred and it has been replicated using the irrigation system.

In order to analyze the role played by the climate characteristics in the behavior of the GRs, the following key parameters have been investigated for each storm event (Table 5.2): cumulative rainfall depth, duration, rain peak intensity. The peak intensity with duration of 5 minutes has been considered for real events because they have a temporal evolution including pre-onset, onset, peak, decay, and post-decay where the peak is clearly distinguishable. Instead, the average intensity has been considered for the simulated events because this kind of event has an even distribution of rainfall in time so the peak can't be detected. Duration reaches a maximum value of 2230 minutes and a minimum value of 5 minutes, cumulative rainfall values range between 1.8 mm and 79 mm, maximum intensity with duration of 5 minutes (for real events) ranges from 7.2 to 112.8 mm/h, while the average intensity (for simulates events) varies between 22 and 168 mm/h (Table 5.2).
For each test bed and recorded event, the hydrological performance in term of retention capacity "R" have been derived. The retention capacity is given by:

$$R = 1 - C^* \tag{5-6}$$

where C* is the coefficient of discharge regarded as the ratio between runoff depth stored in the tank and rainfall depth fallen on the experimental bed. The retention coefficients have been studied, considering the entire dataset of events (real and simulated) with regard to the relationship with the cumulative rainfall and the duration. A distinction between real and simulated events has been made when the relation with the rainfall intensity has been investigated. In addition, the differences appeared from an experimental point of view, between the observations related to the two different construction types of the roof have been highlighted. Concerning to the cumulative rainfall, both for GR1 and GR2, it has been found to have an inverse relationship to the retention capacity: events with a large amount of rainwater are associated with low retention capacity (Figure 5.8). The lowest value observed is about of 50% corresponding to the maximum value of cumulative rainfall of 140 mm. The highest retention coefficient is of 100% occurring during events with low values of cumulative rainfall and in particular during the summer period (when the retention capacity is supported by a dry weather condition due to the remarkable evapotranspiration losses). The relationship between the cumulative

rainfall and the retention capacity is the same for the two construction types even if GR2 has been proved to have slightly higher value of R (about 10% more) for same values of cumulative rainfall. Figure 5.10 shows how green roof retention efficiency decreased with intensity for both the event types. The slope of the curve related to simulated events for which the average intensity has been accounted for (Figure 5.10 right panel), is less pronounced than the slope related to the real events for which the maximum intensity with duration of 5 minutes has been considered (Figure 5.10 left panel). The reason is that the simulations have been carried out during the summer/spring seasons when considerable percentages of retention have been achieved for each kind of the event because the very high ET fluxes regenerate the storage capacity quickly. Indeed, the average percentage of retention reached during the real events is smaller than the value related to the simulated events respectively 60% vs 96% . The inverse relationship between the intensity and the retention capacity, has been found because during high-intensity events featured by a substantial volume of rain falling in a short time, a small amount of rainwater infiltrates into ground and can be stored due to the rainfall intensity bigger than the infiltration capacity of the vegetation support layer. That is clearly reflected in the values of the better performances of 78% (for real events) against 100%(for simulated events) occurring for the lowest rainfall intensities respectively of 18 and 22 mm/h. For a certain duration, an event with a higher intensity will be featured by a bigger return period "T" than an event with equal duration but lower intensity. Consequently, in accord with the previous remarks about the relationship between rainfall intensity and the retention capacity of the roof, it can be said that the performances worsen for higher T because the event is more severe and the effectiveness of the green roof is lower

Table 5.2 Real and simulated events.

Event	From	To	Duration	Cumulative rainfall	Maximum intensity	Retention capacity (%)	
-	-	-	min	mm	mm/h	GR1	GR2
Real	18/02/2017 00:00	19/02/2017 00:00	180	5,8	7,2	50,1	40,2
	25/02/2017 00:00	26/02/2017 00:00	535	5,8	9,6	47,8	34,1
	01/03/2017 00:00	02/03/2017 00:00	105	1,8	7,2	56,8	56,2
	06/03/2017 19:00	07/03/2017 09:00	790	67,1	100,584	62,4	63,0
	07/03/2017 14:00	08/03/2017 09:00	1080	30,5	15,24	58,5	47,3
	26/07/2017 13:10	26/07/2017 18:55	350	22,1	51,816	70,7	68,5
	07/09/2017 12:10	07/09/2017 21:15	545	6,6	18,288	77,7	77,9
	11/09/2017 03:15	12/09/2017 06:05	1615	79,8	57,912	53,3	53,1
	22/10/2017 17:50	24/10/2017 07:00	2235	48,5	79,248	49,5	57,3
	06/11/2017 00:45	07/11/2017 13:50	2230	143,3	112,8	42,9	49,6
Simulated	23/05/2017 12:25	23/05/2017 12:30	5	6,0	72	100	100
	01/06/2017 11:30	01/06/2017 11:35	5	11,2	134,4	89,9	98,4
	05/06/2017 11:25	05/06/2017 11:55	30	11,2	22,4	98,6	99,9
	08/06/2017 14:25	08/06/2017 14:40	15	11,2	44,8	98,9	99,8
	11/06/2017 14:25	11/06/2017 14:30	5	8,4	100,8	100,0	100,0
	15/06/2017 14:15	15/06/2017 14:20	5,0	14,0	168,0	92,0	100,0
	26/06/2017 10:00	26/06/2017 10:30	30,0	30,0	60,0	92,6	99,7
	10/07/2017 10:40	11/07/2017 11:40	60,0	60,0	60,0	84,7	80,0
	24/07/2017 10:00	24/07/2017 10:45	45,0	45,0	60,0	99,2	99,5

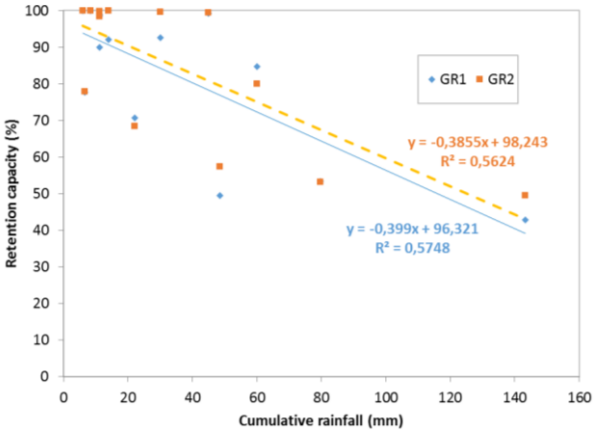

Figure 5.9 Retention capacity of two green roofs vs cumulative rainfall depth.

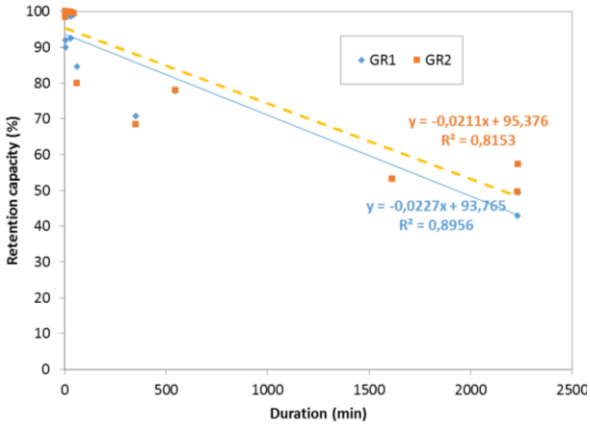

Figure 5.10 Retention capacity of two green roofs vs duration of storm events.

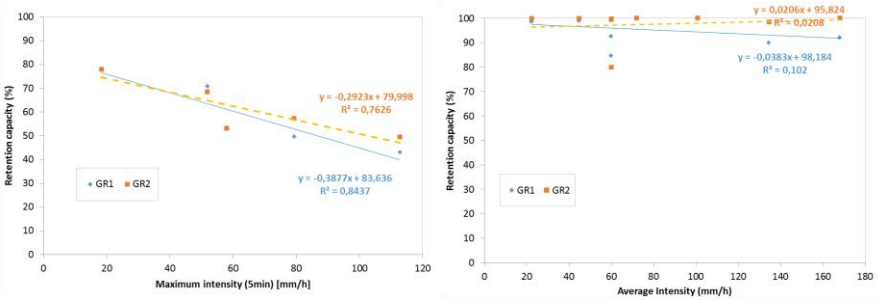

Figure 5.11 left panel-Retention capacity of two green roofs vs intensity of the real events, right panel- Retention capacity of two green roofs vs intensity of the simulated events.

In general the performances of GR2 are slightly higher than GR1 even if the water reserve provided by GR1 is larger than that one of GR2: 32 l/m^2 against 14 l/m^2 corresponding respectively to 32 mm and 14 mm of storable rainwater. This evidence underlines that the storage capacity of the drainage layer of GR is not the only property getting involved in the process of retention but the mode of operation of the drainage layer plays an important role too. In light of this, more insights about this latter aspect are required and the investigation of a larger number of events is of primary importance. Finally, rainfall attenuation ranged from minimum value of 43% during winter to maximum value of 100% during Spring consistently with other results found in a mediterranean area of about 60% reported by Fioretti et al. 2010 and Palla et al. 2009.

6 SUDS, HYDROLOGICAL IMPACT AT BASIN SCALE

In this chapter, the hydrologic impact of a widespread implementation of green roofs within a virtual basin has been investigated using the Storm Water Management Model (SWMM) of the US Environmental Protection Agency (USEPA). For the virtual basin, the performances have been evaluated at the outlet section of the drainage system in terms of decrease in runoff volume and peak discharge and increase in the peak delay comparing the scenario under investigation with the baseline scenario (no GR facilities). The simulations have been performed for design storms with different return periods, durations and temporal distributions and they have analyzed how the GRs response at basin scale varies according with the percentages of retrofitted roofs, the spatial GRs distribution and the catchment spatial scale aggregation.

6.1 STORM WATER MANAGEMENT MODEL

The analysis of the performances of GRs at the basin scale has been performed using the Storm Water Management Model (SWMM). SWMM of the US Environmental Protection Agency (USEPA) is a model able to simulate the runoff generated within urban areas during single and long term rainfall events. SWMM is divided into several computational "blocks" but the main ones are the RUNOFF and TRANSPORT blokes.
The RUNOFF Block generates surface runoff in response to a precipitation input. A number of subcatchments with homogeneous characteristics or a single watershed with parameters averaged over the numbers of homogeneous watersheds should be considered. Each basins can be sketched like a non-linear reservoir (Figure 6.1) where the inflow is an arbitrary rainfall hyetograph while the outflows are evaporation, infiltration and the surface runoff.

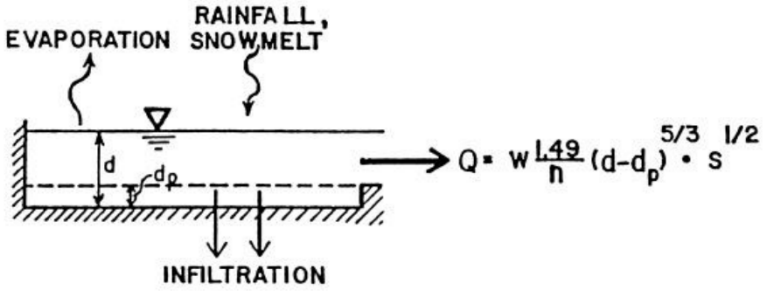

Figure 6.1 Basins sketched like non linear reservoirs.

Total runoff "R" occurs only when the depth of water in the "reservoir" "d" (unknow) is higher than the maximum depression storage of the ground (or reservoir) "d_s" consisting of ponding, surface wetting and interception. R is provided by Manning's equation:

$$Q = W \cdot \frac{1.49}{n}\left(d - d_p\right)^{\frac{5}{3}} S_0^{1/2} \tag{6-1}$$

Where W is the subcatchment width, n is the Manning's roughness coefficient, n is the depth of depression storage and S_0 is the subcatchment slope. Depth of water over the subcatchment (d) can be depleted by infiltration and evaporation. Evapotranspiration is provided by the user but it is negligible at event scale, while infiltration is modeled by the method selected by the user that in this case is the SCS method (Mishra S. K. et al. 2013). This approach assumes that the total infiltration capacity of a soil can be found from the soil's tabulated Curve Number (CN) and the direct runoff Q can be expressed through:

$$Q = \frac{\left(P - 0.2S\right)^2}{P + 0.8S} \tag{6-2}$$

and

$$S = \frac{1000}{CN} - 10 \tag{6-3}$$

With P cumulative precipitation and S maximum water storage function of the land use and 0.2S is (Ia) Initial abstraction (i.e. water constituting the short term surface storage such as puddles or detention ponds).

The unknow parameter d is continuously updated with time by solving numerically a water balance equation (continuity mass equation) over the subcatchment which therefore tracks the volume or depth of water on the surface of the subwatershed.

$$\frac{dV}{dt} = A\frac{dd}{dt} = A \cdot i^* - Q \tag{6-4}$$

Where V is the volume of water on the subarea, t is the time, A is the surface area of subarea, i* is the rainfall excess given by rainfall minus evapotranspiration/infiltration. Substituting eq. 6-1 into eq. 6-4 and dividing by A, the result the equation is:

$$\frac{dd}{dt} = i^* - \left[(1.49 \cdot W)/(A \cdot n)\right] \cdot \left(d - d_p\right)^{5/3} \cdot S_0^{1/2} \tag{6-5}$$

The equation became:

$$\frac{d_{n+1} - d_n}{\Delta t} = i^* - \left[(1.49 \cdot W)/(A \cdot n)\right] \cdot \left(d - d_p\right)^{5/3} \cdot S_0^{1/2} \tag{6-6}$$

Where the differential term dd/dt is approximated by a finite difference of values for depth at two points in time separated by Δt. $\Delta t = t_{n+1} - t_n$ is the time step size while n and n+1 are subscripts indicating respectively conditions at the start of time step n and the end of time step n+1. d became $d = (d_n + d_{n+1})/2$ representing the depth of flow during time step n+1. The equation becomes a nonlinear, algebraic relationship with one unknown at any time, d_{n+1} (The value of dn is, of course, known from the end of the previous time step) solvable numerically using the Newton-Raphson technique. The calculated value of d_{n+1} (instantaneous outflow at the end of a time step) is then used in eq. 6-1 to calculate the value of Q at the same time. In the next step the calculated d_{n+1} becomes the new d_n already known and so on.
The TRANSPORT block routes flows generated by the RUNOFF block through a sewer system. Flow in the conduits can be represented by the continuity equation:

$$\delta Q / \delta t + \delta A / \delta t = 0 \tag{6-7}$$

and by the Momentum equation which in a simplified version can be expressed as:

$$S_f = S_0 \tag{6-8}$$

Where S_f is friction slope estimated from Manning's equation:

$$S_f = \frac{Q^2}{\left[(1.49/n)^2 \cdot A^2 \cdot R^{4/3}\right]} \tag{6-9}$$

The continuity equation can be approximated by a finite difference relationship:

$$\left[(1-w_t)(A_{j,n+1} - A_{j,n}) + w_t(A_{j+1,n+1} - A_{j+1,n})\right]/\Delta t + \left[(1-w_x)(Q_{j+1,n} - Q_{j,n}) + w_x(Q_{j+1,n+1} - Q_{j,n+1})\right]/\Delta x = 0 \tag{6-10}$$

Where $\Delta x = x_{j+1} - x_j$ is the distance interval length and j, j+1 the subscripts indicating conditions at the upstream and the downstream end of the conduit, and w_t, w_x the weights set to 0.55 after tests of stability.
The two equations (eq. 6-9 and eq. 6-10) are used together to route flows through a sewer system. At the end of any time step n+1, the unknown quantities are the flow $Q_{j+1,n+1}$ and cross-sectional area of flow $A_{j+1,n+1}$ at the downstream end of conduit. (The variables $Q_{j,n}$ and $A_{j,n}$ are known from the previous time step and conditions at the upstream end of the conduit). With only two unknowns, these two equations are sufficient to determine the value of both. The calculations are carried out from the most upstream conduit to the most downstream conduit during each time step.
Total Runoff consists of both surface runoff from non linear-reservoir representing the sub-basin and SUDS drain flow (or outflow). SUDS controls are represented by a combination of vertical layers:

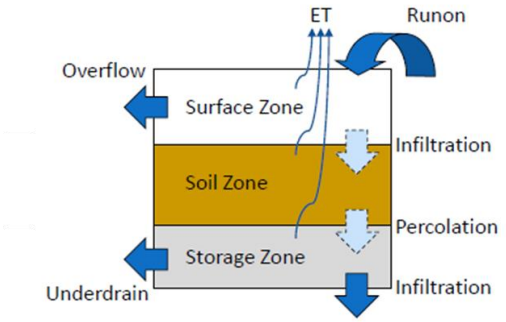

Figure 6.2 Vertical layers of SUDS infrastructures.

The Surface Layer is the ground surface. It receives directly rainfall input, it stores excess inflow in depression storage, and generates overflow that the can enter into the drainage system or flow on the subcatchment area depending on network capacity.
-The Pavement Layer is the layer of porous concrete or asphalt used in continuous permeable.
-The Soil Layer is the vegetation support layer.
-The Storage Layer is a bed rock or gravel that provides storage of water, it can contain a drain system conveying water out of the storage layer typically with slotted pipes into a common outlet pipe or chamber.
During a simulation SWMM performs a moisture balance that keeps track of how much water moves between and is stored within each SUDS layer. The flows balance equations are:

$$\frac{\delta d_1}{\delta t} = q_0 - e_1 - f_1 - q_1 \qquad (6\text{-}11)$$

$$D_2 \frac{\delta \theta}{\delta t} = f_1 - e_2 - f_p \qquad (6\text{-}12)$$

$$\phi \frac{\delta d_3}{\delta t} = f_p - e3 - f3 - q_3 \qquad (6\text{-}13)$$

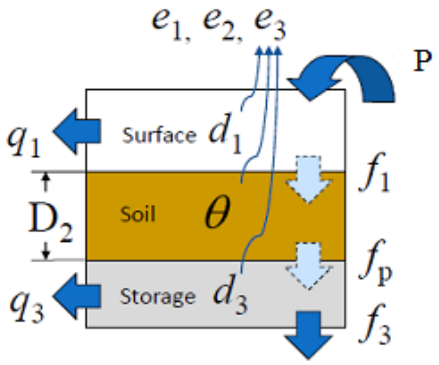

Figure 6.3 Parameters used in the flows balance equations.

Where:
q_1 is the overflow flux, 1,2,3 are the number of the layers, e is evapotranspiration flux provided by the user even if negligible at event scale, f is the infiltration flux in the underlying layers or in the native soil given by Green-Ampt Equation:

$$f = K_{sat}\left(1+\frac{(\phi-\theta)(d+\psi)}{F}\right) \tag{6-14}$$

Where K_{sat} is the saturated hydraulic conductivity, ϕ is the porosity, θ is the moisture content, ψ is the suction head depending on the field capacity θ_{FC}, F is the cumulative amount of infiltrated water and d is the zone's water depth. f_p is the percolation flux from Darcy's law:

$$f_p = K(\theta)\left(1+\frac{\psi(\theta)}{D}\right) \tag{6-15}$$

q_3 is the drain flow provided by:

$$q_3 = C \cdot h^n \tag{6-16}$$

Where C and n are respectively the drain coefficient and exponent and h is the height of the drain above the bottom of the unit's storage layer.

The following table (Table 6.1) indicates which combination of layers applies to each type of SUDS (x means required, o means optional):

Table 6.1 Combination of layers for each SUDS technique.

SUDS Tipe	Surface	Pavement	Soil	Storage	Drain
Bio-retention Cell	x		x	o	o
Rain Garden	x		x		
Green Roof	x		x		
Permeable pavement	x	x	o	x	o
Infiltration Trench	x			x	o
Rain Barrel				x	x
Roof Disconnection	x				x
Vegetative Swale	x				

The parameters of bio-retention cell (used for the simulations of green roofs) required in the SUDS-SWMM section are listed in Table 6.2.
About the Surface layer, for the green roof has been set a height of the confining walls for the pond of the water above the surface of 100 mm. The volume fraction occupied by stems and leaves is of 0.8 which means very dense vegetative growth. For dense grass surface the Manning coefficient is 0.24. The soil characteristics have been suggested by Rawls et al. 1983 for a soil layer of loam. About the storage layer, the thickness of extensive green roof is around 10 cm while for porous pavement it goes from 60 to 90 cm. The rate at which water seeps into the native soil below the storage layer of the permeable pavement would typically be the Saturated Hydraulic Conductivity of the surrounding subcatchment if Green-Ampt infiltration is used and for silt loam or loam (Group B) with moderate infiltration rate the range of values are between 3.8 and 7.6 mm/h (Hydrology 2017). In green roof there is an impermeable floor below the storage layer then value 0 for seepage rate has been used. The GRs technology doesn't use a drainage system while in the permeable pavement the drain is located the top of the storage layer in order to allow the full storage volume to fill before draining occurs, n and C have been set respectively equal to 0.5 and 2 as the drain act like an orifice.

Table 6.2 Parameters used for Bio-retention cells.

Surface	
Berm Height (mm)	100
Vegetation Volume fraction (-)	0,8
Mannings roughness (-) [n]	0,24
Surface slope (%) [S_0]	1
Pavement	
Thickness (mm)	-
Void ration (Voids/solids)	-
Impervious Surface (fraction)	-
Permeability (mm/h)	-
Soil	
Thickness (mm)	100
Porosity (volumetric fraction) [φ]	0,85
Field capacity (volumetric fraction) [θ_{FC}]	0,2
Hydraulic conductivity (mm/h) [K]	0,5
Suction head (mm) [Ψ]	3,5
Storage	
Thickness (mm)	100
Seepage rate (mm/h) [mm/h]	0
Drain	
Drain coefficient (-) [C]	-
Drain exponent (-) [n]	-
Offset Height (mm) [h]	-

6.2 THE VIRTUAL BASIN

In order to study the effects of the percentages of retrofitted roofs, of the relative spatial distribution and spatial scale of aggregation, simulations have been initially performed for a virtual basin. A real catchment would have been featured by heterogeneous characteristics contrary to a virtual catchment. In the analysis of a real system then it could be difficult to distinguish between the hydrological effects caused by the peculiarities of the real basin from those resulting from the above said scenarios to be investigated.
The virtual basin consists of 4 sub-basins of 1 hectare and an average surface slope of 1% (Figure 6.4).

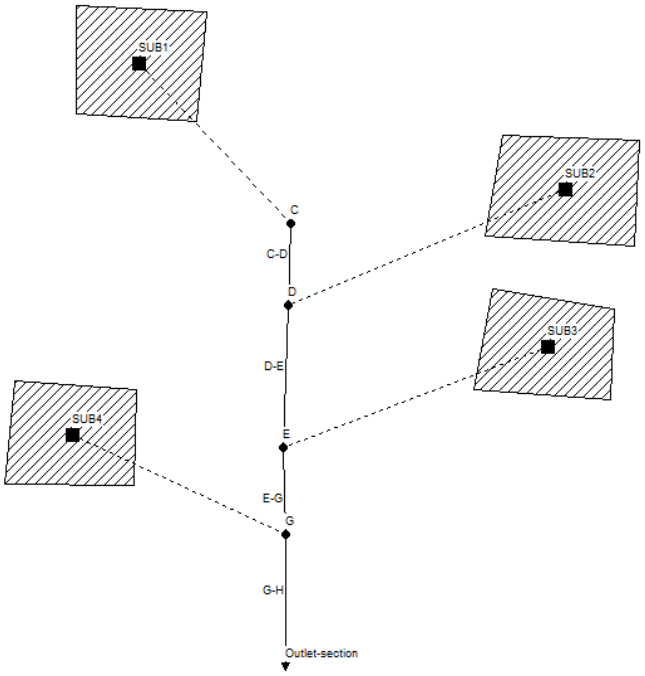

Figure 6.4 The virtual basin.

As preliminary to the application to a particular case study, the virtual basis is supposed to be located in a Mediterranean area where the weather is characterized by warm to hot, dry summers and mild to cool, wet winters. The meteorological station providing the data required for the analysis is located in the campus of University of Salerno in Fisciano, in Southern Italy with a typical Mediterranean climate. The site-specific Intensity-duration-frequency curves are shown in the Figure 6.5.

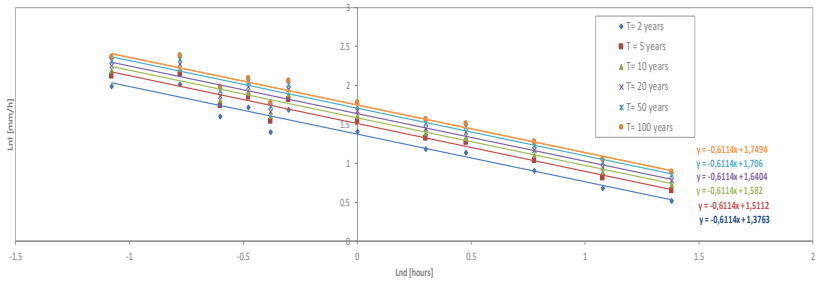

Figure 6.5 IDF curves.

As GR facilities are particularly attractive in densely urbanized areas, each sub-basin is considered highly urbanized, with 80% impervious area (the baseline scenario) and so a CN of 98 related to paved area with parking lots, roofs and driveways(Cronshey 1986).
The combined drainage network includes a main collector and four secondary sewer pipes of 1 Km length for which a preliminary design has been carried out assuming satisfied the final design checks. Pipes design has been performed according to conventional methodologies used in the region where the virtual basin is supposed to be located. Each pipe can carry both wastewater and stormwater, so the design flow is:

$$Q_{Design} = Q_{waste} + Q_{stormwater} \tag{6-17}$$

Where Q_{waste} and $Q_{stormwater}$ are respectively waste and stormwater flows. Assuming that 80% of average water supply goes to sewers as waste water:

$$Q_{waste}\left(m^3/s\right) = 0.8\frac{K_p \cdot N \cdot q}{86400 \cdot 10^3} \tag{6-18}$$

Where N is design population in thousands depending on the current population density "d" (pop/km^2) of the study area multiplied by the surface of the catchment, q is the average daily per capita domestic flow (litres/capita/day), K_p (-) is the peak factor, function of the population of the whole basin, 86400 is a conversion factor. $Q_{wastwater}$ is calculated according to index flow formula:

$$Q_{stormwater}(m^3/s) = K_T\frac{A \cdot C \cdot i_m}{3.6} \tag{6-19}$$

A (Km^2) is the drained area, C (-) is the run-off coefficient which is dependent on the characteristics of the drained area:

$$C = 0.14 + 0.65P_i + 0.05P_m \tag{6-20}$$

Pi (-) is the ratio between the imperviousness area of the basin and the total area, Pm (%) is the slope of the pipe, K_T is the probabilistic factor of growth depending on the return period "T" (10 years):

$$K_T = -0.45 - \frac{1}{1.28}\ln(-\ln(1-\frac{1}{T})) \quad (6\text{-}21)$$

i_m is the average rainfall intensity in millimeters/hour.
Because of the lack of sub-hourly rainfall data provided by the meteorological station of campus of University of Salerno, a statistically significant sample related to the rainfall events of short duration is not available. In the case of short duration events (below 1 hour interval) the maximum rainfall intensity has been computed according to an empirical law with 4 parameters, proposed into the project "Vapi Campania" (Rossi et al. 1994), for regional analysis in ungagged catchments. It consists of a regional analysis of the averages of annual maximum values of rain with a given duration and according to this law:

$$i_m = \frac{i_0}{\left[1+\frac{d}{d_c}\right]^{c-D\cdot Z}} \quad (6\text{-}22)$$

Where i_0 is the limit of the rainfall intensity for the duration of the event which tends to zero, expressed in mm/hour, d is the duration of rainfall in hours set equal to Schaake's the delay time:

$$d = 1.40 L^{0.24} P_i^{-0.24} P_m^{-0.16} \quad (6\text{-}23)$$

Where L (m) is length of pipe, dc is the characteristic duration of the rain on the basin in hours, c and D are dimensionless parameters, z is the average height in meters of the basin set at 255 m and corresponding to the average altitude of the campus of Fisciano. According to the VAPI project (Rossi et al. 1994) there are 6 homogeneous rainfall areas in Campania, identified on the basis of characteristics of spatial contiguity and physiographic, thermometric and hydrological homogeneity. In each area the parameters of the equation are constant. The basin into analysis falls in homogeneous area A2.

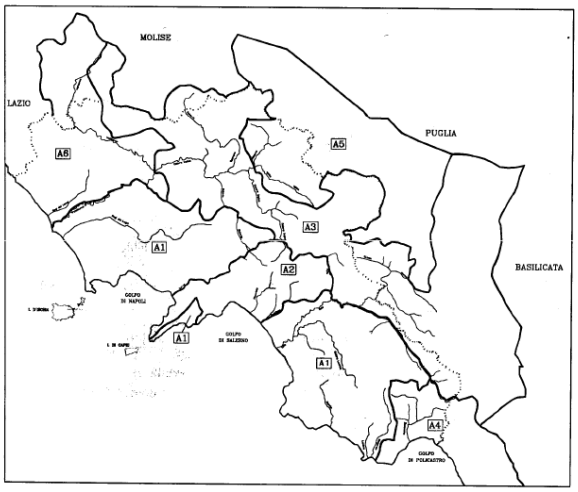

Figure 6.6 Homogeneous rainfall areas in Campania.

All the values required for the design are shown in the Table 6.3:

Table 6.3 Values required for the design.

A (Km^2)	0,01	P_i (-)	0,8	d_c (h)	0,3312
d (pop/Km^2)	223	P_m (%)	2	c (-)	0,7031
N,i (pop)	2,23	C (-)	0,76	D(-)	7,74E-05
N (pop)	8,92	T (Years)	10	z (m.s.l.m.)	255
q (l/capita/day)	300	K_T (-)	1,308099	d (h)	0,12
Kp (-)	10,98	L (m)	1000	i_m (mm/h)	68,24
$Q_{waste,i}$ (m^3/s)	6,80E-05	i_0 (mm/h)	83,8	**$Q_{stormwater,i}$ (m^3/s)**	0,19

Finally, the total flow in the pipes is:

Table 6.4 Flows in the pipes.

Section	Q (m^3/s)	D (m)
C,D	0,19	0,4
D,E	0,57	0,6
E,G	0,94	0,6
G,H	1,32	0,8

The diameters of the channels have been calculated by means of successive iterations, changing their values until the total flow equals uniform flow given by Gauckler and Strickler:

$$Q_u = K_{st} \cdot A_f \cdot R^{2/3} \cdot P_i^{1/2} \tag{6-24}$$

With R hydraulic radius (m), K_{st} Gauckler and Strickler coefficient (=70 $m^{1/3}/s$ for concrete section), A_f flow area (m^2).

6.3 RAINFALL INPUT

The simulations have been performed for design storms with return periods of 2, 5, 10 years, different distribution of the hyetographs and different durations, if compared to the time of concentration t_c.
The concentration time is the current time water takes to propagate from the most distant point in the watershed to the outlet section. It has been detected according to the formula proposed by Carter 1961 that is the most suitable for the considered virtual basin because it has been calibrated for urban basins with area less than 20.7 Km^2 and channel length less than 11 km:

$$t_c = 0.0015476 \cdot L^{0.6} \cdot P_m^{-0.3} \tag{6-25}$$

Where L (m) is length of the watershed along the main channel from the hydraulically most distant point to the channel assumed equaling the length of the main channel of 4000 m, P_m (m/m) is the average slope of the water route that can be express using the Taylor-Schwartz equation:

$$P_m = \left(\frac{L}{\sum_{j=1}^{n} \frac{l_j}{\sqrt{P_i}}} \right)^2 \tag{6-26}$$

With lj and Pj the length and the slope of of each j-th section being part of the main course and obviously:

$$\sum_{i=1}^{n} l_j = L \tag{6-27}$$

Table 6.5 Average slope of the water route.

Section	z_0 (m)	z_f (m)	Dz/2 (m)	Pj (%)	lj (m)	lj/(Pj)^0.5
C-D	50	40	5	0,50	1000	1414,21
D-E	40	30	5	0,50	1000	1414,21
E-G	30	20	5	0,50	1000	1414,21
G-Outlet	20	10	5	0,50	1000	1414,21
				S	4000	5656,85
				Pm (%)	0,50	

Finally, t_c is about 1 hour. Tc helps to distinguish short, medium and long events having respectively comparable, higher and much higher duration than the lag time.

Events with duration less than 1 hour have not been investigated because they require a too high level of detail of the used SWMM model, leading to not significant simulations with potentially incorrect assessment of the performances. In confirmation of the above said, in literature, in order to model runoff from extensive or intensive green roofs using SWMM, many authors consider single storm events with different durations but no one of them looks at events lasting less than about 1 hour. Peng et al. 2017 model runoff in response to eight single rainfalls with minimum duration of 2 hours while Kong et al. 2017 examine the hydrological response of SUDS controls using a rainfall event occurred from 23 to 24 June 2015. Zhu et al. 2017 analyze the influence of rainfall duration on SUDS techniques selecting three rainfall scenarios of 1hour, 1.5 hours and 2 hours. Krebsat et al. 2016 use for calibration and validation of SWMM single storm events with duration ranging from 9 to 41 hours, Cipolla et al. 2016 use events with minimum duration of 65 minutes, Haichun et al. chose for calibration/validation rainfall events mostly around 1 h.

Wu et al. 2016, Masseroni et al. 2016, Ghimire et al. 2016, and Krebs et al. 2013 use for parameter calibration and model validation single rainfall events respectively with duration of 24 hours, 45 or 75 minutes and at least 7 hours. For very short events whose duration is lower than the time of concentration, the hydrological impacts of GR spatial distribution is unpredictable and its trend is not linear with distance from

the downstream point as confirmed by Versini et al. 2016. He considered a highly impervious 65 ha test-basin (Versini et al. 2014) called Loup near to Paris, with an elevation difference of 12.5 m (Gires et al. 2015) and a length of the main channel deduced by graph scale in Versini et al. 2016 of about 1500 m. Using these information and according to Carter 1961, a time of concentration of 0.63 hours has been calculated. For short events compared to t_c with duration of 30 minutes, despite, the run-off model (Multi-Hydro) used by the author differs from that one used in this study, the non-linear behavior along the basin in terms of hydrological efficiency is proved. Short and intensive events with duration of 1 hour, long and low-intensity events lasting 24 hours and events with medium intensity and duration of 3 hours have been chosen.

Another rainfall characteristic which has been considered, is the shape of the hyetographs. Chicago, rectangular and triangular hyetographs (Fletcher et al. 1975, Yen et al. 1980, Westphal 2001, Asquith 2003, Yalin 2015) have been designed in order to investigate the hydrological behavior of the basin in response to different rainfall patterns. In literature different authors used synthetic hyetographs for computing the inlet hydrographs (Fletcher et al. 1975) some of them studied the storm runoff response to a triangular rainfall pattern (Yen et al. 1980, Asquith 2003), others used rectangular hyetograph shape for investigating the runoff production (Yalin 2015), still others used Chicago method for computation of peak rate and volume of runoff (Westphal 2001).

The three synthetic hyetographs have been derived from the rainfall Intensity-duration-frequency curves (Figure 6.5) they return the same volume of rain. The rectangular hyetograph has, regardless for the duration of the event, a constant-intensity derived from the IDF relationships while for the other distributions, the equations for estimating the synthetic hyetographs are shown in (Becciu 2004):

Rectangular:

$$i = \frac{A \cdot \delta^n}{\delta} = A \cdot \delta^{n-1} \tag{6-28}$$

Triangular:

$$\text{if } t_m \le t_p \Rightarrow i = 2A\delta^{n-2}\left(\frac{t_m}{K}\right); \text{ if } t_m > t_p \Rightarrow i = 2A\delta^{n-2}\left(\frac{\delta - t_m}{1-K}\right) \quad (6\text{-}29)$$

Chicago:

$$\text{if } t_m \le t_p \Rightarrow i = n \cdot a \cdot \left(\frac{t_p - t_m}{K}\right)^{n-1}; \text{ if } t_m > t_p \Rightarrow i = n \cdot a \cdot \left(\frac{t_m - t_p}{1-K}\right)^{n-1} \quad (6\text{-}30)$$

With δ duration of the rainfall event (1 hour, 3 hours, 24 hours), A and n are the intercept and the slope of the IDF curves, t_m is sampling time for mean value of duration, having fixed a time step of 10 minutes and t_p is the time to peak. It is the time when the hyetographs reaches the highest rainfall and it is calculated as the rate "K" commonly of about one-half the precipitation duration:

$$t_p = K \cdot \delta = 0.4 \cdot \delta \quad (6\text{-}31)$$

Table 6.6 Intercept and the slope of the IDF curves.

T(years)	$Log_{10}A$	A (mm/h^n)	n
2	1.376	23.768	0.388
5	1.511	32.434	0.388
10	1.582	38.194	0.388

Using the above said relationships, the synthetic hyetographs with triangular, rectangular and Chicago distributions have been defined (Figure 6.7).

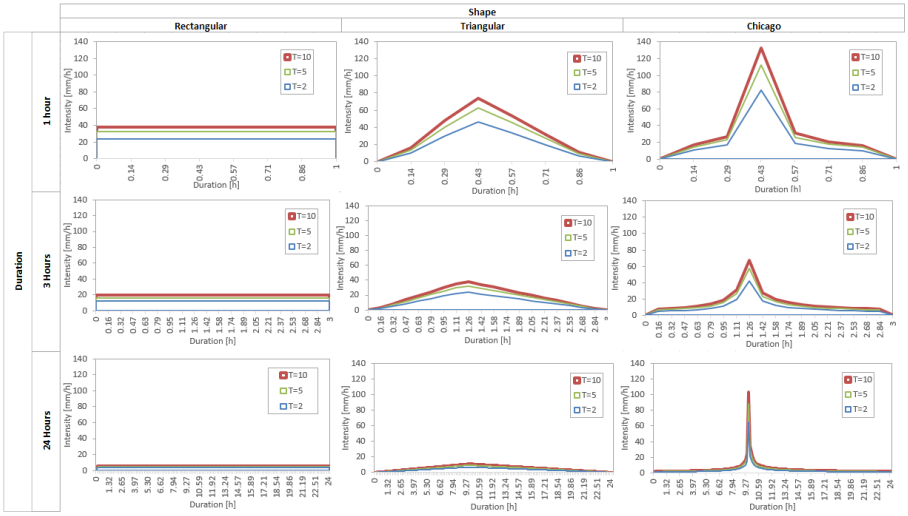

Figure 6.7 Synthetic hyetographs for duration of 1, 3, 24 hours.

6.4 SIMULATIONS SCENARIOS FOR THE VIRTUAL BASIN

Once the geometric characteristics of the virtual basin and the design rainfall input have been described, it is possible to investigate, using SWMM simulations, how the response of the virtual catchment varies with:

- Percentages of retrofitted roofs
- Spatial GRs distribution
- Spatial scale of aggregation

For this purpose, several greening scenarios with different percentage of retrofitted roofs have been proposed and analyzed. The comparison between the performances of each greening scenario and the baseline scenario (without green roof infrastructures) estimated in the outlet section of the sewage network, has been performed using three indices: the percentage of reduction in runoff volume (ΔR_V), peak flow (ΔP_F) and increase in the delay time (ΔD_T). The indices have been estimated as follows:

$$\Delta R_V = \frac{R_{V,0} - R_{V,i}}{R_{V,0}} \cdot 100 \qquad (6\text{-}32)$$

$$\Delta P_F = \frac{P_{F,0} - P_{F,i}}{P_{F,0}} \cdot 100 \quad (6\text{-}33)$$

$$\Delta D_T = \frac{D_{T,0} - D_{T,i}}{D_{T,0}} \cdot 100 \quad (6\text{-}34)$$

$R_{V,0}$, $P_{F,0}$, $D_{T,0}$ are respectively the runoff volume (m^3), the peak flow (m) and the delay time (min) referred to the baseline scenario, while $R_{V,i}$, $P_{F,i}$, $D_{T,i}$ are the same parameters but referred to the i-th scenario of greening.

6.5 RESULTS OF THE SIMULATIONS

At first, the simulations have been focused on GR response varying the percentage of retrofitted roofs and ten scenarios, with increasing percentages, from 0% to 100%, of impervious surface, converted into GRs and evenly distributed within the four sub-basins of the virtual catchment, have been analyzed. Table 6.7 shows how the percentage reduction of runoff volume (ΔR_V) and peak flow (ΔP_F) and the percentage increase in the delay time (ΔD_T) vary with return period, duration and temporal distribution of the precipitation input and the percentage of greening of the basin. The results highlight that the larger the percentage of converted traditional roofs, the better the performances in terms of ΔR_V, ΔP_F, ΔD_T with a range of effectiveness from 0 to 100% in the most favorable cases and from 0 to 48.3%, 27.7%, 0.14% correspondingly for ΔR_V, ΔP_F, ΔD_T in the worst cases. Looking at these values, it can be deducted that for equal percentage of greening, greater benefits can be observed on the reduction of runoff volume and peak flow than on the increase of delay time (Figure 6.8). For same duration, the shape of the hyetograph seems to affect the hydrological response less than the return period does. Changing the distribution of the precipitation with an assigned rate of conversion in GR and return period, the maximum range of variation of the performances is higher than changing T and fixing the shape, respectively 25%, 18.8%, 39.9% for ΔR_V, ΔP_F, ΔD_T against 10.5%, 43.5% and 85.9% of the opposite case. Fixing a target value of retrofitted area, the response of a green roofing scenario improves moving from long to short events in fact the maximum percentages of reduction

achievable during long events is at most of 77.5% for ΔR_V, 81.2% for ΔP_F, 36.2% for ΔD_T against 100% for both events with medium and short duration.

Table 6.7 GR response varying the percentages of retrofitted roofs.

T= 2 Years

Percentage	1 Hour									3 Hours									24 Hours								
of Greening	Rectangular			Triangular			Chiacago			Rectangular			Triangular			Chiacago			Rectangular			Triangular			Chiacago		
(%)	ΔR_V	ΔP_F	ΔD_T	ΔR_V	ΔP_F	ΔD_T	ΔR_V	ΔP_F	ΔD_T	ΔR_V	ΔP_F	ΔD_T	ΔR_V	ΔP_F	ΔD_T	ΔR_V	ΔP_F	ΔD_T	ΔR_V	ΔP_F	ΔD_T	ΔR_V	ΔP_F	ΔD_T	ΔR_V	ΔP_F	ΔD_T
0	0	0,0	0,0	0,0	0,0	0,0	0,0	0,0	0,0	0,0	0,0	0,0	0,0	0,0	0,0	0,0	0,0	0,0	0,0	0,0	0,00	0,0	0,0	0,0	0,0	0,0	0,0
10	18	6,5	4,7	17,0	10,7	7,4	16,2	13,1	9,1	12,5	3,1	0,3	12,0	3,0	2,3	14,1	7,0	4,0	8,7	3,7	0,00	8,4	3,4	0,2	8,7	0,0	0,1
20	33	20,1	10,2	31,7	26,1	15,7	30,1	28,4	19,2	23,8	6,7	0,6	22,9	9,5	7,4	26,8	22,0	10,6	17,0	8,0	0,07	16,3	7,4	1,0	16,8	1,3	0,3
30	47	38,6	17,3	45,6	43,6	24,1	43,5	44,1	29,3	34,7	10,6	0,6	33,3	19,4	14,8	39,0	38,9	19,1	25,2	12,5	0,10	24,0	11,8	1,6	24,7	4,9	0,5
40	61	57,8	26,0	59,2	60,5	32,4	56,5	59,3	38,4	45,3	15,5	0,8	43,6	31,1	22,2	50,9	54,6	28,6	33,2	16,7	0,10	31,6	16,6	1,5	32,3	10,9	0,8
50	74	74,3	32,3	71,9	75,0	40,7	69,0	72,8	47,5	55,7	23,1	0,8	53,7	43,6	30,6	62,5	68,0	41,2	41,1	21,2	0,10	38,9	22,3	4,4	39,8	22,5	1,3
60	85	86,9	36,2	83,1	86,3	47,2	80,2	83,9	54,5	65,8	34,8	0,8	63,6	55,9	38,9	73,6	78,8	60,3	48,8	26,0	0,14	46,1	29,2	8,1	47,1	37,5	2,1
70	93	94,6	37,0	91,5	94,0	52,8	89,3	92,2	61,6	75,4	50,5	1,1	73,0	67,6	47,2	83,8	87,0	84,9	56,3	30,8	0,14	53,2	37,0	14,3	54,4	51,8	3,1
80	97	98,0	37,8	96,4	97,9	47,2	95,5	97,2	60,6	84,2	68,0	1,4	81,9	78,2	55,1	92,4	94,0	93,0	63,6	35,8	0,14	60,1	44,9	21,5	61,5	63,9	4,4
90	98	99,2	38,6	98,4	99,3	50,0	98,4	99,3	76,8	91,8	84,0	1,9	89,8	87,7	63,9	97,9	98,8	43,7	70,7	40,8	0,14	66,8	52,7	29,1	68,4	73,6	6,1
100	100	100,0	-	100,0	100,0	-	100,0	100,0	-	97,7	95,8	3,3	96,3	95,5	76,9	100,0	100,0	-	77,5	46,4	0,14	73,4	60,3	36,2	75,1	81,2	8,5
Baseline value	847,5	0,2	63,5	867,0	0,3	54,0	911,8	0,3	49,5	###	0,1	180,5	1353,5	0,2	108,0	1148,8	0,212	99,5	3168,3	0,038	1442,5	3170,3	0,073	625,5	3127,6	0,299	597,0
UM	m^3	m	min	m^3	m	min	m^3	m	min	m^3	m	min	m^3	m	min	m^3	m	min	m^3	m	min	m^3	m	min	m^3	m	min

T= 5 Years

Percentage	1 Hour									3 Hours									24 Hours								
of Greening	Rectangular			Triangular			Chiacago			Rectangular			Triangular			Chiacago			Rectangular			Triangular			Chiacago		
(%)	ΔR_V	ΔP_F	ΔD_T	ΔR_V	ΔP_F	ΔD_T	ΔR_V	ΔP_F	ΔD_T	ΔR_V	ΔP_F	ΔD_T	ΔR_V	ΔP_F	ΔD_T	ΔR_V	ΔP_F	ΔD_T	ΔR_V	ΔP_F	ΔD_T	ΔR_V	ΔP_F	ΔD_T	ΔR_V	ΔP_F	ΔD_T
0	0,0	0,0	0,0	0,0	0,0	0,0	0,0	0,0	0,0	0,0	0,0	0,0	0,0	0,0	0,0	0,0	0,0	0,0	0,0	0,0	0,00	0,0	0,0	0,0	0,0	0,0	0,0
10	12,8	2,8	1,6	12,3	5,9	3,9	11,7	8,8	6,5	9,1	2,3	1,1	8,8	1,7	1,0	10,4	2,8	2,1	6,4	2,9	0,07	6,2	2,5	0,2	6,4	0,0	0,1
20	23,9	9,5	4,8	23,0	15,9	9,7	21,9	20,2	14,1	17,5	4,9	1,4	16,9	5,5	4,4	19,7	11,8	6,3	12,5	5,8	0,07	12,1	5,3	0,6	12,5	0,5	0,3
30	34,6	20,6	8,8	33,4	28,5	16,5	31,8	32,7	20,7	25,7	7,6	1,7	24,7	11,8	9,2	28,8	24,8	10,9	18,6	8,7	0,07	17,8	8,4	1,0	18,4	3,2	0,4
40	45,2	34,5	13,6	43,7	41,7	22,3	41,6	44,9	29,3	33,8	10,6	2,0	32,5	20,0	15,5	37,8	38,5	16,7	24,6	11,8	0,07	23,5	11,7	0,6	24,2	7,1	0,6
50	55,7	49,1	18,4	53,8	54,5	27,2	51,4	56,1	35,9	41,8	14,2	2,2	40,2	29,1	21,4	46,6	51,3	22,4	30,6	15,3	0,07	29,1	15,4	1,7	29,8	12,0	0,8
60	65,8	62,8	23,2	63,7	66,2	33,0	60,9	66,4	42,4	49,7	18,9	2,5	47,8	38,5	28,2	55,4	62,5	30,7	36,4	18,8	0,07	34,6	19,5	3,4	35,4	19,0	1,0
70	75,3	74,7	28,0	73,0	76,4	38,8	70,1	75,5	48,9	57,5	25,3	3,1	55,5	47,8	34,5	64,0	71,8	39,6	42,3	22,1	0,07	40,1	24,0	4,7	40,9	28,8	1,4
80	83,8	84,7	35,2	81,6	84,9	45,6	78,6	83,4	57,6	65,2	33,6	3,7	63,0	56,6	41,3	72,4	79,3	56,3	48,0	25,6	0,07	45,4	29,2	8,2	46,4	39,9	2,0
90	91,0	92,3	41,6	89,1	91,8	56,3	86,4	90,0	67,4	72,7	44,1	5,3	70,3	64,8	48,1	80,4	85,1	76,0	53,7	29,1	0,07	50,7	34,8	12,9	51,8	50,7	2,9
100	96,7	97,6	56,8	95,2	96,8	69,9	93,0	95,3	85,9	79,9	55,9	7,3	77,5	72,5	56,3	87,9	89,6	93,2	59,3	32,8	0,14	56,0	40,4	17,2	57,1	60,0	3,9
Baseline value	1193,8	0,3	62,5	###	0,4	51,5	1280,8	0,4	46,0	###	0,2	178,0	1883,0	0,3	103,0	1604,1	0,3	96,0	4358,3	0,052	1442,0	4359,4	0,100	620,5	4301,4	0,4	594,5
UM	m^3	m	min	m^3	m	min	m^3	m	min	m^3	m	min	m^3	m	min	m^3	m	min	m^3	m	min	m^3	m	min	m^3	m	min

T= 10 Years

Percentage	1 Hour									3 Hours									24 Hours								
of Greening	Rectangular			Triangular			Chiacago			Rectangular			Triangular			Chiacago			Rectangular			Triangular			Chiacago		
(%)	ΔR_V	ΔP_F	ΔD_T	ΔR_V	ΔP_F	ΔD_T	ΔR_V	ΔP_F	ΔD_T	ΔR_V	ΔP_F	ΔD_T	ΔR_V	ΔP_F	ΔD_T	ΔR_V	ΔP_F	ΔD_T	ΔR_V	ΔP_F	ΔD_T	ΔR_V	ΔP_F	ΔD_T	ΔR_V	ΔP_F	ΔD_T
0	0,0	0,0	0,0	0,0	0,0	0,0	0,0	0,0	0,0	0,0	0,0	0,0	0,0	0,0	0,0	0,0	0,0	0,0	0,0	0,0	0,00	0	0,0	0,0	0	0	0
10	10,8	1,9	1,6	10,4	4,1	4,0	9,9	6,9	5,6	7,8	2,0	0,0	7,5	1,3	1,0	8,8	1,5	1,6	5,5	2,5	0,07	5,27	2,12	0,16	5,45	0,00	0,08
20	20,3	6,4	3,2	19,6	11,9	8,0	18,6	16,5	11,2	15,0	4,2	0,3	14,4	4,1	3,0	16,8	8,0	4,2	10,7	4,9	0,07	10,31	4,48	0,49	10,63	0,09	0,25
30	29,5	14,3	5,6	28,4	22,3	14,0	27,1	27,6	18,0	22,0	6,5	0,3	21,1	9,0	6,9	24,6	18,6	7,9	15,9	7,6	0,14	15,25	7,11	1,14	15,71	2,49	0,42
40	38,6	25,2	8,9	37,2	33,8	19,0	35,5	38,8	23,6	28,9	9,0	0,6	27,8	15,6	12,4	32,3	30,8	12,7	21,0	10,0	0,14	20,14	9,90	1,38	20,69	5,89	0,51
50	47,7	37,5	12,9	46,1	45,3	24,0	44,0	49,3	30,3	35,9	11,7	0,6	34,5	23,4	17,3	40,0	42,9	17,5	26,1	12,7	0,14	24,95	12,94	2,03	25,61	10,08	0,67
60	56,7	50,2	16,1	54,8	56,3	28,0	52,4	58,9	38,2	42,8	15,0	0,6	41,2	31,6	23,3	47,7	53,9	22,2	31,2	15,7	0,14	29,72	16,24	3,09	30,45	15,15	0,84
70	65,5	62,1	20,2	63,4	66,4	33,0	60,7	67,5	43,8	49,7	19,3	0,8	47,8	39,7	29,2	55,3	63,6	29,6	36,2	18,8	0,17	34,44	19,80	4,22	35,23	21,68	1,01
80	73,8	72,8	25,0	71,6	75,3	39,0	68,7	75,3	50,6	56,6	24,6	1,1	54,5	47,6	35,1	62,8	71,6	39,7	41,2	21,7	0,17	39,10	23,69	5,69	39,96	29,93	1,43
90	81,6	82,0	31,5	79,4	83,1	46,0	76,4	82,2	58,4	63,3	31,4	1,7	61,1	55,0	41,6	70,1	78,0	51,3	46,2	24,7	0,17	43,73	28,00	8,37	44,65	39,24	1,94
100	88,6	89,6	41,9	86,5	89,6	58,0	83,6	88,1	70,8	70,0	39,7	3,0	67,6	62,1	48,5	77,3	83,1	68,3	51,1	27,7	0,17	48,32	32,57	11,62	49,32	48,35	11,12
Baseline value	1424,2	0,4	62,0	###	0,5	50,0	1526,3	0,5	44,5	###	0,2	181,0	2235,3	0,4	101,0	1907,2	0,4	94,5	5149,4	0,1	1441,0	5149,99	0,12	615,50	5081,74	0,53	593,50
UM	m^3	m	min	m^3	m	min	m^3	m	min	m^3	m	min	m^3	m	min	m^3	m	min	m^3	m	min	m^3	m	min	m^3	m	min

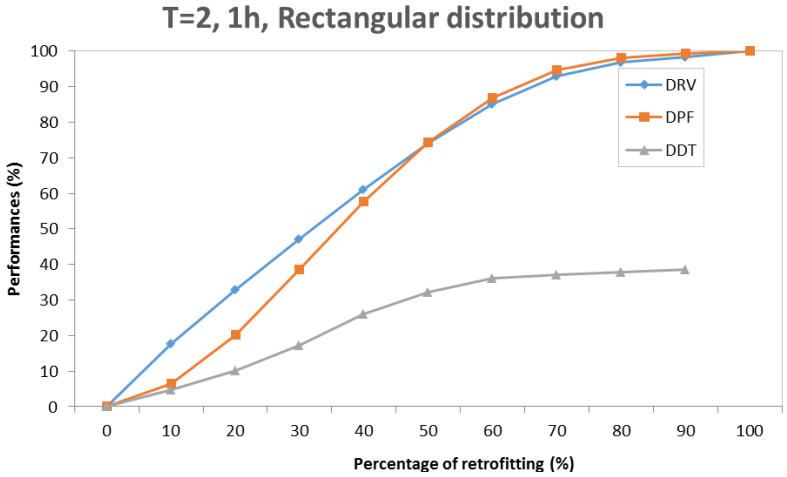

Figure 6.8 Performances in terms of ΔR_V, ΔP_F, ΔD_T varying the percentage of retrofitting.

The performances worsen for higher T because the event is more severe and the effectiveness of the green roof is lower. For instance, for short event with a rectangular distribution and a percentage of conversion of 100%, ΔR_V go from 100% (T=2 years) to 96.7% (T=5 years) to 88.6% (T=10 years). The next step has been the analysis of GR response varying the spatial GRs distribution in the basin so, the simulations have concerned four further scenarios corresponding to convert in GRs surfaces alternatively the far north (SUB1) and north (SUB2), the middle (SUB3) and the south (SUB4) side of the catchment. For illustrative purpose, an average percentage of green roofing of 50% (for a total amount of covered area of 0.5 ha), the rectangular distribution shape of the hyetographs and the duration of 1 hour have been set. The hydrological behavior for the period of 10 years has been investigated in order to consider the worst condition because green roofs return the lowest performances for 10 years storm events. Again, the percentage of reduction in runoff volume (ΔR_V), peak flow (ΔP_F) and increase in the delay time (ΔD_T) of the new scenarios compared to the baseline one has been evaluated in the outlet section of the sewer system. The results show how ΔR_V is steady, no matter the converted sub-basin because the same percentage of covered area has been set for each of them. ΔP_F decreases from the northern to the southern part of watershed while ΔD_T increases and so, closer the converted part to the outlet section of the sewer, slower the wave of runoff flow but higher its peak.

Table 6.8 GR response varying the spatial GRs distribution in the basin.

T= 10 Years			
Converted Sub-basin (50%)	1 Hour		
	Rectangular		
	ΔR_V	ΔP_F	ΔD_T
SUB1	11,5	14,1	1,6
SUB2	11,5	11,6	1,6
SUB3	11,5	8,4	1,6
SUB4	11,5	5,0	2,4
Baseline value	1424	0,4	62,0
UM	m^3	m	min

Anyway, the increase in peak delay is less significant than the attenuation of runoff volume and peak discharge. Another aspect, here investigated, is the effect of spatial scale of aggregation on GRs response and namely if and how the detail in spatial modeling of the basin can affect the simulation. For this purpose, each sub-basin has been divided into two and four smaller catchments respectively having half and one quarter of the initial area of 1 hectare and with same hydraulic characteristics. In the first scenario, a drainage system with 8 pipes of 500 meters length and eight sub-basins with an area of 0.5 ha have been considered. A conversion in GRs has been carried out alternatively on each of them using a percentage of greening of 100% in order to get the same amount of covered area of 0.5 ha as that one achieved in the previous simulations, using 50% of conversion on the initial area of 1 ha of the sub-basins(Figure 6.9). The simulations have been performed, by way of explanation, only for duration of 1 hour, return period of 10 years and rectangular distribution of the rainfall inputs. The results are shown in the following table (Table 6.9):

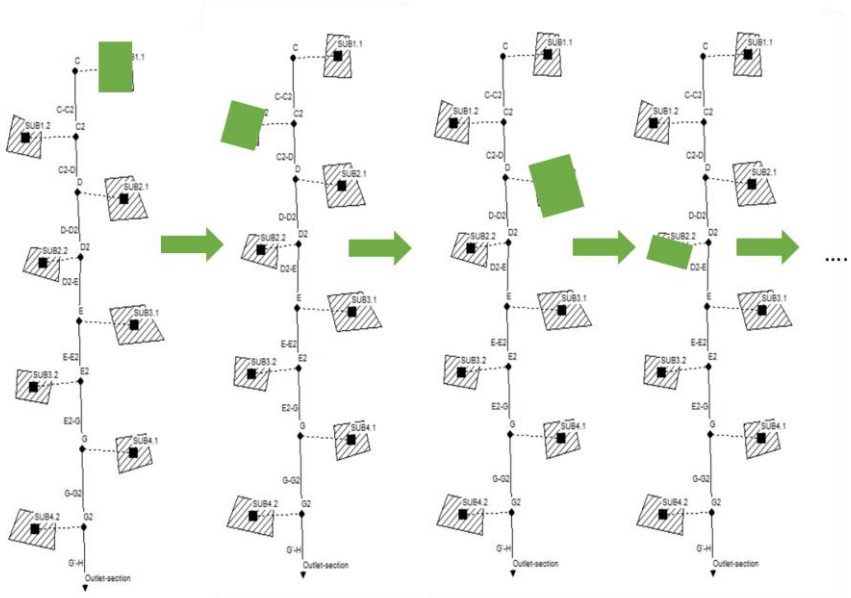

Figure 6.9 Virtual basin with 8 sub-catchment.

Table 6.9 Effect of spatial scale of aggregation on GRs response (8 sub-basins).

T= 10 Years			
Converted Sub-basin (100%)	1 Hour		
	Rectangular		
	ΔR_V	ΔP_F	ΔD_T
SUB1.1	10,42	12,24	0,00
SUB1.2	10,42	12,22	0,82
SUB2.1	10,42	11,93	0,82
SUB2.2	10,42	11,42	0,82
SUB3.1	10,42	10,72	0,82
SUB3.2	10,42	10,01	0,82
SUB4.1	10,42	8,99	0,82
SUB4.2	10,42	8,05	2,46
Baseline value	1424	0,4	61,0
UM	m^3	m	min

In the second scenario, sixteen sub-basins with an area of 0.25 ha and a sewer with 16 conduits of 250 meters have been analyzed (Figure 6.10).

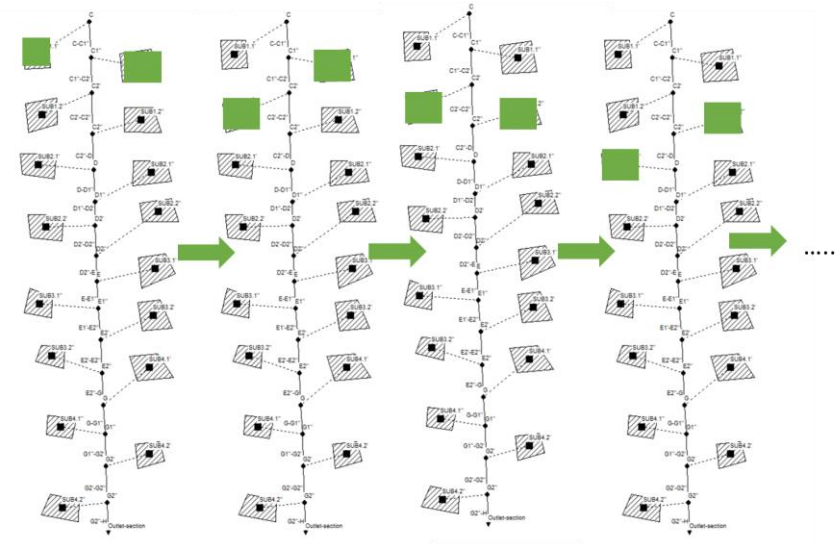

Figure 6.10 Virtual basin with 16 sub-catchment.

In this case a greening of 100% on two watersheds at once has been applied in order to reach an amount of covered area of 0.5 hectares. The results in the table below (Table 6.10).

The detailed analysis related to the hydrological impacts of GR spatial distribution along the whole catchment confirm that ΔR_V is steady, the peak linearly decreases when the variation of land use concerns the more downstream sub-basins while the opposite situation occurs for ΔD_T decreasing from the northern to the southern part of watershed. About the performances, ΔR_V and ΔD_T decreases from the scenario with 4 sub-basins to that one with 16 sub-basins while ΔP_F increases. The spatial analysis highlights that the scale used for sketching the basin isn't a basic parameter in the model and its variation doesn't return substantial changes in the results of the simulations.

Table 6.10 Effect of spatial scale of aggregation on GRs response (16 sub-basins).

T= 10 Years			
Converted Sub-basin (100%)	1 Hour		
	Rectangular		
	ΔR_V	ΔP_F	ΔD_T
SUB1.1'+SUB1.1"	10,09	12,40	0
SUB1.1"+SUB1.2'	10,09	12,43	0
SUB1.2'+SUB1.2"	10,09	12,31	0
SUB1.2"+SUB2.1'	10,09	12,02	0
SUB2.1'+SUB2.1"	10,09	11,67	0
SUB2.1"+SUB2.2'	10,09	11,21	0
SUB2.2'+SUB2.2"	10,09	10,62	0,82
SUB2.2"+SUB3.1'	10,09	9,98	0,82
SUB3.1'+SUB3.1"	10,09	9,29	0,82
SUB3.1"+SUB3.2'	10,09	8,64	0,82
SUB3.2'+SUB3.2"	10,09	8,00	0,82
SUB3.2"+SUB4.1'	10,09	7,36	0,82
SUB4.1'+SUB4.1"	10,09	6,83	0,82
SUB4.1"+SUB4.2'	10,09	6,40	0,82
SUB4.2'+SUB4.2"	10,09	5,64	1,64
Baseline value	1424	0,4	61,0
UM	m^3	m	min

7 SUDS, APPLICATION IN AN EVOLVING CATCHMENT IN THE MEDITERRANEAN BASIN

In an evolving basin where the climate change and/or the rapid urbanization are altering the rainfall-runoff response and increasing urban flooding events, the use of SUDS technique, in addition to all the benefits of different types, which have not been investigated in the present PhD dissertation, could represent a good solution for the mitigation of hydrologic and hydraulic risk, by increasing the resilience of the study area to the changing conditions. Sarno river Basin has been selected as case study because Multiple Damaging Hydrological Events (MDHEs) (Petrucci and Polemio 2003) like flooding and landslides occurred rather frequently, especially during the last fifteen years within this catchment. One of the cause of the increase of flooding events occurrences probability could be the evolving climate condition, with precipitation events featured by an increase in extreme values. Another cause could be the increase in urbanization that has a significant impact on hydrologic and ecosystems functions, and often results in excess runoff, whilst depleting groundwater and baseflows, thus increasing the vulnerability of these areas to floods, droughts and water quality problems (Jacobson 2011). The process of transformation of the natural soils to impermeable and sealed surfaces, leads indeed to an increase in the amount of surface runoff, limiting the natural phenomena of infiltration and evaporation into and from the soil surface. Since the results of the monitoring campaign conducted at the experimental site of UNISA, have confirmed the positive impact of green roofs at the building scale in the Mediterranean climate, the analysis has been focused at a greater scale (basin scale) within the same climate area.

7.1 ANALYSIS OF THE CLIMATE VARIABILITY

In order to understand the role played by the climate change in the problem of an increased frequency of flooding events within the basin under investigation, sub-hourly, hourly and daily rainfall data collected by five rain-gauge stations located within the study area, have been tested for temporal trend detection and significance (Califano et al. 2015) For stationarity analysis long term time series are needed and only five meteorological stations located within the studied catchment met those requirements. The five rain gauges (Table 7.19) close to the Solofrana basin are located in the municipalities of Baronissi, Forino, Mercato San Severino, Sarno and Serino. Stations location is indicated in the Figure 7.19. Rainfall data, for different duration and with different consistency, are available from the period 1920-2013, as indicated in Table 7.1. Failure in data collection and thus missed data has mainly occurred during the period 1940–1950, which is during and immediately after the Second World War.

Table 7.1 Rain gauge stations metadata indications.

Station	Period of observation	# of records (years)
Baronissi	1964-2013	48
Forino	1920-2013	72
M.S.S.	1920-2013	77
Sarno	1919-2013	79
Serino	1919-2013	76

As a first step analysis of climate variability, precipitation data have been screened to assess data quality, searching for potential change points in temporal patterns. A homogeneous climate data series is defined as one where variations are caused only by variations in weather and climate (Conrad et al 1950). Most long-term climatic series are affected by non-climatic factors indeed: changes in instruments, station location, station environment and so on make climate data unrepresentative of temporal climate variability. Non homogeneities produce either sharp discontinuities or gradual bias in the data, which can be detected with the use of statistical tests. A large number of approaches for change point detection have been indeed proposed and when applied to the same

series, they could actually yield conflicting conclusions, because of different climate elements relevant to the time series under investigation (Reeves et al. 2007). Given to this reason, it could be advisable to apply a number of regime shift detection methods and further critically compare them. For this purpose, four different statistical tests have been considered. These are 1) the parametric t-test, 2) the non-parametric U-test, 3) the non-parametric Pettitt's test and 4) the cumulative CUMSUM test. These tests were selected due to their proven capability in atmospheric studies (Rodionov 2005).

1) The t-test (Hald 1953) assesses whether the means of two groups (n_1 and n_2) are not statistically different from each other (null hypothesis H_0: $\mu_1 = \mu_2$). The t test statistic, which has a Student's distribution, is defined as:

$$t = \frac{\left(\overline{x_1} - \overline{x_2}\right)}{\sqrt{\frac{S_1^2(n_1-1)+S_2^2(n_2-1)}{n_1+n_2-2}\left(\frac{1}{n_2}+\frac{1}{n_2}\right)}} \qquad (7\text{-}1)$$

Where $\overline{x_1^2}, \overline{x_2^2}$ = two samples means, S_1^2, S_2^2 =the two samples variances, n_1, n_2= the two simples size. If the calculated t value is above the threshold chosen for statistical significance α, then the null hypothesis H_0: $\mu_1 = \mu_2$ that the two groups do not differ is rejected in favor of an alternative hypothesis, which states that the groups do differ (H_a: $\mu_1 \neq \mu_2$).

2) The Wilcoxon-Mann-Whitney's test is a nonparametric test used for change point detection. The null hypothesis H_0 stresses the existence of no change point. The time series is split into two samples (n_1= first sample size, n_2=second sample size) and the following indices are calculated:

$$U_1 = n_1 n_2 + \frac{1}{2} n_1(n_1+1) - R_1 \qquad (7\text{-}2)$$

$$U_2 = n_1 n_2 + \frac{1}{2} n_2(n_2+1) - R_2 \qquad (7\text{-}3)$$

$$T = \min(U_1, U_2) \tag{7-4}$$

Where R_1= sum of ranks in sample 1, R_2= sum of ranks in sample 2. If the number of elements in each sample is larger than 10, T has a standard normal distribution with mean μ_T and standard deviation σ_T:

$$\mu_T = \frac{n_1 n_2}{2} \tag{7-5}$$

$$\sigma_T = \frac{n_1 n_2 (n_1 + n_2 + 1)}{12} \tag{7-6}$$

The test statistic Z is then:

$$Z = \frac{T - \mu_T}{\sigma_T} \tag{7-7}$$

and the null hypothesis H_0 is accepted if Z is smaller than the Z-value corresponding to the chosen significance level.

3) Pettitt's test is a nonparametric test, that requires then no assumption about the distribution of data. It tests the H_0: the T variables follow one or more distributions that have the same location parameter (no change), against the alternative H_a: a change point exists. If T is the length of the time series, $x_t = \{x_1, x_2, \ldots, x_t\}$ and $x_j = \{x_{t+1}, x_{t+2}, \ldots, x_T\}$, the non-parametric statistic is defined as:

$$K_T = \max|U_{t,T}| \tag{7-8}$$

Where:

$$U_{t,T} = \sum_{i=1}^{t} \sum_{j=1}^{T} \operatorname{sgn}(x_i - x_j) \tag{7-9}$$

The change-point of the series is located at K_T , provided that the statistic is significant. For the change point, the probability of occurrences is:

$$p(t) = 1 - \exp\left(\frac{-6U_{t,T}^2}{T^3 + T^2}\right) \tag{7-10}$$

4) The CUMSUM test is a cumulative test which statistic S is defined as:

$$S_t = S_{t-1} + (x_t - \mu) \qquad for\, t = 1.....T \tag{7-11}$$

where T is the sample length and μ is the sample mean. The series is homogeneous if S is approximately 0. If St shows a maximum (minimum) a negative (positive) shift would be detected. The significance of the shift can be evaluated calculating the 'rescaled adjusted range' variable:

$$R = \frac{\max S_t - \min S_t}{\sigma_x} \tag{7-12}$$

where σ_X is the time series standard deviation. Critical values for R are given in (Buishand 1982).

The described tests have been applied to detect non homogeneities within long-term yearly precipitation data set of the 5 rain gauge stations in the Solofrana river basin, over the period from 1920 to 2013. For each gauging station and for each test, Table 7.2 indicate the relevant results, for a significance level α = 10%. Metadata have also been inspected to search for changes in rain gauge settings, in particular, in station elevation. From this point of view, metadata inspection has been considered as an additional test. Regardless for the method, if a change point is detected, a "non-homogeneity" label is associated to the station (for the particular test) and the year of occurrence is also provided. Table 7.2 clearly indicates that the five different approaches, applied to a particular time series, have provided contrasting results. As a general rule, it has been decided to critically compare the results of the tests and to conceptually intersect them. Then it has been assumed that a time series can be defined homogeneous if three of five tests provide a favorable result. Homogeneous rainfall time series will be then further analyzed for trend detection. As the number of investigated stations is rather limited, comments are provided individually. Illustrations of tests

application are provided instead for a single station (Baronissi) as an example in Figure 7.1 and Figure 7.2.

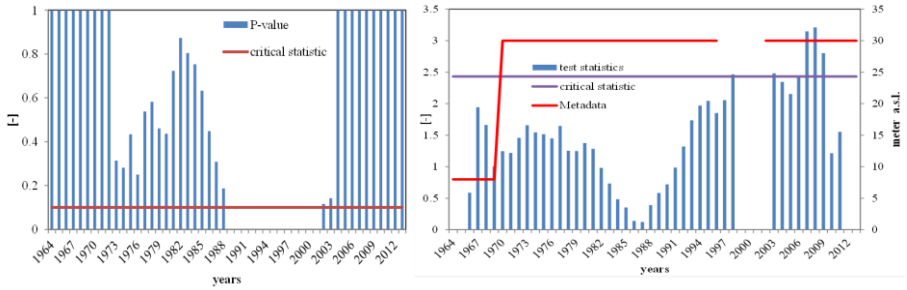

Figure 7.1 Baronissi rain gauge station change point detection test. Left panel: U-test. Right panel: t-test.

CUSUM test (Fig. 7.2 lower panel) and Student's t-test (Fig.7.1 right panel) both predict a breakpoint occurrence around 2008. Metadata, do not indicate changes in the rain gauge location. Detected shift points are not probably related to the station geographical settings but, perhaps, related to climate variability, discussed in the following paragraphs. CUMSUM test and Pettitt's test results for Forino data set do not detect a change point, whereas both Student's t-test and U-test detected it, even though located in different time period, respectively around the year 2002 and 1931. The probability of occurrence of the change point provided by the Pettitt's test is however rather small (p value= 0.430). Metadata inspection does not indicate changes in the station setting. As three of five test have provided favorable results and a fourth (Pettitt's test) has yield a very small probability of change point occurrences, the time series for the Forino station is further considered ad homogeneous. Analyzing the results of the tests on Baronissi data set, it appears that both the U-test (Fig.7.1 left panel) and Pettitt's test (Fig. 7.2 upper panel) do not predict a change point occurrence. CUMSUM test and Pettitt's test results for Mercato San Severino's data set do not detect a change point, whereas both Student's t-test and U-test detected it around the year 1942. The probability of occurrence of the change point provided by the Pettitt's test is however rather small (p value= 0.269). Metadata inspection does not indicate changes in the station setting. As three of five tests have provided favorable results and a fourth (Pettitt's test) has yield a very small probability of change point occurrences, the time series

for the Mercato San Severino station is further considered ad homogeneous.

Table 7.2 Change point detection analysis results (significance level 10%). Indication of change points occurrence year is also given.

Station	Student's t-test	U-test	Pettitt's test	CUSUM test	Metadata
Baronissi	Non homogeneity -2008	Homogeneity -	Homogeneity -	Non homogeneity -2008	Homogeneity -
Forino	Non homogeneity -2002	Non homogeneity -1931	Homogeneity -	Homogeneity -	Homogeneity -
Mercato S	Non homogeneity -1942	Non homogeneity -1942	Homogeneity -	Homogeneity -	Homogeneity -
Sarno	Non homogeneity (1959-1988)	Non homogeneity (1967-1999)	Non homogeneity -1941,1988	Non homogeneity -1941,1988	Non homogeneity -
Serino	Non homogeneity -1926	Homogeneity -	Homogeneity -	Homogeneity -	Homogeneity -

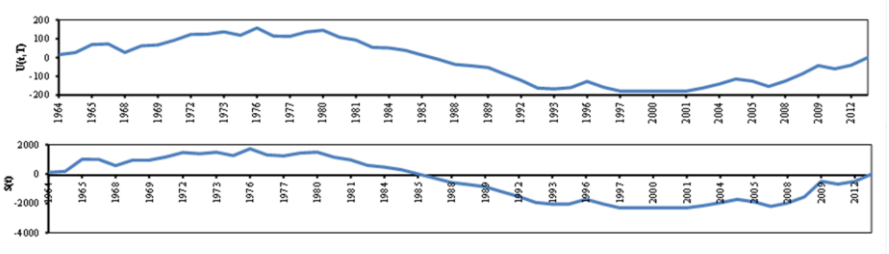

Figure 7.2 Baronissi rain gauge station change point detection test. Upper panel: Pettitt's test. Lower panel: CUMSUM test.

CUMSUM test, Pettitt's test and U-test results for Serino data set do not detect a change point, whereas the Student's t-test detected it around the year 1926. The reliability of this results is however undermined by the fact that the change point detected is located really close to the beginning of the observation. Metadata inspection does not indicate changes in the station setting. As four of five tests have provided favorable results, the time series for the Serino station is further considered ad homogeneous. In the case of the Sarno station none of the tests, included the metadata inspection, provided a favorable result in terms of time series homogeneity. The time series is then excluded from the following trend detection analysis. Subsequently time series of maximum annual rainfall, for different duration (10, 20, 30 min, and 1, 2, 3, 6, 12, 24 h), for homogeneous rain gauge stations, have been tested for linear trend detection in time. A trend is a significant change over time exhibited by a

random variable (Onoz et all. 2003) here investigated using parametric (Pearson test) and non-parametric (Mann Kendall test and Sen's test) approaches. In Pearson parametric test, the significance of the regression line is evaluated indirectly, by assessing the significance of the correlation coefficient Pearson:

$$\rho = \frac{codeviance(X,Y)}{\sqrt{dev(X)dev(Y)}} \tag{7-13}$$

High values of the correlation coefficient indicate that observed rainfall heights do vary jointly to the time variable, both in ascending or descending tendencies. It's possible use the statistics t, distributed according to the Student distribution, to define:

$$t = \frac{\rho\sqrt{n-2}}{(1-\rho^2)^{0.5}} \tag{7-14}$$

where n is the sample size and ρ is the Pearson correlation coefficient. It is possible to test the null hypothesis $H_0 \rightarrow \rho = 0$ against the alternative hypothesis $H_1 \rightarrow \rho \neq 0$ comparing the test statistic with the critical value $t_{\alpha/2}$. If t is larger than $t_{\alpha/2}$, the null hypothesis of no trend is rejected. The Pearson's test can be applied only if the observations of maximum annual rainfall heights of different duration are normally distributed. This condition has been verified with the application of the Jarque-Bera test.
One of the most used non-parametric test for the detection of monotonous trend (linear or not) is the test of Mann-Kendall (Mann 2003, Kendall 1945). Given a time series of observations $\mathbf{X}_t$, with t = 1, ..., T (sample size), the test is based on the comparison of pairs of observations (x_i, x_j), with i>j to determine whether $x_i > x_j$ or $x_i < x_j$. The test statistic is expressed formally by the relationship:

$$S = \sum_{k=1}^{T-1} \sum_{j=k+1}^{T} \mathrm{sgn}(X_j - X_k) \tag{7-15}$$

where:

$$\mathrm{sgn}(\theta)=\begin{cases}+1.....\theta>0\\ 0.....\theta=0\\ -1.....\theta<0\end{cases} \tag{7-16}$$

Under the hypothesis of independent and randomly distributed x random variable, when n ≥ 8, S statistic is approximately normally distributed, with zero mean and variance as follow:

$$\sigma^2=\frac{n(n-1)(2n+5)}{18} \tag{7-17}$$

As a consequence, the standardized Z statistics follows a normal standardized distribution:

$$Z=\begin{cases}\dfrac{S-1}{\sigma} & if \quad S>0\\ 0 & if \quad S=0\\ \dfrac{S+1}{\sigma} & if \quad S<0\end{cases} \tag{7-18}$$

The hypothesis that there is no trend is rejected when the Z value computed by eq 7-18 is greater in absolute value than the critical value Z α, at a chosen level of significance α.
The Sen's test (Sen 1962) is a non-parametric procedure providing a robust estimate for the magnitude of trend at the correspondent significance. The sample slope for each location is:

$$Q_i=\frac{x_j-x_k}{j-k}\ for \quad i=1....,N' \tag{7-19}$$

Where x_j and x_k are the data values at times j and k (j>k), respectively, N' is the number of data pairs for which j>k. The median value of N' values of Q, S, is the Sen's estimator of trend, computed as:

$$\begin{cases} S = Q_{(N'+1)/2} & if \quad N' is\, odd \\ S = \dfrac{Q_{N'/2} + Q_{(N'+2)/2}}{2} & if \quad N' is\, even \end{cases} \tag{7-20}$$

To assess whether the median slope is statistically different from zero, the confidence interval for S, for a given level of significance α, has to be computed. The confidence interval (Gilbert 1987) can be computed as follows:

$$C_\alpha = Z_{1-\alpha/2}\sqrt{Var(S)} \tag{7-21}$$

Where Var(S) is defined by:

$$Var(S) = \frac{1}{18}\left[n(n-1)(2n+5) - \sum_{p=1}^{q} t_p(t_p-1)(2t_p+5) \right] \tag{7-22}$$

and q is the number of values for which there are ties and t_p is the number of tied measurements for a particular value. $Z_{1-\alpha/2}$ is obtained from the standard normal distribution table. The approximate normal theoretical lower and upper confidence limit are respectively the M_1th largest and the (M_2+1)th largest of value of Q, where:

$$M_1 = \frac{N' - C_\alpha}{2} \tag{7-23}$$

$$M2 = \frac{N' + C_\alpha}{2} \tag{7-24}$$

The slope S is statistically different from zero if the two limits $Q(M_1)$ and $Q(M_2)$ have same sign.
The illustrated tests have been applied to detect for linear trend in long-term maximum annual rainfall heights of different duration (10, 20, 30 min, and 1, 2, 3, 6, 12, 24 h), for the data set of the 4 homogeneous rain gauge stations in the Solofrana river basin, over the period from 1920 to

2013. For each gauging station and for each test, Table 3, 4,5 and 6 indicate the relevant results, for a significance level α = 10%. The Sen's slope S is reported along with the results in terms of trend significance for each of the mentioned tests. As the time series patterns for each station produces different tendency, but essentially because the number of rain gauge stations is rather limited, it appears quite difficult to comment on a general tendency for the river basin under investigation. Regardless for the test significance, the robust S Sen's slope estimator appear to be consistently positive, for the different stations and the different rainfall duration, entailing an overall tendency toward an increase in maximum sub-daily rainfall heights and consequently intensity. Rainfall heights, compared to maximum annual average for different duration, increase on average of about 5-10% (on a ten-years base). Larger increase occurs for the Mercato San Severino station, where sub-hourly rainfall heights increases up to 40% (on a ten-years base). As an example, Figure 4 illustrates the temporal pattern of maximum annual 24 h rainfall height for the four analyzed rain gauge stations. With reference to the significance of the linear trend, provided by the different tests, differently from the case of change point analysis, the results appear to have more consistency. Baronissi (Table 7.3) and Mercato San Severino (Table 7.5) tendencies do not appear significant for none of the durations, with an exception for 24 h rainfall heights, significant according only to the Mann-Kendall test. Forino rain gauge station tendencies (Table 7.4) appear contrarily significant, for all of the durations, according to two of the three applied tests. Significant for all of the three tests appear the 24 h trend for the Serino rain gauge station (Table 7.6). From the results of the analysis, it appears quite difficult to comment on a general tendency for the river basin under investigation, since the time series patterns for each station produces different tendency, but essentially because the number of rain gauge stations is rather limited. The robust S Sen's slope estimator appear to be consistently positive, for the different stations and the different rainfall duration, entailing an overall tendency toward an increase in maximum sub-daily rainfall heights and consequently intensity, of about 5-10% (on average, on a ten-years base). However, the role assumed by climate variability in the increase of the numbers of severe events occurred within the studied river basin during the last fifteen years, cannot be established for sure. The investigation of the impact of urbanization

could guide towards a better understanding of the reasons behind the massive increase of flooding events.

Table 7.3 Baronissi rain gauge station trend detection analysis results.

Duration	mean max annual rainfall (mm)	S (Sen's slope)	Pearson's test	Mann Kendall test	Sen's test
10 min	14.4	0.05	Not significant	Not significant	Not significant
20 min	21.76	0.09	Not significant	Not significant	Not significant
30 min	26.42	0.07	Not significant	Not significant	Not significant
1 hour	39.18	0.06	Not significant	Not significant	Not significant
3 hours	62.58	-0.13	Not significant	Not significant	Not significant
6 hours	76.65	-0.11	Not significant	Not significant	Not significant
12 hours	88.90	0.03	Not significant	Not significant	Not significant
24 hours	95.90	-0.57	Not significant	Significant	Not significant

Table 7.4 Forino rain gauge station trend detection analysis results.

Duration	mean max annual rainfall (mm)	S (Sen's slope)	Pearson's test	Mann Kendall test	Sen's test
10 min	13.94	0.1	Not significant	Significant	Not significant
20 min	19.10	0.16	Significant	Significant	Not significant
30 min	23.14	0.17	Significant	Significant	Not significant
1 hour	35.02	0.19	Significant	Significant	Not significant
3 hours	43.56	0.19	Significant	Significant	Not significant
6 hours	55.86	0.24	Significant	Significant	Not significant
12 hours	73.59	0.30	Significant	Significant	Not significant
24 hours	95.91	0.39	Significant	Significant	Significant

Table 7.5 Mercato San Severino rain gauge station trend detection analysis results.

Duration	mean max annual rainfall (mm)	S (Sen's slope)	Pearson's test	Mann Kendall test	Sen's test
10 min	12.66	0.12	Not significant	Not significant	Not significant
20 min	18.64	0.20	Not significant	Not significant	Not significant
30 min	23.74	0.29	Not significant	Not significant	Not significant
1 hour	35.38	1.48	Not significant	Not significant	Not significant
3 hours	51.14	0.09	Not significant	Not significant	Not significant
6 hours	69.15	0.12	Not significant	Not significant	Not significant
12 hours	85.42	0.10	Not significant	Not significant	Not significant
24 hours	90.10	-0.11	Not significant	Significant	Not significant

Table 7.6 Serino rain gauge station trend detection analysis results.

Duration	mean max annual rainfall (mm)	S (Sen's slope)	Pearson's test	Mann Kendall test	Sen's test
24 hours	80.05	0.24	significant	Significant	significant

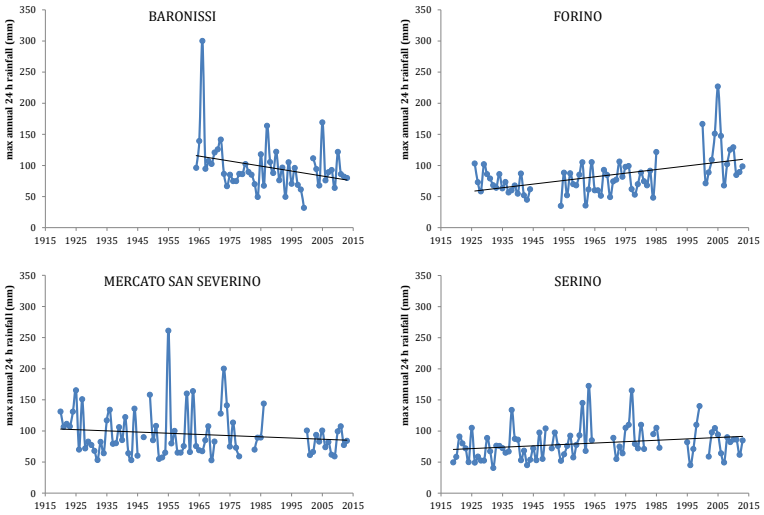

Figure 7.3 Maximum annual 24 h rainfall time series for the four investigated rain gauge stations.

7.2 ANALYSIS OF THE RAINFALL EVENTS DRIVING THE DAMAGIN EVENTS

Another aspect to be investigated is the relationship between the risk of occurrence of damaging events, and rainfall triggering event types, for the Solofrana peri-urban basin (Mobilia et al. 2015c,d, Longobardi et al. 2016, 2017). Within the Solofrana peri-urban basin, MDHEs have occurred rather frequently, especially during the last decade. A number of about 25 MDHE, occurred during the period 1951-2014, have been selected and analyzed for the purpose. Governmental agencies documentary evidences, paper and book reviews, press articles and floods/landslides catalogues have been searched and crossed to originate the MDHE inventory for the Solofrana basin, which are listed in Table 7.7. Events mainly involved the urban areas of Solofra, Montoro and Mercato San Severino municipalities (Figure 7.4) and, although they have never caused losses of lives, severe and costly damaging to the urban environment and interruption of local motorways occurred, where at least more than 50 people reported affected (Figure 7.5).

Figure 7.4 Site locations where MDHE have been recorded during last 60 years. Blue lines indicate main streams and red circles flooded areas (most frequent occurrences).

Figure 7.5 Documentary photos.

Table 7.7 MDHEs inventory for the Solofrana peri-urban catchment.

Date	Main stream	Locations	Event	Source
26/09/1951	Solofrana	Montoro	F	Vallario (2001)
22/11/1951	Solofrana	Solofra	L	SICI-CNR
02/11/1951	Solofrana	Solofra	F	Vallario (2001)
02/11/1951	Calvagnola	M.S.S.	F	Vallario (2001)
03/02/1960	Solofrana	Solofra	F	SICI-CNR
03/02/1960	Solofrana	Forino	L	SICI-CNR
18/10/1961	Solofrana	Montoro	F	Vallario (2001)
07/03/1964	Solofrana	Solofra	F	SICI-CNR
25/10/1966	Solofrana	M.S.S.	F	Vallario (2001)
29/08/1974	Solofrana	Solofra	F	SICI-CNR
29/08/1974	Solofrana	Montoro	F	SICI-CNR
29/08/1974	Solofrana	Forino	L	SICI-CNR
21/10/1981	Solofrana	Montoro	F	SICI-CNR
21/01/1981	Solofrana	Montoro	F	Vallario (2001)
18/11/1985	Solofrana	Forino	L	SICI-CNR
14-16/07/1986	Solofrana	Montoro	F	Vallario (2001)
23/12/1986	Solofrana	Solofra	L	Vallario (2001)
20/08/1993	Solofrana	Solofra	L	Landslides/flood catalogue, Vallario (2001)
04/03/1995	Solofrana	Solofra	F	SICI-CNR
02/04/1996	Solofrana	Solofra	F	SICI-CNR
01/09/1997	Solofrana	Solofra	F	SICI-CNR
01/12/1997	Solofrana	Forino	L	SICI-CNR
05/05/1998	Solofrana	Montoro	F/ L	Landslides/flood catalogue, Vallario (2001)
21/08/1998	Solofrana	Montoro	F	SICI-CNR
04/11/2000	Solofrana	Solofra	F	SICI-CNR
04/11/2000	Solofrana	M.S.S.	F	SICI-CNR
04/11/2000	Solofrana	Montoro	F	SICI-CNR
04/11/2000	Solofrana	Forino	L	SICI-CNR
09/11/2001	Solofrana	Montoro	F /L	Local municipalities website
09/11/2001	Calvagnola	M.S.S.	F	Local municipalities website
28/09/2007	Solofrana	Montoro	L	newspaper database
28/09/2007	Calvagnola	M.S.S.	F	newspaper database
13/09/2008	Calvagnola	M.S.S.	F	Local municipalities website
05/10/2008	Calvagnola	M.S.S.	F	newspaper database

Date	Main stream	Locations	Event	Source
08/01/2010	Solofrana	Montoro	L	newspaper database
08/01/2010	Solofrana	Solofra	L	landslides catalogue
30-31/07/2010	Calvagnola	M.S.S.	F	newspaper database
06/09/2011	Solofrana	Solofra	F	newspaper database
19/09/2011	Solofrana	Solofra	F	newspaper database
19/09/2011	Solofrana	Montoro	L	newspaper database
13/09/2012	Solofrana	Montoro	F	Local municipalities website
13/09/2012	Calvagnola	M.S.S.	F	newspaper database
08/10/2013	Solofrana	Solofra	L	newspaper database
01/09/2014	Solofrana	Montoro	F	newspaper database
01/09/2014	Solofrana	Solofra	F /L	flood catalogue, landslides catalogue

As a streamflow measurement database is not available for the investigated basin, the risk of occurrences of MDHE has been mainly investigated with reference to the study of the triggering rainfall events. For the studied area, the rain gauges network is made by 5 historical rain gauges, for which rainfall data observation are available, from 1920-2000 at the daily scale, and from 2000 till present at a resolution time interval of 10 minutes. They are indicated with red circles in Figure 7.6. After the 2000, two more rain gauge stations have been installed, for which rainfall data observation are available, from 2002 till present at a resolution time interval of 10 minutes. They are indicated with magenta circles in Figure 7.6. In the same figure, the municipalities affected by MDHE and main river network are also illustrated. In order to investigate the risk of occurrences of MDHE, a temporal characterization and a rainfall characterization are reported for each of the rainfall events triggering the MDHEs indicated in Table 7.7. The analysis is aimed at a classification of the meteorological events to supply a set of precipitation event types and related risk of occurrences classes. Preliminarily, the temporal characterization of the MDHEs occurrences has been investigated. Results are indicated in Figure 7.7. On a seasonal base, it is rather evident how the largest fraction of damaging events occurs within the autumn station, where, in particular for the months of September and October, about 58% of the total number of events have been reported.

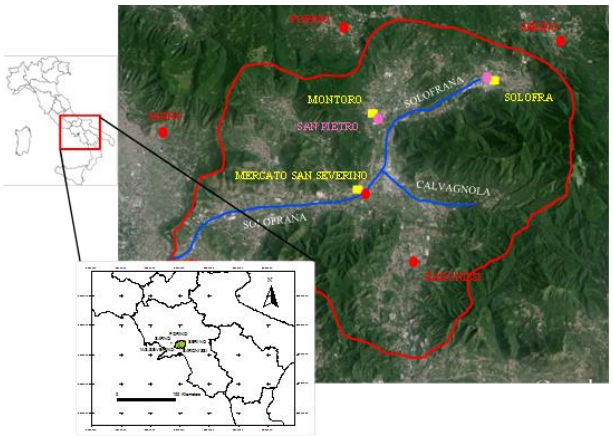

Figure 7.6 The area under investigation and the rain gauges network. Yellow squares: site locations where MDHE have been recorded during last 60 years. Red circles: historical rain gauge stations. Magenta circles: rain gauge station installed after 2000. Blue lines: main streams network.

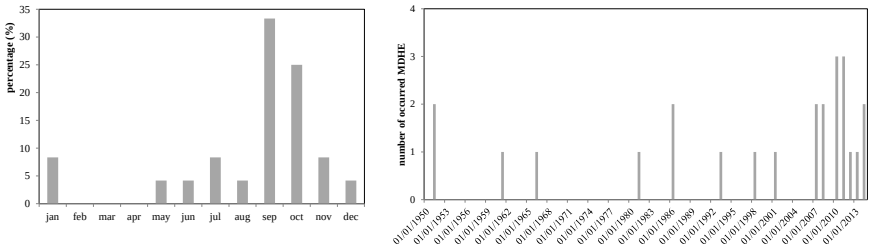

Figure 7.7 Temporal distribution and characterization of occurred MDHE in the Solofrana river basin.

The large percentage of occurrences in this period of the year could be related to the synoptic dynamics of hazardous winter precipitation and cyclones events moving and evolving along the Mediterranean basin within this particular season (Diodato et al. 2014). It is also worth indicate that, however, a significant number, about 12%, also occur during the summer period (from June to August). Figure 7.7 also shows that the frequency of occurrences of MDHEs has changed in time. About 60% of total investigated events are indeed reported within the last decade, from 2007 till present. Subsequently a precipitation event characterization has been performed. Because of the need for short time scale rainfall measurements, for only eighteen of the twenty-five events, a

number of characteristics have been assessed. They are reported in Table 7.9. Among these, the assessment of rainfall duration, maximum intensity, for a duration of 10 min, and cumulative precipitation volume, do not need clarifications. Precipitation events have been also distinguished on the base of the cumulative rainfall profile and on the base of the estimated return period. The event cumulative rainfall pattern, along with storm duration and intensity, provides useful information about the rainfall temporal structure. Introduced by Huff 1969, the standardized rainfall profile (SRP) represent a probabilistic description of the high variability of rainfall in time. Because of the straightforward information provided by the BSC (Binary Shape Code), the rainfall cumulative shape profile proposed by Terranova et al. 2011 has been used in the current study. BSC code is based on the comparison between the SRP and the USRP (Uniform SRP) for 0.25, 0.5, 0.75 quantiles. Considering the dimensionless duration interval 0-0.25, if the area below the USRP is larger than the area below the SRP, the relevant code for this dimensionless duration interval would be "0" and "1" in the reverse case. The same hold for the remaining dimensionless duration interval. An example of application is provided in Figure 7.8.

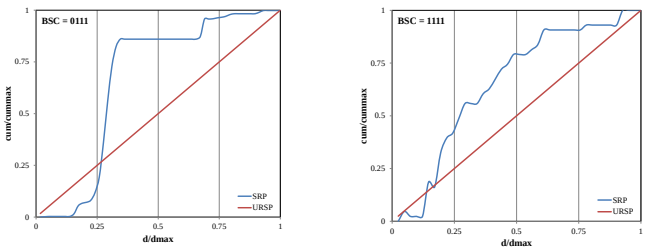

Figure 7.8 MDHEs BSC types most frequently occurring within the Solofrana river basin. Left panel represent BSC for the 19/09/2011 event. Right panel represent BSC for the 08/10/2013 event.

To assess the return period (T) the method of the index flow has been used:

$$i_T(d) = K_T \cdot i_m(d) \tag{7-25}$$

With:

im(d) is the average value of annual maximum intensity of rain with duration "d" of 10 minutes.
It derives by the regional law in four parameters of VAPI Campania report:

$$i_m = \frac{i_0}{\left[1+\frac{d}{d_c}\right]^{c-D\cdot Z}} \tag{6-22}$$

Where:
i0, dc, C, D are the parameters of the law, tabulated according to homogeneous areas (Area 2), z is the altitude of the basin (400 m.a.s.l.), iT(d) is the intensity of rain with assigned return period corresponding to the observed intensity and KT is probabilistic factor of growth expressed as:

$$K_T = -0.0373 + 0.517 \cdot LnT \tag{7-26}$$

Reversing the equation, T can be calculated for each event.

Table 7.8 Parameters for the homogeneous areas.

Homogeneus area	i_0 (mm/h)	d_c(h)	C	D*10^5
1	77.08	0.3661	0.7995	36.077
2	83.75	0.3312	0.7031	77.381
3	116.7	0.0976	0.7360	87.300
4	78.61	0.3846	0.8100	24.874
5	231.8	0.0508	0.8351	10.800
6	87.87	0.2205	0.7265	88.476

Table 7.9 reports the main characteristics of occurred MDHE, from 1998 till current time. Prior that period, detailed rainfall records for short time interval are indeed not available. Overall, MDHE are featured by average duration of 510 min (± 49 min, 5% significance level), max intensity (10 min) of 66 mm/h (± 4 mm/h, 5% significance level) and cumulative rainfall of 54 mm/h (± 4 mm, 5% significance level). BSC type 0111 and BSC type 1111 occur with the same frequency, of about 85%, typical of thunderstorm and convective rainfalls (Terranova et al.

2014). BSC type 0000, typical of stratiform precipitations, occurs with a frequency of about 19%. With reference to the return period T associated to each of the event, stratiform rainfall are generally associated to ordinary events (T < 10 year) whereas convective and thunderstorms could originate different event types, from ordinary to extremely severe.
The 50% of analyzed events fall into the category of ordinary events. MDHE with T < 5 years are characterized by maximum rainfall intensity (10 min) lower than the average maximum value of about 64 mm/h (10 min). Durations and cumulative rainfall ae also below the relevant average values. One of nine MDHEs with T < 5 years (13/09/2012 in Montoro) has been featured by very long duration, about 1000 min, however with a moderate cumulative rainfall amount. Within this class of event, the most frequent BSC is represented by type 1111, occurred with a frequency of 43%.
The 33% of analyzed events fall into the category of moderate events. MDHE with 5 < T < 25 years are characterized by maximum rainfall intensity (10 min) comparable with the average maximum value of about 64 mm/h (10 min). Durations are quite variable, from a minimum of 270 min to a max of 1800 min, but there is no clear tendency between durations and cumulative rainfall, which is however mainly above the average value of 51 mm. Within this class of event, the most frequent BSC is represented by type 1111, occurred with a frequency of 50%.
Respectively two and one of eighteen events (11%) and (5%) fall into the category of severe (25 < T < 100) to extremely severe events (T > 100). The reduced number of events makes meaningless any statistical consideration, but it appears clear that they are featured by very large max intensities, with an increase, compared to the average max value, of about 150% for the 01/09/2014 event, the most severe occurred so far within the studied basin. The analysis highlights that flooding and landslides events occurred within the studied catchment also for rainfall events of very moderate intensity and/or severity and low return period. They represent the 50% of total analyzed critical situation and this proportion is likely the expression of the fragile equilibrium and scarce resilience of peri-urban surfaces expanded in areas unsuitable for settlements and developments. In light of this, the SUDS techniques, proved to be particularly effective for rainfall events with low return period, could be successfully used in order to solve the issue of urban flooding events in this context.

Table 7.9 MDHEs and main rainfall characteristics.

Date	Main stream	Duration [min]	Max intensity (10 min)[mm/h]	cum rainfall [mm]	BSC	Return period [years]
05/05/1998	Solofrana	1800	7.6 (60min)	93.6	0	10
09/11/2001	Solofrana (Montoro)	43	31.8	33.6	0	2
09/11/2001	Calvagnola (MS Severino)	720	63.6	43	111	10
28/09/2007	Solofrana (Montoro)	270	64.8	44.8	1111	10
28/09/2007	Calvagnola (MS Severino)	300	86.4	54.6	1111	15
13/09/2008	Calvagnola	90	39.6	16	111	4
05/10/2008	Calvagnola	310	24	18.6	1111	2
08/01/2010	Solofrana (Solofra)	600	58.5	80	0	5
08/01/2010	Solofrana (Montoro)	-	-	-	-	-
30-31/07/2010	Calvagnola	120	32.4	17.4	111	5
06/09/2011	Solofrana	60	103.2	38	111	25
19/09/2011	Solofrana (Solofra)	640	106.8	91	110	25
19/09/2011	Solofrana (Montoro)	-	-	-	-	-
13/09/2012	Solofrana (Montoro)	990	54	56.4	1111	5
13/09/2012	Calvagnola (MS Severino)	450	64.6	73.8	111	10
08/10/2013	Solofrana	410	9.6	8.6	1111	2
01/09/2014	Solofrana (Montoro)	860	82.8	57.4	1111	15
01/09/2014	Solofrana (Solofra)	580	166.8	140	111	> 100

7.3 SAR IMAGES ELABORATION

The results provided by the previous analysis don't allow to indicate the role played by the climate variability in the increase of the numbers of severe events occurred within the Solofrana river basin during the last fifteen years but perhaps the investigation of the impact of urbanization could provide better results. ISPRA (Istituto Superiore per la Protezione

e la Ricerca Ambientale- National Institute for Environmental Protection and Researc) provides a report where it shows the percentage of soil imperviousness in time derived by monitoring network and national map for North, South, Center of Italy (Ispra Ambiente 2017).

Table 7.10 Soil consuption Assessment (%) related to the geographical areas. Source:ISPRA-ARPA-APPA monitoring network.

Zone	50s	1989	1996	1998	2006	2008	2013	2015
North-West	3.7%	6.2%	6.8%	7.0%	7.4%	7.6%	8.4%	8.5%
North-East	2.7%	5.3%	6.1%	6.3%	6.8%	7.0%	7.2%	7.3%
Center	2.1%	4.7%	5.6%	5.7%	6.3%	6.4%	6.6%	6.6%
South	2.5%	4.6%	5.0%	5.2%	5.8%	6.0%	6.2%	6.3%

Unfortunately, the report stops in 2015 so no indications are provided about the current years, in addition it returns values related to macro-areas of Italy and not site-specific information. For these reasons, in the present study, the above said parameter has been estimated by the use and the elaboration of SAR (Synthetic aperture radar) images of the Sarno basin (Mobilia et al. 2018c). The process, here proposed, for the elaboration of SAR images (Figure 7.9) of the studied basin, can be organized in three chains: data acquisition, pre-processing and feature extraction blocks as the following diagram shows.

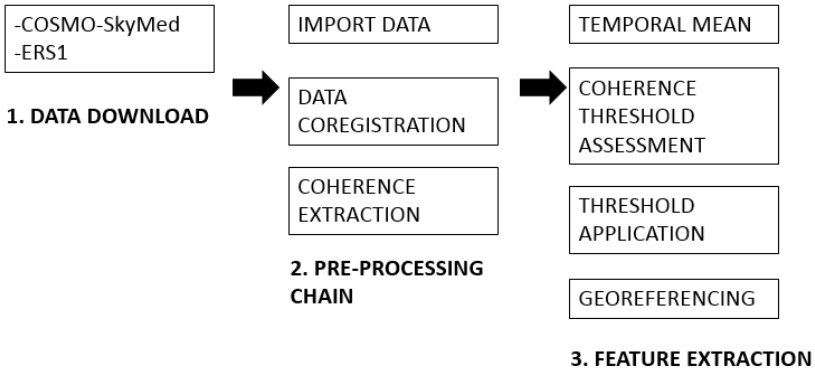

Figure 7.9 Process for the elaboration of SAR images.

The first step was the data download. Two sets of archive satellite images have been used. The first set of images consists of 6 images acquired between March and December 1995 by the ERS-1 satellite and distributed by the European Space Agency (ESA) free of charge. The

second dataset has been acquired by the COSMO-SkyMed sensor between May and December 2016, and consists of 7 images distributed free of charge by the Italian Space Agency (ASI) after the award of an "Open Call for Science". The two synthetic aperture radars have been selected because they provide the oldest and the most recent images of the considered basin. In the following, some sensor characteristics are listed:

Table 7.11 Characteristics of the two sensors.

Characteristics	COSMO-SkyMed	ERS1
Pixel size	3mx3m	8m (range) x 4m(azimuth)
Spectral band	X	C
Frequency	9.6 GHz	5.3 GHz
Wavelength	3.1 cm	5.8 cm
Orbit period	97.2 minutes	100 minutes
Nominal Repeat cyde	16 days	35 days

Finally, the two sets of images are:

Table 7.12 The two sets of SAR images.

ERS1	COSMO-SkyMed
24/03/1995	03/05/2016
08/07/1995	20/06/2016
12/08/1995	06/07/2016
21/10/1995	08/09/2016
25/11/1995	24/09/2016
30/12/1995	27/11/2016
-	13/12/2016

The Remote Sensing Software used for the elaboration is Exelis' ENVI allowing to readily read and process SAR data. The pre-processing block includes the data import, the coregistration and the coherence extraction. Coregistration is the process shifting a slave image to match the reference image. The image assigned as the master is the first, in chronological order of series while the others of the set are the slave images. In the images acquired by ERS1 and COSMO, the master images are respectively those ones acquired on March 1995 and May 2016. The next step of the block is the coherence extraction. Coherence is a measure of the phase consistency in the received signal between two SAR acquisitions (Parihar et al. 2014). So it is estimated by the cross-correlation measurements between phase values for each pair of

corresponding pixels in the two SAR images averaged over a small moving window of pixel as shown in the following formulation:

$$\gamma = \frac{\left|\Sigma S_1(x) \cdot S_2^*(x)\right|}{\sqrt{\Sigma|S_1(x)|^2 \cdot |S_2(x)|^2}} \quad (7\text{-}27)$$

Where s_1 and s_2 represent the values of phase for each couple of corresponding pixels in the two images and S_2* is the complex conjugate of S_2. In the end it highlights the variations in backscattering characteristics in terms of the radar wavelenght (Lu et al. 2014). In this work, the window size for the coherence images generation is of 3 pixels × 3 pixels. The coherence image for all interferometric pairs for the years 1995 and 2016 has been produced using as reference image the master image of the previous step. The coherence ranges between 0 and 1 where 0 represents irrelevant and 1 represents totally relevant. Built-up areas have high backscattering values because of rebound signal, single from roofs or double from the wall-ground structures and high values of coherence in time, because of the stable scattering configuration. (Strozzi et al. 1998; Chini et al., 2017) The feature extraction block includes the temporal mean of the coherence consisting of averaging per year the multi-temporal SAR images of coherence in order to reduce the speckle but not the spatial resolution. The second activity of the block is the coherence threshold assessment carried out using Otsu's method (Otsu 1979). It is a binarization algorithm allowing to convert a grey level image to monochrome (or binary) image which is particularly useful in this study for a clear distinction between the built-up areas and the other land cover classes. The assumption of this procedure is that the image contains two classes of pixels falling in foreground and background (black and white pixels) and following bimodal histogram. It iteratively calculates among all possible threshold values, the optimum threshold of intensity level "t" separating the two classes that minimizes the weighted within-class variance of the black and white pixels:

$$\min\left(\sigma_w^2(t)\right) = \min\left(W_b(t) \cdot \sigma_b^2(t) + W_f(t) \cdot \sigma_f^2(t)\right) \rightarrow \; for \quad t = \min \ldots \max \quad (7\text{-}28)$$

Where "min" and "max" are respectively the minimum and maximum intensity, σ^2_w is the intra-class variance, σ^2_f and σ^2_b are the variances of

the foreground and background classes of pixels, W_b and W_f are the weights of the two classes. The resulting threshold is about 0.3 for both series of images. After the assessment and the application of the threshold, the images have been georeferenced and converted into geotiff for GIS analysis. In the following (Figure 7.10), the clustering-based thresholding images of the basin related to the year 1995 and 2016 are shown.

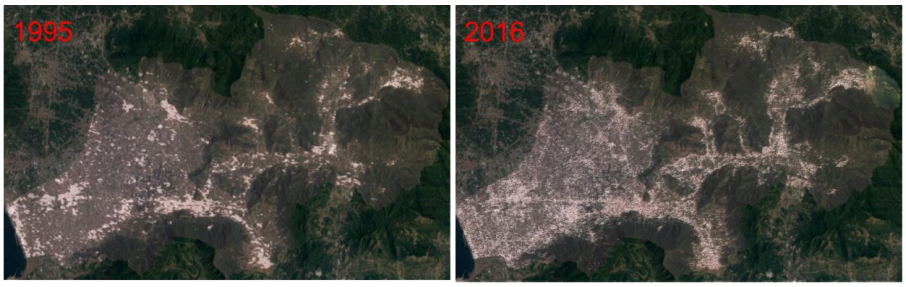

Figure 7.10 The clustering-based thresholding images of Sarno river basin.

Finally, the percentage of soil sealing for Sarno basin and its sub-catchments has been deducted from the ratio between the number of pixels of the images related to the built-up area (white pixels) and the total number of pixels(Table 7.13).

Table 7.13 Built-up area in each sub-basin.

Basin	Total area	1995		2016	
Name	Pixel	Impervious area (Pixel)	Built-up area (%)	Impervious area (Pixel)	Built-up area (%)
Sarno	736237	54494	7,40	91123	12,38
Calvagnola	71087	7105	9,99	9203	12,95
Complementary	300314	31638	10,53	55320	18,42
Solofrana	364836	15751	4,32	26600	7,29
ISPRA (South)	-	-	5,00	-	6,30

The percentage of soil imperviousness increases from 1995 to 2016 for each basin. The maximum range of variation over this period, has been reached by the complementary basin while the minimum one by Calvagnola basin with 7.89% against 2.95%. For the Southern Italy where the studied basin is located, ISPRA report proposed a percentage of soil sealing of 5% in 1996 and 6.3% in 2015. These percentages are consistent with that one found using SAR images for Solofrana basin (4.32% in 1995 and 7.29% in 2016) while they show an overbuilding in the rest of the catchment compared to the regional average and anyway

they highlight a rapid increase of the sealing areas in the last decades (Figure 7.11).

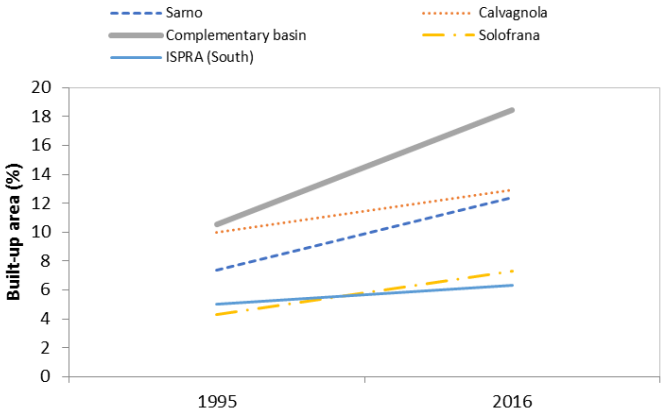

Figure 7.11 Evolution of build-up area in time.

The results of SAR images elaboration confirm that the large number of damaging events, and the relative increase in the last decade, is most likely caused by the increase in sealed surfaces. Because the reason of the increased number of flooding events within the Sarno basin is mainly attributable to the overbuilding of the surface, the retrofitting of buildings with green roofs could represent a valid solution.

7.4 SIMULATION AND RESULTS FOR SARNO RIVER BASIN

The rapid urbanization occurring in Sarno river basin and its high vulnerability also to rainfall events of very moderate intensity and/or severity, suggest that the use of SUDs could represent a good solution for the mitigation of hydrologic and hydraulic risk. In order to check whether that objective can really be achieved in the Sarno catchment, an analysis of the hydrological impact at basin scale resulting from the widespread implementation of green roofs, has been performed. Sarno river basin is a catchment of about 434 Km^2 located in Campania region, in the South of Italy that can be inscribed within a box whose corners have the following geographic coordinates:

Table 7.14 Coordinates of the study area.

E			N			Corner
14°	27'	43"	40°	53'	58"	Upper left
14°	26'	29"	40°	41'	30"	Bottom left
14°	52'	36"	40°	40'	23"	Bottom right
14°	54'	39"	40°	53'	30"	Upper right

The basin has three major tributaries: Sarno, Solofrana and Cavaiola with a length of the main courses respectively of 18.4 km, 24.8 km, 10.2 km whose sub-basins have an area of 177 km^2, 216 km^2, 41 km^2. Analisys of Digital elevation model (DEM) within GIS software return average watershed slope respectively of about 13%, 32%, 17%.

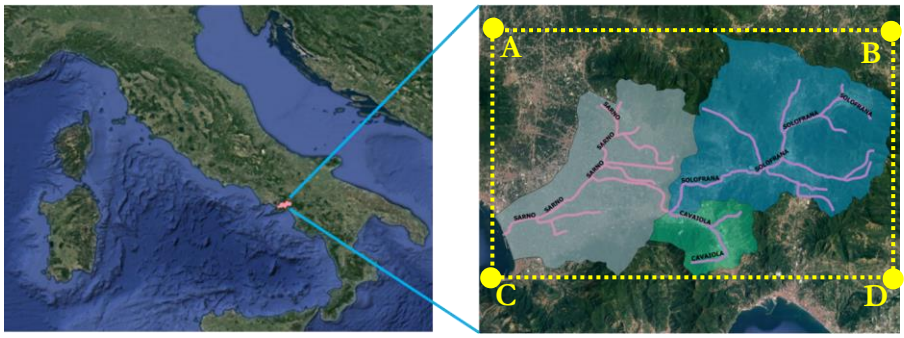

Figure 7.12 The area under investigation.

The catchment has a time of concentration (tc) of about 10 hours. It has been detected according to Haktanir et al. 1990 formula that is the most suitable for the Sarno basin because it has been calibrated for urban basins with area between 11 and 9867 Km^2:

$$t_c = 26.85 \cdot L^{0.841} \qquad (7\text{-}29)$$

Where L (m) is length of the main course.

The name and location of each node, sub-catchment and link useful for the modeling in SMWW are shown in the Figure 7.13:

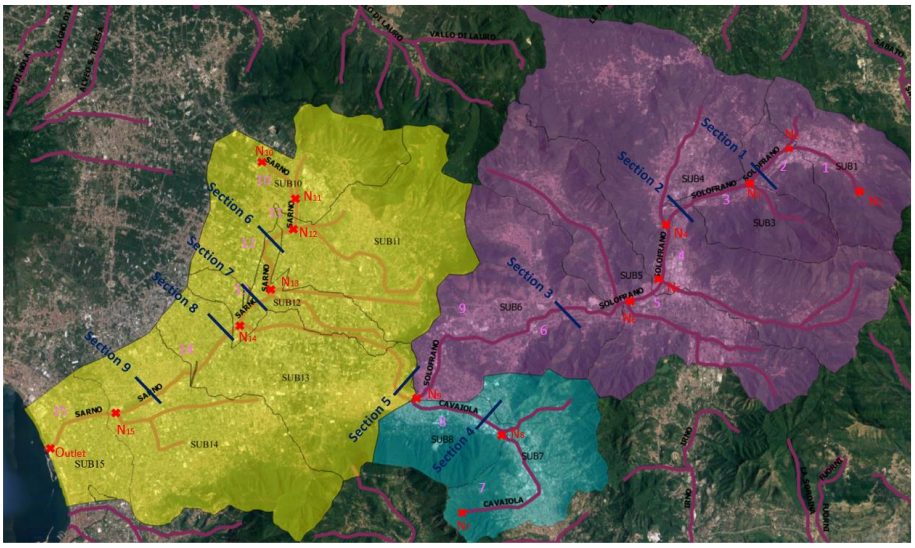

Figure 7.13 Sub-catchments, trunks and nodes of Sarno river basin.

Finally, in SWMM, Sarno river basin can be sketched as in Figure 7.14. The main properties of the elements like the area of sub-catchments, the width of overland flow, the average surface slope, the elevation of junctions, the conduit length (provided by GIS analysis of DEM with QGIS), the percentage of impervious area (provided by SAR images), and the conduit's cross section geometry (Figure 7.15) provided by Arcadis 2017 for each section where the main river joins its tributaries, are listed in the table 7.15.

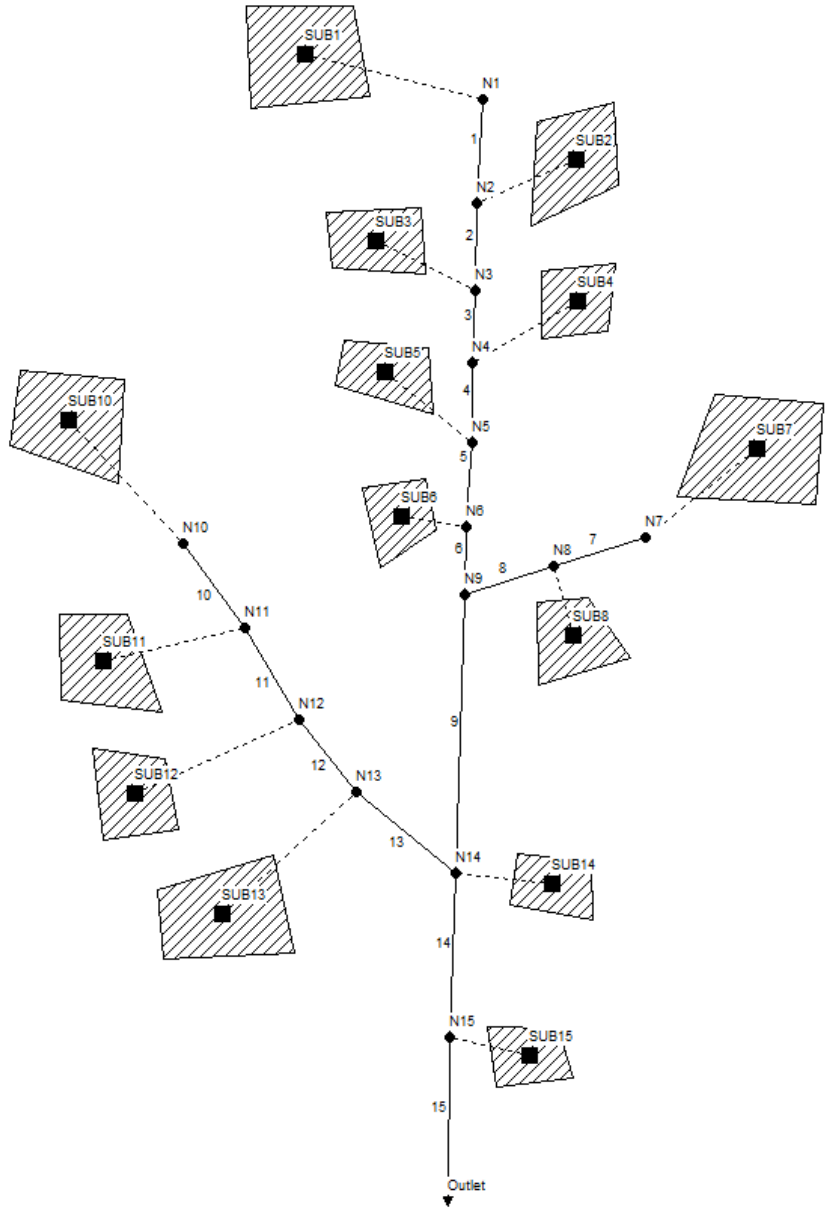

Figure 7.14 Sarno river basin in SWMM.

Table 7.15 The main properties of the sub-catchments, trunks and nodes of Sarno river basin.

BASINS				
	AREA (m^2)	WIDTH (m)=A/L	Slope (%)	Imperviousness (%)
SUB1	20729768	5670	50,76	4,11
SUB2	7208400	3356	31,08	8,64
SUB3	12926400	3474	46,86	3,61
SUB4	86120357	38412	31,06	5,46
SUB 5	46277145	22389	36,51	7,71
SUB6	41805449	3803	42,50	13,08
SUB 7	27857817	4417	29,29	12,55
SUB 8	13999902	3551	2,46	14,01
SUB10	30484451	14139	30,89	8,24
SUB11	38240603	32966	7,73	10,06
SUB12	12749286	3755	0,72	14,68
SUB13	38054512	19882	2,29	21,92
SUB14	44142885	7027	9,35	26,27
SUB15	13991174	3961	22,92	32,58

RIVERS			
	Trunk	Lenght (m)	Shape (-)
Solofrana (24826 m)	1	3656	Section 1
	2	2148	
	3	3721	Section 2
	4	2242	
	5	2067	
	6	10992	Section 3
Cavaiola (10250 m)	7	6307	Section 4
	8	3943	
S. Mauro (8880 m)	9	8880	Section 5
Sarno (18439 m)	10	2156	Section 6
	11	1160	
	12	3395	
	13	1914	Section 7
	14	6282	Section 8
	15	3532	Section 9

NODES	
	Altitude (m a.s.l.)
N1	562,5
N2	300
N3	250
N4	175
N5	162,5
N6	125
N7	600
N8	100
N9	50
N10	24
N11	22
N12	20
N13	16
N14	13
N15	5
Outlet	0

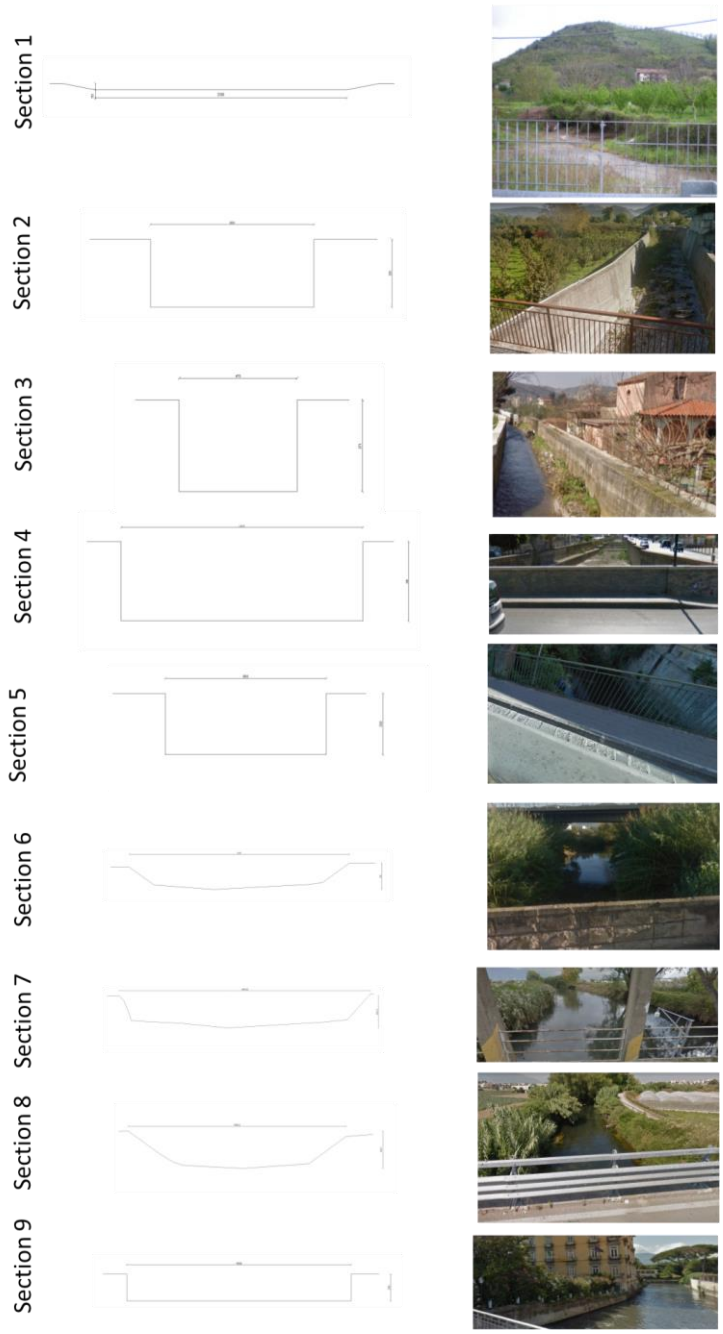

Figure 7.15 Conduit's cross section geometry (in centimeters) for each section where the main river joins its tributaries.

Because the percentage of imperviousness in the sub-basins (from SAR images) is at most of 32%, a CN of 61 has been set (Table 7.16).

Table 7.16 SCS Runoff Curve Numbers (Antecedent moisture condition II).

	Hydrologic Soil Group			
Land Use Description	**A**	**B**	**C**	**D**
Cultivated land				
Without conservation treatment	72	81	88	91
With conservation treatment	62	71	78	81
Pasture or range land				
Poor condition	68	79	86	89
Good condition	39	61	74	80
Meadow Good condition	30	58	71	78
Wood or forest land				
Thin stand, poor cover, no mulch	45	66	77	83
Good cover[2]	25	55	70	77
Open spaces, lawns, parks, golf courses, cemeteries, etc.				
Good condition: grass cover on 75% or more of the area	39	61	74	80
Fair condition: grass cover on 50 - 75% of the area	49	69	79	84
Commercial and business areas (85% impervious)	89	92	94	95
Industrial districts (72% impervious)	81	88	91	93
Residential[3]				
Average lot size (% Impervious[4])				
1/8 ac or less (65)	77	85	90	92
1/4 ac (38)	61	75	83	87
1/3 ac (30)	57	72	81	86
1/2 ac (25)	54	70	80	85
1 ac (20)	51	68	79	84
Paved parking lots, roofs, driveways, etc.	98	98	98	98
Streets and roads				
Paved with curbs and storm sewers	98	98	98	98
Gravel	76	85	89	91
Dirt	72	82	87	89

This value is related to a surface with grass cover on 75% or more of the area with a hydrological group B of mid-level (A,B,C,D respectively

stand for high, moderate, slow and very slow infiltration rates) and for antecedent moisture condition II related to average condition of moisture of the pervious surfaces prior to the rainfall event (Table 7.17).

Table 7.17 Seasonal rainfall limits for AMC.

	Total 5-day antecedent (mm)	
AMC group	**Dormant season**	**Growing season**
I	Less than 13	Less than 36
II	13 to 28	36 to 53
III	More than 28	More than 53

The model has concerned only the superficial drainage system because of the lack of data related to the urban drainage system.
The study has been carried out considering a baseline scenario and a scenario with 50% of impervious surface converted into GRs and evenly distributed in each sub-basin. The simulations have been run with a 5 years return period design storm, rectangular distribution of the hyetographs, and durations of 3, and 24 hours (Figure 6.7) respectively shorter and higher than the lag time of the basin and finally 10 hours comparable to the t_c. (Figure 7.14)

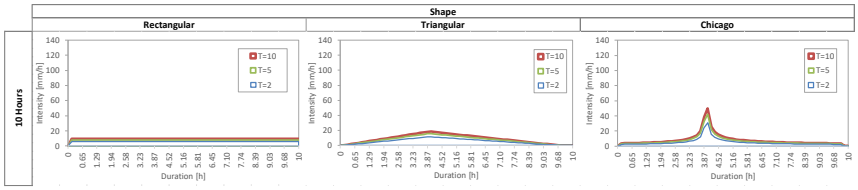

Figure 7.16 Synthetic hyetographs for duration of 10 hours.

The analysis of the performances has concerned only the reduction of runoff production in terms of flooding volume which has been proved to be (Table 6.7) the major benefit the green technologies bring. The design events cause flooding in several sections of the catchment, the use of GRs allows a decrease of the flooding volume and a reduction of number of sections affected by this damaging event (Table 7.18, Figure 7.17). The average reduction is about of 57% against 43% of the virtual basin for the same return period and percentage of greening but with different cover types and so CN (61 vs. 98) influencing the peak rate of runoff from rainfall. In addition, as suggested by the analysis of the

virtual basin (Table 6.7), the reduction increases for shorter events. The percentage of flooded sections decreases more than half.

Table 7.18 Percentage of reduction of flooded sections and flooding volume occurring for design storm events in Sarno basin.

		Flooding		
Duration	Percentage of Greening	Volume (m^3)	Reduction (%)	Flooded sections (%)
3H	0%	2188159,65	61,34	31,25
	50%	846045,69		12,50
10H	0%	8153567,05	54,09	37,50
	50%	3742926,25		18,75
24H	0%	15080789,80	57,04	31,25
	50%	6478548,11		6,25

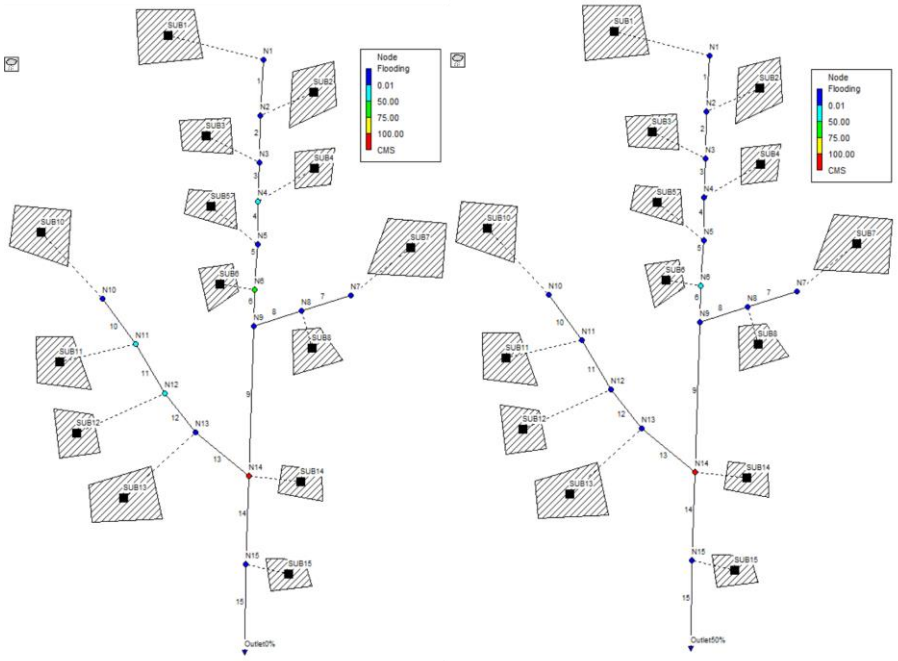

Figure 7.17 Flooded sections and flooding volume before (left panel) and after (right panel) the retrofitting, occurring for design storm events

These simulations have been run with a constant and uniform spatial distribution of rainfall over the watershed. This condition can affect both the hydrological response and the effect of the mitigation due to GR retrofitting. In order to avoid these situations, in the following,

simulations have been run with an actual event also in relation to the spatial distribution of rainfall. In the end, after the analysis with design events, the study involves simulations with actual events occurred in the past and causing MDHEs (Multiple Damaging Hydrological Events) (Table 7.7).
Event analysis has been carried out with the rainfall event occurred on 13 September 2012, belonging to the collected database of the MDHEs, as it known that during this period a real event has occurred. The event has a return period of 5 years, a duration between 7 and 8 hours and it has been chosen for the simulations because the GR technique is more effective for low T (Table 6.7).
A rainfall time series, defined with Thiessen method, has been assigned to each sub-basin. Thiessen (Voronoi) polygons identify the area of influence around each rain gauge so that any point inside the polygon is closer to the considered rain gauge than any of the other ones. The construction of a polygon requires to draw the perpendicular bisectors of the lines between all neighboring rain gauges of the set. In the table 7.19, a list of rain gauges in the Sarno river basin is shown.

Table 7.19 List of rain gauges in the Sarno river basin.

Rain Gauge	ID	Longitude	Latitude	Altitude (m a.s.l.)
Solofra	18933	14,855111	40,823667	534
S. pietro	12290	14,786972	40,818472	209
Serino	21746	14,844528	40,891361	327
Forino	18939	14,745806	40,860056	399
Mercato S.S.	17406	14,752889	40,778417	141
Barnonissi	21774	14,766278	40,751278	226
Pellezzano	18925	14,756528	40,728806	369
Cava de' tirreni	18917	14,702306	40,705972	195
Bracigliano	38443	14,711167	40,824806	349
Cetronico	15279	14,708417	40,809611	265
Ponte camerelle	12298	14,684833	40,73425	97
S. Mauro	12294	14,632333	40,764083	29
Corbara S.Egidio	18923	14,601278	40,724833	475
Chiusura sarno	15276	14,47725	40,732028	24
Lettere	18927	14,532028	40,703556	291
S Marzano sul sarno	36887	14,573306	40,779944	14
Sarno	15276	14,614139	40,8295	124
Sarno acqu. Campano	38445	14,595194	40,835194	162
Piani di Prato	15280	14,648722	40,834889	840
Toriello	15285	14,625861	40,847528	840
Quindici torre vecchia	15282	14,657333	40,855083	357
Pizzolano	38977	14,786639	40,785028	244
Giffoni valle piana	18964	14,912083	40,786806	980
Castiglione del Genovesi	21778	14,848306	40,720028	512

Figure 7.18 reports the main characteristics of the rainfall event occurred on 13/09/2012 and recorded by the several rain gauges.

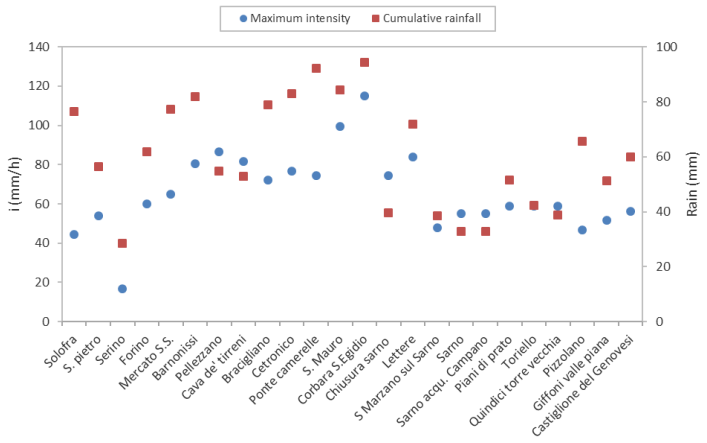

Figure 7.18 Characteristics of the studied rainfall event.

As the Figure 7.18 has pointed out, the same event, occurred in different locations, has different characteristics but also a different temporal evolution (Figure 7.19) (different pre-onset, onset, peak, decay, and post-decay). This underlines the rainfall variability in the basin, hence the need to consider a spatial distribution of the rain using the Thiessen method.

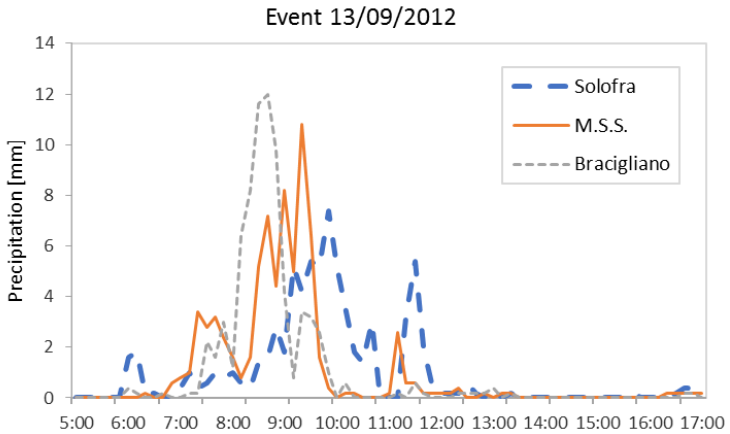

Figure 7.19 Rainfall records from 3 rain gauge stations in Sarno basin.

For the study area, the polygons appear as in the following:

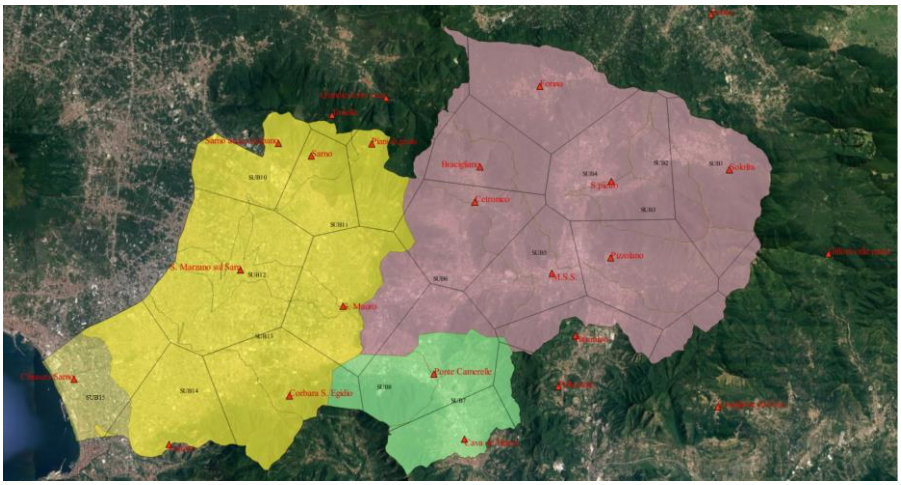

Figure 7.20 Thiessen polygons for the basin under investigation.

Each sub-basin falls into the area of influence of two or more rain gauges so the time series related to the single catchment is an average series. The results show a percentage of reduction of about 60% (Table 7.20) consistent with those ones derived from the design events for precipitation with 5 years return period and duration of 7-8 hours and a reduction of the flooded sections from 31% to 18%.

Table 7.20 Percentage of reduction of flooded sections and flooding volume occurring for actual event in Sarno basin.

		Flooding		
Duration	**Percentage of Greening**	**Volume (m^3)**	**Reduction (%)**	**Flooded sections (%)**
7-8 h	0%	5930297,43	60,25	31,25
	50%	2357421,61		18,75

The simulation highlights the sections where the flooding events occur. The section N4 corresponds to the sub-basin "SUB4" (Figure 7.21) including the municipality of Montoro where a MDHE has been reported by local websites and by newspapers database .

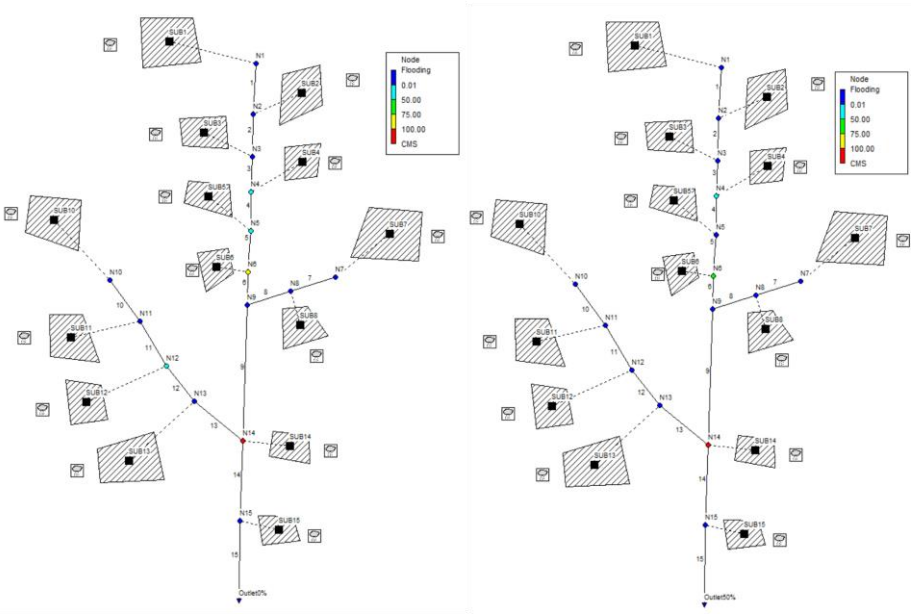

Figure 7.21 Flooded sections and flooding volume before (left panel) and after (right panel) the retrofitting, occurring for the actual event.

In particular, the damaging event occurred in via Marconi, Preturo district of Montoro, for this reason the analysis has been further deepened considering a most detailed scale of modeling (Figure 7.22).
This analysis helps to take into account the interaction between the surface hydrology because only the natural drainage system has been considered in the simulations of Sarno river basin, and the urban drainage system of the municipality of Preturo.

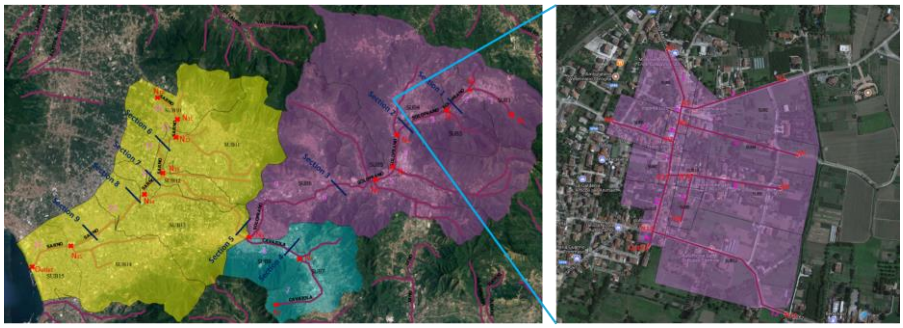

Figure 7.22 The urban drainage system of Preturo.

For the study area surrounding Via Marconi (link 1,3,5,7,11,13) the combined urban drainage network has been designed as in chapter 6 for the virtual basin. In SWMM, the urban basin can be sketched as follows:

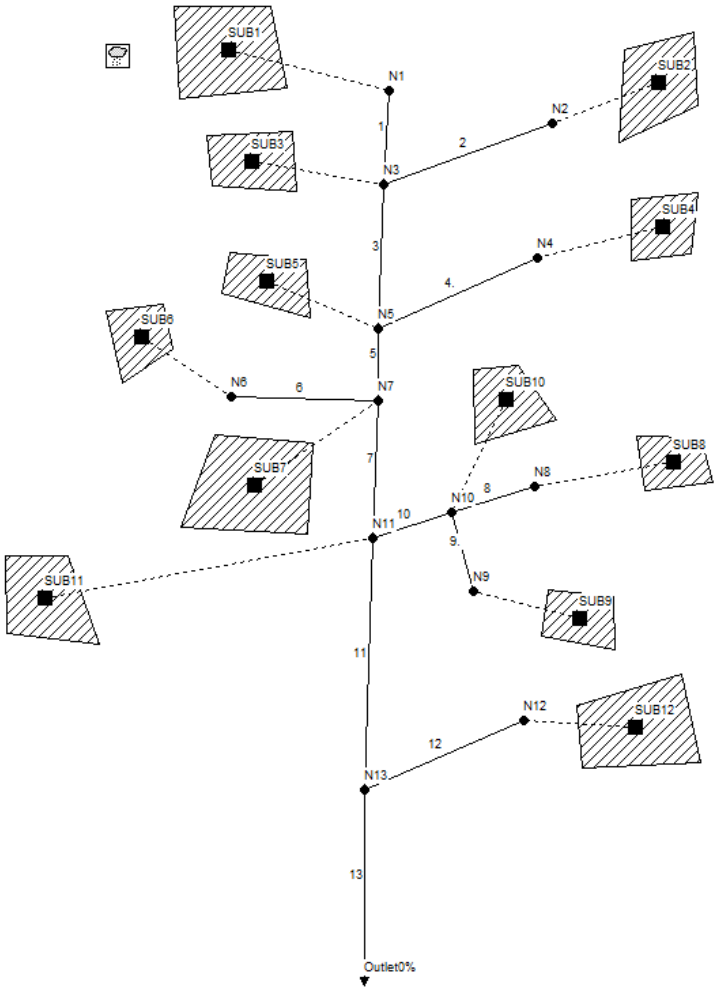

Figure 7.23 Urban drainage system of Preturo in SWMM.

The main properties of the elements required for the simulation, are listed in the following table:

Table 7.21 The main properties of the sub-catchments, trunks and nodes of Preturo district.

BASINS				
	AREA (m^2)	WIDTH (m)=A/L	Slope (%)	Imperviousness (%)
SUB1	20512	129	1	74,97
SUB2	39368	135	1	28,45
SUB3	3090	69	1	93,50
SUB4	32123	97	1	22,11
SUB 5	3665	70	1	89,52
SUB6	16939	101	1	55,24
SUB 7	12159	134	1	59,15
SUB 8	44409	186	1	27,23
SUB 9	7900	62	1	36,75
SUB10	7129	113	1	71,43
SUB11	16278	104	1	68,14
SUB12	76811	169	1	18,27
CONDUITS				
Trunk	Lenght (m)	Diameter (Circular pipes)		
1	159	DN400		
2	291	DN400		
3	45	DN600		
4	330	DN400		
5	52	DN600		
6	168	DN400		
7	91	DN800		
8	239	DN400		
9	127	DN200		
10	63	DN500		
11	157	DN800		
12	455	DN500		
13	37	DN1000		
NODES				
ID	Altitude (m a.s.l.)			
N1	188			
N2	188			
N3	186,41			
N4	188			
N5	185,96			
N6	188			
N7	185,44			
N8	188			
N9	188			
N10	185,61			
N11	184,53			
N12	188			
N13	182,96			
Outlet	182,59			

The rainfall time series used as input in the simulation refers to rainfall event occurred on 13/09/2012 and recorded by the rain gauges located

in S. Pietro in whose area of influence, defined with Thiessen method, is Preturo. In this case the comparison has been carried out between the baseline scenario (NO GRs) and a scenario where the percentage of GRs-conversion has been not set a priori but with an analysis of the green roof retrofit potential of the buildings. The identification has been performed by means of a visual inspection of the buildings using the Google Earth, Google Map and Google Streetview softwares while the detection of the buildings which can accommodate a retrofitted green roof has been based mainly on 4 criteria (Wilkinson et al. 2009):

- Roof slope

The greening should be applied to roof with a minimum slope of 2% and a maximum slope of 45%. Roofs with a slope less than 2% require additional drainage measures in order to avoid waterlogging in the vegetation support course. On the other hand, a sloped roof retains less water and structural and vegetation problems could occur like the slip of the plant layer. With Google Map the roofs of the buildings have been observed from the close quarters and they have distinguished between steeply pitched or flat roofs. All the buildings in the basin meet the requirements of the slope.

- Number of stories

Taller buildings could partially or totally overshadow the adjacent lower edifices and the shadow could affect negatively the grow of the plants and reduce ET fluxes. Because the height of each buildings is unknown, the number of stories has helped to achieve this purpose.

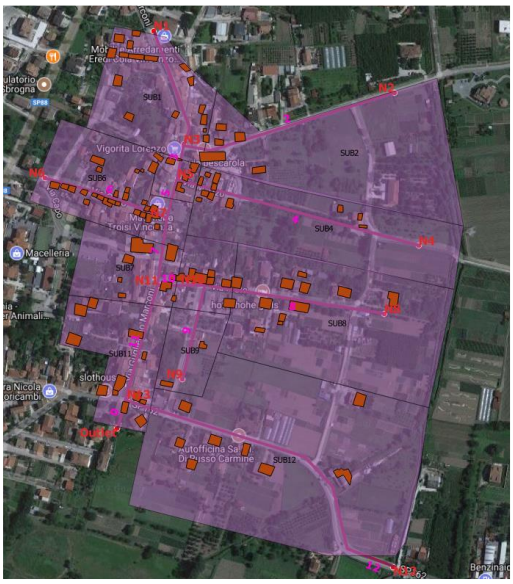

Figure 7.24 Buildings selected according to the number of stories.

- Orientation of the roof

In general, the sunlight contributes to the welfare of the vegetation and in the northern hemisphere, the exposure to direct sun is higher for south-facing buildings.

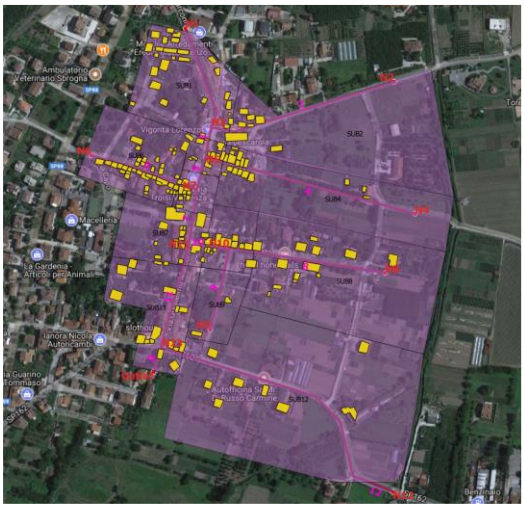

Figure 7.25 Buildings selected according to the orientation of the roof.

- Number of site boundaries

If a building is attached to others on 4 sides, during the construction of GR, the access for machinery and delivery or storage of materials tend to be difficult just like the subsequent access for maintenance. In view of this, the buildings bounded on 4 sides have been discarded.

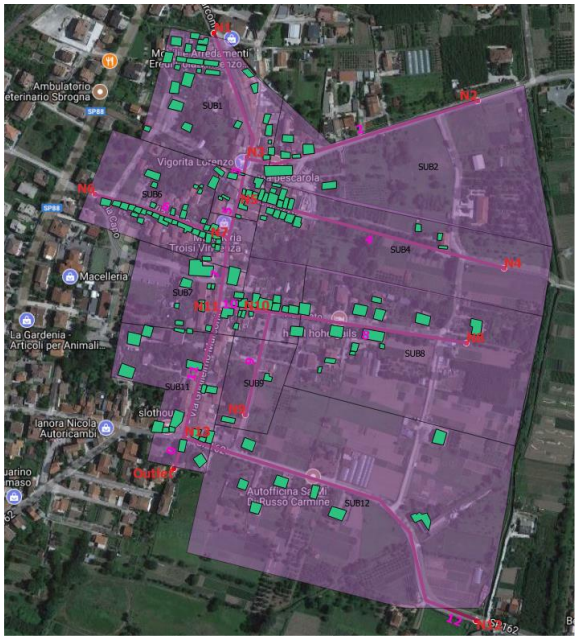

Figure 7.26 Buildings selected according to the number of site boundaries.

Finally, the buildings which contained the attributes required for green roof adaptation occupied on average about the 7% of the area of the whole basin. The percentages of green roof retrofit potential in each basin are:

Table 7.22 Percentages of green roof retrofit potential in each basin.

	% Green roof retrofit potential
sub1	7,57
sub2	2,38
sub3	12,46
sub4	2,25
sub5	8,46
sub6	8,31
sub7	9,88
sub8	4,03
sub9	2,30
sub10	14,28
sub11	10,90
sub12	2,00
Average %	7,07

The average percentage of conversion of about 7% returns a reduction in flooding volume of 11% while the number of flooding section remains unchanged.

Table 7.23 Percentage of reduction of flooded sections and flooding volume occurring using GRs for actual event in Preturo district.

		Flooding		
Duration	Average Percentage of Greening	Volume (m3)	Reduction (%)	Flooded sections (%)
7-8h	0	821,35	11,17	71,43
	7% (GR)	729,64		71,43

In situations like this where there are few buildings which can accommodate a retrofitted green roof or in a not highly urbanized urban basin, an effective management of rainfall damaging events can be reach coupling the GR technology to another SUDS technology for instance the permeable pavements (PPs) which have been proved to be very useful in reducing the surface runoff (Zachary Bean et al. 2007, Fassman et al. 2010, Pratt et al. 1989). Since GRs are not alone able to fully solve the flooding problem for the investigated basin, as also stated, for instance, with regard to a different case study by Mentens et al. 2006 who suggested to accompany the green roofs with other tools of runoff reduction, their ability in combination with PPs in addressing the issue has been investigated. The latter technique would require further

insights if interested in a sensitivity analysis aiming at verifying its performances but as the final goal is the assessment of how vegetated covers work in synergy with other sustainable urban drainage systems, in order to overcome the restrictions associated with the GRs retrofit potential, these information have been not required and default parameters for PPs have been accounted for the simulations. PPs should not been used for high speed roads, although they have been successfully applied for low speed residential streets, parking lots and paths (Virginia dcr stormwater design specification no.7 2017). The average percentage of conversion within the city of Preturo is about 15% while a detail report for each basin has been shown in the following table and Figure 7.24:

Table 7.24 Percentage of potential use of permeable pavements in Preturo district.

Basin	% of conversion
sub1	21,66
sub2	12,81
sub3	15,53
sub4	7,31
sub5	18,69
sub6	9,97
sub7	23,89
sub8	6,42
sub9	22,84
sub10	19,74
sub11	13,65
sub12	7,22
Average %	14,98

The context studied at a most detailed scale, is not characterized by a high percentage of urbanization because of this condition, the effect resulting from GRs use in term of mitigation of hydraulic risk cannot be fully highlighted. However, it should be considered that SUDS technology involves, by definition, the extensive implementation of different types of techniques, in order to reach the final goal of sustainable development. With regard to the proposed case study, by way of example, without having conducted any impact assessment, simulations have been run in SWMM considering the combination between the use of green roofs and permeable pavements. With a

combined conversion of about 7% in GRs and of about 15% in PPs, a reduction of 60% in flooding volume and of 7% in flooded sections can be reached. The use of PPs, in addition to GRs, allows a significant reduction of the flooding volume, of about 50% furthermore they can be placed on a larger area than the vegetated covers. The percentage of flooded sections hasn't significantly improved but this parameter is not indicative of the flooding problem if it is not related to the volume of runoff that actually overflows from the urban drainage system and to the geometric characteristics of the area where the flooding event occurs.

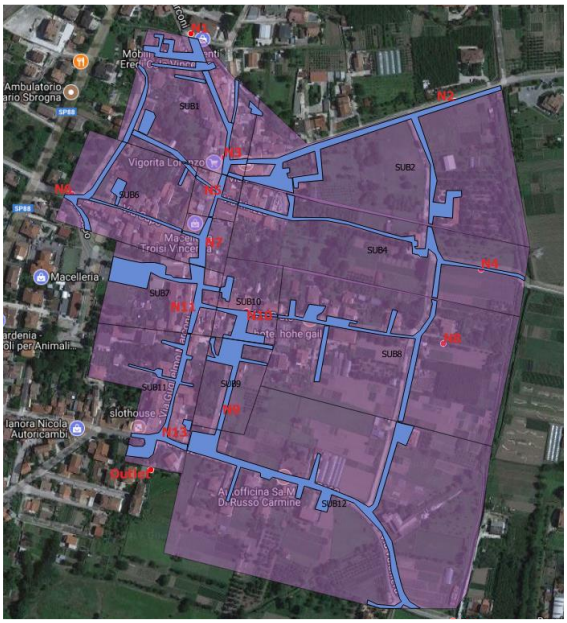

Figure 7.27 Areas selected according for the replacement with Permeable Pavements.

Table 7.25 Percentage of reduction of flooded sections and flooding volume occurring using GRs and Permeable Pavements for actual event in Preturo district.

Duration	Average Percentage of Greening	Volume (m^3)	Reduction (%)	Flooded sections (%)
7-8h	0%	821,35	-	71,43
	7% (GR)	729,64	11,17	71,43
	15%(PP)+7% (GR)	344,328	58,08	64,29

8 CONCLUSION

In this PhD dissertation, the problem of sustainable management of stormwater within a Mediterranean area with evolving climate and urban conditions and by means of SUDSs has been approached. In particular the effectiveness of the green roof technology has been explored. The GR hydrological behavior is generally modeled by soil water balance approaches where evapotranspiration loss plays an important role because it directly affects the retention effect of the eco-roofs in terms of runoff volume reduction and the original contribution of the present PhD dissertation to this aspect has been twofold. On one side, the proposal for an actual evapotranspiration assessment model which summarize the switching mechanism between energy and water limited conditions able to simulate the ET fluxes with an error of prediction at most of 20%. On the other side the integration of the latter in a conceptual water balance model approach for green roof hydrological behavior which is simply based on meteorological data but nevertheless returns an good forecasting of the storage capacity of green roofs at daily scale with maximum RMSE value of 15% . Besides the ability of the water balance approach in describing the GR behavior, the tool appears, for its peculiarities, particularly suitable for studies devoted to green-roof installation planning in a given area and also for climate sensitivity analysis. The research work has been further focusing on starting filling a gap about experimental green roof behavior in Mediterranean areas. From an experimental point of view, the contribution of the present research lies in particular in the implementation of two green roof test beds located in the campus of University of Salerno. The two GRs differ for the construction type of the drainage layer (expanded clay vs commercial drainage panel filled with expanded clay) which slightly affects the performances of the system. Preliminary results about the hydrological behavior have been shown in order to analyze the role played by the climate conditions and the GR structure in the relative behavior. The monitoring campaign confirm the effectiveness of the eco-roofs in term of the retention capacity, within the Mediterranean climatic at building scale. In fact, despite the prolonged drought periods occurring during the hot seasons in this area, survival of the plants is not

compromised and an optimal retention capacity (ranging between 35% and 100% depending on the rainfall event) is achieved during this particular period of the year. To conclude, a further novel contribution is represented by the analysis of a widespread use of GR technology to mitigate the hydrological hazard in a changing environment. The Sarno peri-urban basin in Campania region, has been selected as it represents a hydrogeological hazard prone system where flooding and landslide events have occurred rather frequently, especially during the last fifteen years. About the causes of the increase of flooding events occurrences within the study catchment, the changing climate conditions wouldn't appear to play the main role. Actually, their role cannot be established for sure because the time series patterns for the investigated stations produce different tendencies and because the number of rain gauge stations is rather limited. With the elaboration of SAR images acquired over the basin at different times, the rapid urbanization has been proved to be the main cause of the increasing urban flooding events

Subsequently, the hydrologic behavior resulting from the extensive use of SUDS technologies at basin scale has been investigated. As no green roof installations are placed in the study areas, the research efforts have focused on the potential hydrological benefits of hypothetical scenarios of rainfall and GR retrofitting. The SWMM of the US Environmental Protection Agency has been used to predict the hydraulic performances corresponding to the different greening and rainfall scenarios.

The results show that green roofs in urban areas can be a valuable tool for flood risk mitigation reaching percentage of reduction of stormwater from roofs even nearly to 100% with regard to certain rainfall characteristics and percentage of green retrofitting. These findings can be extended also to the case of the peculiar Italian building heritage, where the use of SUDS techniques and the integration of the sustainable urban drainage concept are not at all common. The results also pointed out how, in a perspective of a retrofitting scenarios, the low percentage of traditional roofs that can be converted into green is not alone able to solve the issue associated with the urban runoff management and it needs to be used in combination with other runoff reduction measures such as permeable pavements. The undertaken research work actually open the road for a multiplicity of future research perspectives, both on the theoretical, practical and experimental side.

About the experimental site, the short period of monitoring was not actually adequate to fully characterize the broad spectrum of climate

conditions that can feature the Mediterranean climate, which is known to be an extremely variable climate type. Long term measurement would most likely characterize the GR behavior under climate stress conditions, which is one of the most important concernments about the GR applicability in semi-arid areas. Furthermore, since the analysis have highlighted that the behavior of the experimental benches is strongly driven by the mode of operation of the drainage layer, a wider effort should be spent in order the improve the knowledge of the processes occurring to identify the dependence on the GR constructive properties. On the practical perspective, the potentiality of the Italian building heritage to host to broad spectrum of SUDS technology has to be analyzed in more detail. The introduction of an automated procedure able to discern green roof (or others SUDS) retrofit potential of the urban scale based on the use of remotely sensed areas could help to plan where and at which extent GRs (or other SUDS) adaptation can take place, accelerating the identification performed in the presented work by means of a visual inspection.

BIBLIOGRAPHY

Abbaspour K. C., Rouholahnejad E., Vaghefi S., Srinivasan R., Yang H., Kløved B. (2015). A continental-scale hydrology and water quality model for Europe: Calibration and uncertainty of a high-resolution large-scale SWAT model. *Journal of Hydrology*, 524: 733-752.

AgrarMeteorologie. Rheinland-Pfalz. Available from: www.am.rlp.de [*Accessed 28 April 2017*].

Ahern J. (2007). *Green infrastructure for cities: the spatial dimension*. London: IWA Publishing.

Ali M.F., Mawdsley J.A. (1987). Comparison of two recent models for estimating actual evapotranspiration using only regularly recorded data. *J. Hydrol*, 93: 257-276.

Allen R.G., Pereira L.S., Raes D., Smith M. (1998). Crop evapotranspiration-Guidelines for computing crop water requirements. *FAO Irrigation and drainage paper 56*. 300(9), D05109.

Arnbjerg-Nielsen K. (2012). Quantification of climate change effects on extreme precipitation used for high resolution hydrologic design. *Urban Water J*. 9: 57–65.

Asquith W. H. (2003). Modeling of runoff-producing rainfall hyetographs in Texas using L-moment statistics. *Doctoral dissertation*.

Ban, Y., Yousif O.A. (2012). Multitemporal spaceborne SAR data for urban change detection in China. *IEEE Journal of Selected Topics in Applied Earth Observations and Remote Sensing*, 5(4): 1087-1094

Becciu G., Paoletti A. (2004). *Esercitazioni di costruzioni idrauliche*. Chia: Cedam.

Benedict, M. A., McMahon E.T. (2002). Green infrastructure: smart conservation for the 21st century. *Renewable Resources Journal,* 20(3): 12-17.

Bengtsson L. (2005). Peak flows from thin sedum-moss roof. *Hydrology Research*, 36(3): 269-280.

Berndtsson, J.C. (2010). Green roof performance towards management of runoff water quantity and quality: A review. *Ecological Engineering*, 36(4): 351-360.

Berthier E., De Gouvello B., Archambault F., Gallis D. (2010). Water Balance of Green Roofs: Contributions to Better Understanding and Simulation. *Techniques Sciences Methodes. Genie Urbain-Genie Rural*, 6: 39–47.

Bonoli A., Conte A., Maglionico M., Stojkov I. (2013). Green roofs for sustainable water management in urban areas. *Environmental Engineering and Management Journal*, 12(S11): 153-156.

Borchard N., Schirrmann M., Von Hebel C., Schmidt M., Baatz R., Firbank L., Vereecken H., Herbst M. (2015). Spatio-temporal drivers of soil and ecosystem carbon fluxes at field scale in an upland grassland in Germany. *Agric. Ecosyst. Environ.*, 211: 84-93.

Bouchet R.J. (1963). Evapotranspiration réelle et potentielle, signification climatique. *IAHS Publ.* ,62: 134-142.

Brouwer C., Heibloem M. (1968). Irrigation water management: irrigation water needs. *Training manual 3*.

Brutsaert W. Stricker H. (1979). An advection aridity approach to estimate actual regional evapotranspiration. *Water resources research*, 15(2): 443-450.

Burszta-Adamiak E., Mrowiec, M. (2013). Modelling of green roofs' hydrologic performance using EPA's SWMM. *Water Science and Technology*, 68(1): 36-42.

Budyko M.I. (1974). *Climate and Life. Academy of Sciences, Main Observatory of Leningrad*. New York: Academic Press.

Buishand T.A. (1982). Some methods for testing the homogeneity of rainfall records. *J. Hydrol.*, 58: 11–27.

Burba G., Anderson D. (2010), A brief practical guide to eddy covariance flux measurements: principles and workflow examples for scientific and industrial applications. *Li-Cor Biosciences*, 1-211.

Califano F., Mobilia M., Longobardi A. (2015). Heavy Rainfall Temporal Characterization in the Peri-Urban Solofrana River Basin, Southern Italy., *Proc. 13th International Conference on Computing and Control for the Water Industry*, 1129–1138.

Carbone M., Nigro G., Garofalo G., Piro P. (2014). The hydrological performance of a green roof: An experimental study in the University of Calabria, Italy. *WIT Transactions on Ecology and the Environment*, 191: 1661-1669.

Carson T., Keeley M., Marasco D.E., McGillis W. Culian P., (2015). Assessing methods for predicting green roof rainfall capture: a comparison between full-scale observations and four hydrologic models. *Urban Water Journal*, 14(6): 1-15

Carter R.W. (1961). Magnitude and frequency of floods in suburban areas. *U.S. Geological Survey Professional Paper*, 424-B: 9-11.

Carter T.L., Rasmussen T.C. (2006). Hydrologic behavior of vegetated roofs. *J. Am. Water Resour. Assoc.*, 42 (5): 1261-1274

Chini M., Hostache R., Giustarini L., Matgen P. (2017). A hierarchical split-based approach for parametric thresholding of SAR images: Flood inundation as a test case. *IEEE Transactions on Geoscience and Remote Sensing*, 55(12): 6975-6988.

Cipolla S. S., Maglionico M., Stojkov I. (2016). A long-term hydrological modelling of an extensive green roof by means of SWMM. *Ecological Engineering,* 95: 876-887.

CLIMATE-DATA.ORG. Available from: https://it.climate-data.org/location/14223/. [*Accessed 20 March 2017*]

Conrad V., Pollak C. (1950). *Methods in Climatology*. Cambridge: Harvard University Press.

Davies J.A., Allen C.D. (1973). Equilibrium, potential and actual evaporation from cropped surfaces in southern Ontario. *Journal of Applied Meteorology*, 12(4): 649-657.

De Bruin H.A.R., Keijman, J.Q. (1979). The Priestley-Taylor evaporation model applied to a large, shallow lake in the Netherlands. *Journal of Applied Meteorology*, 18(7): 898-903.

Dewan A.M., Yamaguchi, Y. (2008). Effect of land cover changes on flooding: example from Greater Dhaka of Bangladesh. *International Journal of Geoinformatics*, 4(1): 11-20.

Di Martire D., Novellino A., Ramondini M., Calcaterra D. (2016). A-differential synthetic aperture radar interferometry analysis of a deep seated gravitational slope deformation occurring at Bisaccia (Italy). *Science of the Total Environment, 550*: 556-573.

Diodato N., Bellocchi G., Fiorillo F., Longobardi A. (2014). *Historical reconstruction of erosive storms driving damaging hydrological events in Southern Italy (Bonea basin), Storminess and Environmental Changes: Climate Forcing and Responses in the Mediterranean Region*. N. Diodato and G. Bellocchi (eds), Springer (2014): 179-192.

Ekström M., Fowler H.J., Kilsby C.G., Jones P.D. (2005). New estimates of future changes in extreme rainfall across the UK using regional climate model integrations. 2. Future estimates and use in impact studies. *J. Hydrol.*, 300: 234–251.

Fassman E. A., Blackbourn S. (2010). Urban runoff mitigation by a permeable pavement system over impermeable soils. *Journal of Hydrologic Engineering*, 15(6): 475-485.

Feitosa R. C., Wilkinson S. (2016). Modelling green roof stormwater response for different soil depths. *Landscape and Urban Planning*, 153: 170-179.

Fioretti R., Palla A., Lanza L.G., Principi P. (2010). Green roof energy and water related performance in the Mediterranean climate. *Building and Environment,* 45(8): 1890-1904.

Fletcher J.E., Chen C.L. (1975). Urban Storm Runoff Inlet Hydrograph Study Volume 3: Hydrologic Data for Two Urban Highway Watersheds in the Salt Lake City Area, Utah. *Reports:* Paper 480.

Fletcher T. D., Shuster W., Hunt W.F., Ashley R., Butler D., Arthur S., Trowsdale S., Barraud S., Semádeni-Davies A., Bertrand-Krajewski, J.L.

(2015). SUDS, LID, BMPs, WSUD and more–The evolution and application of terminology surrounding urban drainage. *Urban Water Journal*, 12(7): 525-542.

Fu Y., Wu J.Z. (2014). Expansion of urbanization based on remote sensing technology research To Zhengzhou city as an example. *Advanced Materials Research*. 926: 4242-4245

Gebler S., Hendricks Franssen H. J., Putz T., Post H., Schmidt M., Vereecken H. (2015). Actual evapotranspiration and precipitation measured by lysimeters: a comparison with eddy covariance and tipping bucket. *Hydrology and earth system science*s, 19(5): 2145-2161.

Ghimire G. R., Thakali R., Kalra A., Ahmad S. (2016). Role of Low Impact Development in the Attenuation of Flood Flows in Urban Areas. *In World Environmental and Water Resources Congress 2016*: 339-349.

Gibler M. R. (2015). Comprehensive benefits of green roofs. *World Environmental and Water Resources Congress 2015*. 2244-2251.

Gilbert R.O. (1987). *Statistical Methods for Environmental Pollution Monitoring*. New York: John Wiley & Sons, Inc

Gires A., Giangola-Murzyn A., Abbes J. B., Tchiguirinskaia I., Schertzer D., Lovejoy S. (2015). Impacts of small scale rainfall variability in urban areas: a case study with 1D and 1D/2D hydrological models in a multifractal framework. *Urban Water Journal*, 12(8): 607-617.

Grande progetto "completamento della riqualificazione e recupero del fiume Sarno" of arcadis (agenzia regionale campania difesa suolo) Available from: http://www.arcadis.campania.it [*Accessed 1 December 2017]*

Granger R. J., Gray D. M. (1989). Evaporation from natural nonsaturated surfaces. *Journal of Hydrology*, 111(1-4): 21-29.

Haas J., Ban Y. (2014). Urban growth and environmental impacts in Jing-Jin-Ji, the Yangtze, River Delta and the Pearl River Delta. *International Journal of Applied Earth Observation and Geoinformation*, 30: 42-55.

Hakimdavara R., Culligana P.J., Finazzia M., Barontinib B.S., Ranzib R. (2014). Scale dynamics of extensive green roofs: Quantifying the effect of drainage area and rainfall characteristics on observed and modeled green roof hydrologic performance. *Ecol. Eng*., 73: 494–508.

Haktanir T., Sezen, N. (1990). Suitability of two-parameter gamma and three-parameter beta distributions as synthetic unit hydrographs in Anatolia. *Hydrological sciences journal*, 35(2): 167-184.

Hald A. (1953). *Statistical Theory with Engineering Applications*. New York: John Wiley & Sons Inc.

Hannover L.G. (2002). *Guidelines for the planning, execution and upkeep of green-roof sites.* Bonn: Forschungsgesellschaft Landschaftsentwicklung Landschaftsbau (F.L.L.)

Hardin M., Wanielista M., Chopra M. (2012). A mass balance model for designing green roof systems that incorporate a cistern for re-use. *Water* , 4: 914–931.

Hilten R.N., Lawrence T.M., Tollner E.W. (2008). Modeling storm water runoff from green roofs with HYDRUS-1D. *J. Hydrol.*, 358: 288–293.

Hobbins M. T., Ramirez J.A., Brown T.C. (2001). The complementary relationship in estimation of regional evapotranspiration: An enhanced advection- aridity model. *Water Resources Research*, 37(5): 1389-1403.

Huff F.A. (1969). Climatological Assessment of Natural Precipitation Characteristics for Use in Weather Modification. *J. Appl. Meteor.*, 8 : 401–410.

Huong H.T.L., Pathirana A. (2013). Urbanization and climate change impacts on future urban flooding in Can Tho City, Vietnam. Hydrol. Earth Syst. Sci. , 17: 379-394.

Hydrology Available from: http://parra.sdsu.edu/roberson_chapter02-2.html [*Accessed 10 June 2017]*.

ISPRA Ambiente Available from: http://www.isprambiente.gov.it/files/pubblicazioni/rapporti/Rapporto_consumo_suolo_20162.pdf [*Accessed 20 April 2017]*.

Jacobson C. R. (2011). Identification and quantification of the hydrological impacts of imperviousness in urban catchments: A review. *Journal of environmental management*, 92(6): 1438-1448.

Jarrett A. R., Hunt W. F., Berghage R. D. (2006). Annual and individual-storm green roof stormwater response models. *ASAE Annual Meeting. American Society of Agricultural and Biological Engineers 2006*. (No. 062310)

Jha A., Lamond J., Bloch R., Bhattacharya N., Lopez A., Papachristodoulou N., Bird A., Proverbs D., Davies J., Barker R. (2011). *Five Feet High and Rising-Cities and Flooding in the 21st Century*. Washington: The World Bank.

Jim C.Y. Peng L.L.H. (2012). Substrate moisture effect on water balance and thermal regime of a tropical extensive green roof. *Ecol. Eng.*, 47: 9-23.

Kasmin H., Stovin V. R., Hathway E. A. (2010). Towards a generic rainfall-runoff model for green roofs. *Water science and technology*, 62(4): 898-905.

Kendall M.G. (1962). *Rank Correlation Methods*. New York: Hafner Publishing Company.

Koeppen W. (1931). *Grundriss der Klimakunde*. Berlin: Walter de Gruyter &Co.

FAO–RN, Koeppen's climate classification map Available from: http://www.fao.org/sd/EIdi rect/climate/EIsp0002.htm [*Accessed 18 May 2017]*.

Kohler M. A., Parmele L. H. (1967). Generalized estimates of free- water evaporation. *Water Resources Research*, 3(4): 997-1005.

Kong F., Ban Y., Yin H., James P., Dronova I. (2017). Modeling stormwater management at the city district level in response to changes in land use

and low impact development. *Environmental Modelling & Software*, 95: 132-142.

Krebs G., Kokkonen T., Setälä H., Koivusalo H. (2016). Parameterization of a Hydrological Model for a Large, Ungauged Urban Catchment. *Water,* 8(10): 443.

Krebs G., Kokkonen T., Valtanen M., Koivusalo H., Setälä, H. (2013). A high resolution application of a stormwater management model (SWMM) using genetic parameter optimization. *Urban Water Journal*, 10(6): 394-410.

Lazzarin R. M., Castellotti F., Busato F. (2005). Experimental measurements and numerical modelling of a green roof. *Energy and Buildings*, 37(12): 1260-1267.

Leopold L.B. (1968). Hydrology for Urban Land Planning. A Guidebook on the Hydrologic Effects of Urban Land Use. *Geological Survey Circular,* (No. 554):1-18.

Linsley R. K., Kohler M.A. (1951). Variations in storm rainfall over small areas. *Eos, Transactions American Geophysical Union*, 32(2): 245-250.

Locatelli L., Mark O., Mikkelsen P.S., Arnberg-Nielsen K., Jensen M.B., Binning P.J. (2014). Modelling of green roof hydrological performance for urban drainage applications. *Journal of hydrology*, 519: 3237-3248.

Longobardi A., Diodato N., Mobilia M. (2016). Historical Storminess and Hydro-Geological Hazard Temporal Evolution in the Solofrana River Basin—Southern Italy. *Water*, 8(9): 398.

Longobardi A., Diodato N., Mobilia M. (2017). Hydro-Geological Hazard Temporal Evolution during the last seven decades in the Solofrana River Basin—Southern Italy, *Proc: European Geosciences Union General Assembly 2017 (EGU2017*), 1-1.

Lu Z., Dzurisin D. (2014). *InSAR imaging of Aleutian volcanoes*. Berlin: Springer Berlin Heidelberg.

Ma Q., He C., Wu J., Liu Z., Zhang Q., Sun Z. (2014). Quantifying spatiotemporal patterns of urban impervious surfaces in China: An improved assessment using nighttime light data. *Landscape and Urban Planning*, 130: 36-49.

Mann H.B. (1945). Non parametric tests again trend. *Econometrica*, 13: 245-259.

Marasco D. E., Culligan P. J., McGillis W. R. (2015). Evaluation of common evapotranspiration models based on measurements from two extensive green roofs in New York City. *Ecological Engineering*, 84: 451-462.

Masseroni D., Cislaghi A. (2016). Green roof benefits for reducing flood risk at the catchment scale. *Environmental Earth Sciences,* 75(7): 579.

Mauder M., Cuntz M., Drüe C., Graf A., Rebmann C., Schmid H.P., Schmidt M., Steinbrecher R. (2013). A strategy for quality and uncertainty assessment of long-term eddy-covariance measurements. *Agricultural and Forest Meteorology*, 169: 122-135.

Mauder M., Foken T. (2011). Documentation and instruction manual of the eddy covariance software package TK3, *Arbeitsergebnisse Mikrometeorologie*, (No. 46): 1-60.

Mawdsley J. A. Ali M. F. (1985). Estimating nonpotential evapotranspiration by means of the equilibrium evaporation concept. *Water Resources Research*, 21(3), 383-391.

McMahon T. A., Peel M. C., Lowe L., Srikanthan R., McVicar T. R. (2013). Estimating actual, potential, reference crop and pan evaporation using standard meteorological data: a pragmatic synthesis. *Hydrology and Earth System Sciences*, 17(4): 1331.

McNaughton K.G., Black A.T. (1973). A study of evapotranspiration from a Douglas fir forest using the energy balance approach. *Water Resources Research*, 9(6), 1579-1590.

Mentens J., Raes D., Hermy M.. (2006). Green roofs as a tool for solving the rainwater runoff problem in the urbanized 21st century?. *Landscape and urban planning*, 77(3): 217-226.

Mguni P., Herslund L., Jensen M.B. (2016). Sustainable urban drainage systems: examining the potential for green infrastructure-based stormwater management for Sub-Saharan cities. *Natural Hazards,* 82(2): 241-257

Mishra S. K., and Singh V.P. (2013). *Soil conservation service curve number (SCS-CN) methodology*. Springer Science & Business Media

Mobilia M., Longobardi A. (2018a). Impact of rainfall properties and green roofs spatial distribution on LID performances at the catchment scale. *Proc. UDM2018 11th International Conference on Urban Drainage Modelling*, Submitted.

Mobilia M., Longobardi A., Amitrano D., Ruello G. (2018c). Analisi dei cambiamenti climatici e di uso del suolo in un bacino prono ad allagamenti urbani, *Proc. IDRA2018 XXXVI Convegno Nazionale di Idraulica e Costruzioni Idrauliche*, Submitted.

Mobilia M., Califano F., Longobardi A. (2015c). Event and long term scale analysis of rainfall triggering MDHE in a peri-urban system, Proc. *Rome2015 Science Symposium on climate*, 1-1.

Mobilia M., Califano F., Longobardi A. (2015d). Analysis of Rainfall Events driving MDHEs Occurred in the Solofrana River Basin, Southern Italy, *Proc. 13th International Conference on Computing and Control for the Water Industry,* 1139–1146.

Mobilia M., Longobardi A., Sartor J. F. (2014). Impact of green roofs on stormwater runoff coefficients in a Mediterranean urban environment, *Proc. 5th International Conference on Urban Sustainability, Cultural Sustainability, Green Development, Green Structures and Clean Cars (USCUDAR'14)*, 100-106.

Mobilia M., Longobardi A., Sartor J.F. (2015a). Green Roofs Hydrological Performance under Different Climate Conditions. *WSEAS transactions on environment and development*, 11: 264-271.

Mobilia M., Longobardi A., Sartor J.F. (2015b). Urban stormwater runoff reduction by green roof under different climate conditions, *Proc. 8th International Conference on Environmental and Geological Science and Engineering (EG '15*), 379-383.

Mobilia, M., Longobardi, A., Sartor J. F. (2016b). Including actual evapotranspiration for green roof modelling at an experimental site, *Proc. IDRA2016 XXXV Convegno Nazionale di Idraulica e Costruzioni Idrauliche*, 959-962.

Mobilia M., Longobardi A., Sartor J.F. (2017). Including A-Priori Assessment of Actual Evapotranspiration for Green Roof Daily Scale Hydrological Modelling. *Water*, 9(2): 72.

Mobilia M., Longobardi A., Schmidt M. (2016a). How good perform complementary evapotranspiration models? – A comparison of modeled versus measured evapotranspiration derived from eddy covariance estimates of latent heat flux, *Proc. CCWI16 Computing and Control for the Water Industry*, 1-8.

Mobilia M., Longobardi A., Schmidt M. (2018b). Evaluation of meteorological data based evapotranspiration models using flux measurements under oceanic climate conditions. *Journal of Hydrologic Engineering*. In review.

Mobilia M., Longobardi A. (2017a). Smart Stormwater Management in Urban Areas by Roofs Greening, *Proc. International Conference on Computational Science and Its Applications*, 455-463.

Morton F. I. (1978). Estimating evapotranspiration from potential evaporation: practicality of an iconoclastic approach. *Journal of Hydrology*, 38(1-2): 1-32.

Morton F. I. (1983). Operational estimates of areal evapotranspiration and their significance to the science and practice of hydrology. *Journal of Hydrology*, 66(1-4): 1-76.

Olivieri F., Di Perna C., D'Orazio M., Olivieri L., Neila J. (2013). Experimental measurements and numerical model for the summer performance assessment of extensive green roofs in a Mediterranean coastal climate. *Energy and Buildings*, 63: 1-14.

Onoz B., Bayazit M. (2003). The power of statistical tests for trend detection. *Turkish Journal of Engineering and Environmental Sciences*, 27: 247–251.

Otsu N. (1979). A threshold selection method from gray-level histograms. *IEEE transactions on systems, man, and cybernetics*, 9: 62-66.

Otsuki K., Mitsuno T., Maruyama T., (1984). Comparison between water budget and complementary relationship estimates of catchment evapotranspiration. *Transactions of The Japanese Society of Irrigation, Drainage and Rural Engineering*, 112: 17–23 (In Japanese with English abstract.)

Palla A., Gnecco I., Lanza L.G. (2009). Unsaturated 2D modelling of subsurface water flow in the coarse-grained porous matrix of a green roof. *Journal of Hydrology*, 379(1-2): 193-204.

Palla A., Sansalone J. J., Gnecco I., & Lanza L. G. (2011). Storm water infiltration in a monitored green roof for hydrologic restoration. *Water Science and Technology*, 64(3): 766-773.

Parihar N., Das A., Rathore V. S., Nathawat M. S., Mohan S. (2014). Analysis of L-band SAR backscatter and coherence for delineation of land-use/land-cover. *International journal of remote sensing*, 35(18): 6781-6798.

Peng Z., Stovin V. R. (2017). Independent Validation of the SWMM Green Roof Module. *Journal of Hydrologic Engineering,* 22(9): 04017037

Penman H.L.T., Schofield R.K. (1951) Some physical aspects of assimilation and transpiration. *Symp. Soc. Exp. Biol.*, 5.

Penman H. L. (1948). Natural evaporation from open water, bare soil, and grass., *Proc. R. Soc. London*, 120–146. The Royal Society.

Petrucci O., Polemio M. (2003). The use of historical data for the characterization of multiple damaging hydrogeological events. *Nat. Hazards Earth Syst. Sci.,* 3: 17–30.

Poë S., Stovin, V., Berretta C. (2015). Parameters influencing the regeneration of a green roof's retention capacity via evapotranspiration. *Journal of Hydrology*, 523: 356-367.

Post H., Hendricks Franssen H.J., Graf A., Schmidt M., Vereecken H. (2015). Uncertainty analysis of eddy covariance CO2 flux measurements for different EC tower distances using an extended two-tower approach. *Biogeosciences*, 12: 1205–1221.

Priestley C. H. B., Taylor R.J. (1972). On the assessment of surface heat flux and evaporation using large-scale parameters. *Monthly weather review*, 100(2): 81-92.

Qu W., Bogena H.R., Huisman J.A., Schmidt M., Kunkel R., Weuthen A., Schiedung H., Schilling B., Sorg J., Vereecken H. (2016). The integrated water balance and soil data set of the Rollesbroich hydrological observatory. *Earth System Science data*, 8: 517–529.

Rawls W. J., Brakensiek D.L., Miller N. (1983). Green-Ampt infiltration parameters from soils data. *Journal of hydraulic engineering*, 109(1): 62-70.

Reeves J., Chen J., Wang X.L., Lund R., Lu Q.Q. (2007). A review and comparison of changepoint detection techniques for climate data. *J. Appl Meteorol Clim*, 46: 900-915

Reichstein M., Falge E., Baldocchi D., Papale D., Aubinet M., Berbigier P., Bernhofer C., Buchmann N., Gilmanov T., Granier A., Grünwald T., Havránková K., Ilvesniemi H., Janous D., Knohl A., Laurila K., Lohila A., Loustau D., Matteucci G., Meyers T., Miglietta F., Ourcival J. M., Pumpanen J., Rambal S., Rotenberg E., Sanz M., Tenhunen J., Seufert G.,

Vaccari F., Vesala T., Yakir D., Valentini R. (2005). On the separation of net ecosystem exchange into assimilation and ecosystem respiration: review and improved algorithm. *Global Change Biology*,11: 1424–1439.

Rodionov S.N. (2005). *A brief overview of the regime shift detection methods*. Varna: Large-Scale Disturbances (Regime Shifts) and Recovery in Aquatic Ecosystems: Challenges for Management Toward Sustainability [V. Velikova and N. Chipev (Eds.)].

Rossi F., Villani P. (1994). *Regional flood estimation methods*. Netherlands: Springer.

Cronshey R. (1986). *Urban hydrology for small watersheds*. Washington: US Dept. of Agriculture, Soil Conservation Service, Engineering Division.

Ryu Y., Baldocchi D.D., Ma S., Hehn T. (2008). Interannual variability of evapotranspiration and energy exchange over an annual grassland in California. *Journal of Geophysical Research: Atmospheres,* 113(D9): 2156-2202.

Salinity management. Available from: http://www.salinitymanagement.org /Salinity%20Management%20Guide/ew/ew_9a_table-8.html. [*Accessed 1 June 2017*].

Sartor J.F., Mobilia M., Longobardi A. (2018). Results and Findings from 15 Years of Sustainable Urban Storm Water Management, *Proc. FRIAR 2018 6th International Conference on Flood and Urban Water Management*, In review.

Semadeni-Davies A., Hernebring C., Svensson G., Gustafsson L.G. (2008). The impacts of climate change and urbanisation on drainage in Helsingborg, Sweden: Suburban stormwater. *J. Hydrol.*, 350: 114-125.

Sen P.K.. (1968). Estimates of the regression coefficient based on Kendall's tau. *J Am Stat Ass,* 63: 1379-1389.

Shaharuddin A., Noorazuan M.H., Yaakob M.J. (2011). Green roofs as best management practices for heat reduction and stormwater flow mitigation. *World Applied Sciences Journal,* 13(13): 58-62.

Sherrard J., James A., Jennifer M.J. (2011). Vegetated roof water-balance model: Experimental and model results. *J. Hydrol. Eng.,* 17:858–868.

Slatyer R. O., McIlroy I.C. (1961). *Practical Microclimatology*. Melbourne: UNESCO.

Starry O., Lea-Cox J., Ristvey A., Cohan S. (2016). Parameterizing a Water-Balance Model for Predicting Stormwater Runoff from Green Roofs. *Journal of Hydrologic Engineering,* 21(12): 04016046.

Stovin V, Poë S., Berretta C. (2013). A modelling study of long term green roof retention performance. *Journal of environmental management,* 131: 206-215.

Stovin V., Poë S., De-Ville S., Berretta C. The influence of substrate and vegetation configuration on green roof hydrological performance. *Ecological Engineering*, 85: 159-172.

Stovin V, Vesuviano G., Kasmin H. (2012). The hydrological performance of a green roof test bed under UK climatic conditions. *Journal of Hydrology*, 414: 148-161.

Strozzi T., Wegmuller U. (1998). Delimitation of urban areas with SAR interferometry. *Geoscience and Remote Sensing Symposium Proceedings*, 3: 1632-1634.

Tanner C. B., Pelton W. L. (1960). Potential evapotranspiration estimates by the approximate energy balance method of Penman. *Journal of geophysical research*, 65(10): 3391-3413.

Taubenböck H., Esch T., Felbier A., Wiesner M., Roth A., Dech S. (2012). Monitoring urbanization in mega cities from space. *Remote sensing of Environment,* 117: 162-176.

Teemusk A., Mander U. (2007). Rainwater runoff quantity and quality performance from a greenroof: The effects of short-term events. *Ecological engineering*, 30(3): 271-277.

Terranova O.G., Gariano S.L. (2014). Regional investigation on seasonality of erosivity in the Mediterranean environment. *Environmental Earth Sciences,* 73: 311-324.

Terranova O.G. Iaquinta P. (2011). Temporal properties of rainfall events in Calabria (southern Italy). *Natural Hazards and Earth System Sciences*, 11: 751–757.

Trinh D. H., Chui T. F. M. (2013). Assessing the hydrologic restoration of an urbanized area via an integrated distributed hydrological model. *Hydrology and Earth System Sciences*, 17(12): 4789.

United Nations. Available from: http://www.un.org/en/ development/desa/ news/population/world-urbanizationprospects-2014.html (*Accessed 14 June 2017*).

Vallario A. (2001). *Il dissesto idrogeologico in Campania*. CUEN.

VanWoert N.D., Rowe D.B., Andresen J.A., Rugh C.L., Xiao L. (2005). Green roof stormwater retention. *Journal of environmental quality,* 34(3): 1036-1044.

Versini P. A., Gires A., Abbes J. B., Giangola-Murzyn A., Tchiguirinskaia I., Schertzer D. (2014). *Simulation of Green Roof Impact at Basin Scale by Using a Distributed Rainfall-Runoff Model.* In 13th International Conference on Urban Drainage (ICUD): 1-9.

Versini P. A., Gires A., Tchinguirinskaia I., Schertzer D. (2016). Toward an operational tool to simulate green roof hydrological impact at the basin scale: a new version of the distributed rainfall–runoff model Multi-Hydro. *Water Science and Technology,* 74(8): 1845-1854.

Villarreal E. L., Bengtsson L. (2005). Response of a Sedum green-roof to individual rain events. *Ecological Engineering*, 25(1): 1-7.

Virginia dcr stormwater design specification no. 7. Available from: http://vwrrc.vt.edu/swc/april_22_2010_update/DCR_BMP_Spec_No_7_ PERMEABLE_PAVEMENT_Final_Draft_v1-7_03082010.htm *Accessed 12 October 2017].*

Voyde E., Fassman E., Simcock R. (2010). Hydrology of an extensive living roof under sub-tropical climate conditions in Auckland, New Zealand. *Journal of hydrology* , 394(3): 384-395.

Weijie X., Xiaojie W. (2015). SAR image simulation and verification for urban structures. *International Journal of Electronics*, 103(2): 1-14.

Westphal J.A. (2001). Design of stormwater inlets. New York: McGraw Hill

Wilkinson S. J., Reed R. (2009). Green roof retrofit potential in the central business district. *Property Management*, 27(5): 284-301.

Willems P., Olsson J., Arnbjerg-Nielsen K., Beecham S., Pathirana A., Gregersen I.B., Madsen H., Nguyen V.T.V. (2012). *Impacts of Climate Change on Rainfall Extremes and Urban Drainage*. London: IWA Publishing.

Woods-Ballard B., Kellagher K., Martin P., Jefferies C., Bray R., Shaffer P. (2007). *The SUDS manual*. London: CIRIA.

Wu H., Huang G., Meng Q., Zhang M., Li, L. (2016). Deep Tunnel for Regulating Combined Sewer Overflow Pollution and Flood Disaster: A Case Study in Guangzhou City, China. *Water*, 8(8): 329.

Yalin M. S. (2015). *River mechanics*. U.K.: Elsevier.

Yen B. C., Chow V. T. (1980). Design hyetographs for small drainage structures. *Journal of the Hydraulics Division*, 106: ASCE 15452.

Zachary Bean E., Frederick Hunt W., Alan Bidelspach D. (2007). Evaluation of four permeable pavement sites in eastern North Carolina for runoff reduction and water quality impacts. *Journal of Irrigation and Drainage Engineering*, 133(6): 583-592

Zhang D., Liu X., Zhang Q., Liang K., Liu C. (2016). Investigation of factors affecting intra-annual variability of evapotranspiration and streamflow under different climate conditions. *Journal of Hydrology*, 543: 759-769.

Zhou Q. (2014). A review of sustainable urban drainage systems considering the climate change and urbanization impacts. *Water*, 6(4): 976-992.

Zhou Q., Mikkelsen P.S., Halsnæs K., Arnbjerg-Nielsen, K. (2012). Framework for economic pluvial flood risk assessment considering climate change effects and adaptation benefits. *J. Hydrol.*, 414: 539–549.

Zhu X.X., Montazeri S., Gisinger C., Hanssen R.F., Bamler R. (2016) Geodetic SAR tomography. *IEEE Transactions on Geoscience and Remote Sensing*, 54(1): 18-35.

Zhu Z., Chen X. (2017). Evaluating the Effects of Low Impact Development Practices on Urban Flooding under Different Rainfall Intensities. *Water*, 9(7): 548.

Zhu Z., Woodcock C.E., Rogan, J., Kellndorfer J. (2012). Assessment of spectral, polarimetric, temporal, and spatial dimensions for urban and peri-urban land cover classification using Landsat and SAR data. *Remote Sensing of Environment*, 117: 72-82.

Zimmer U., Geiger W. F. (1997). Model for the design of multilayered infiltration systems. *Water science and technology,* 36(8-9): 301-306.

Zimmermann E., Bracalenti L., Piacentini R., Inostroza L. (2016). Urban Flood Risk Reduction by Increasing Green Areas for Adaptation to Climate Change. *Procedia Engineering*, 161: 2241-2246.

ACKNOWLEDGMENTS

First, I would like to express my deepest thanks to my supervisor professor Antonia Longobardi. It has been a great honor to be her Ph.D. student. Her guidance helped me all the time and her support was unfailing. I could not have imagined having a better mentor for my Ph.D course.

I am also very grateful to professor Joachim Sartor and professor Britta Schmalz for their useful scientific advice and suggestions. Without their precious support it would not have been possible to conduct a big part of this research. (Danke schön!!!)

I would like to thank my parents, my sister Chiara, my grandparents, my boyfriend Domenico and my best friend Luana for the love, support, and constant encouragement.

I would especially like to thank Luca, Luigi and Francesco, my research lab colleagues and friends, it has been a great honor working with them and I have appreciated very much their advice and good humor.

Many thanks to Dr. Marius Schmidt for his mentorship during my stay in Juelich.

Thanks to the Italian Space Agency (ASI) for providing the satellite images used in this study.

Last but not least, I want to express my sincere gratitude to the reviewers of the present dissertation professors Britta Schmalz and Remy Claverie for their valuable and constructive comments.